Consolidation and Arching Potential of Slurry Backfill

A Thesis

Submitted to the College of Graduate Studies and Research

in Partial Fulfilment of the Requirements

for the

Degree of Master of Science

in the Department of Civil and Geological Engineering

University of Saskatchewan

Saskatoon

By

Rahul Vishwanath Mukherjee

PERMISSION TO USE

The author has agreed that the library, University of Saskatchewan, may make this thesis freely available for inspection. Moreover, the author has agreed that permission for extensive copying of this thesis for scholarly purposes may be granted by the professors who supervised the thesis work recorded herein or, in their absence, by the head of the Department or the Dean of the College in which the thesis work was done. It is understood that due recognition will be given to the author of this thesis and to the University of Saskatchewan in any use of the material in this thesis. Copying or publication or any other use of the thesis for financial gain without approval by the University of Saskatchewan and the author's written permission is prohibited.

Requests for permission to copy or to make any other use of material in this thesis in whole or part should be addressed to:

Head of Department of Civil and Geological Engineering
University of Saskatchewan
Engineering Building
57 Campus Drive
Saskatoon, Saskatchewan
Canada, S7N 5A9

ABSTRACT

Soil-bentonite (SB) slurry walls are one of the most popular techniques for minimizing the horizontal migration of contaminants. Backfill arching, or “hang-up” of the backfilled slurry, on the wall trench has the potential to significantly reduce the effectiveness of these barriers. This research was conducted to supplement the design and installation of an 11,000 m long slurry wall at PotashCorp’s mine in Rocanville, Saskatchewan. The slurry wall is being installed through low permeability glacial till containing permeable granular zones.

This study was undertaken to improve the understanding of vertical stress distribution in these deep barriers. In particular, the objective of this study was to develop an understanding of the factors controlling arching and hydraulic conductivity (k) of SB walls. Slurry wall “hang-up” or arching is dependent on shear along the wall of the trench and on a coefficient of lateral earth pressure (K). Consolidated drained (CD) shear box tests were conducted to study the shear strength parameters of the backfill mixes. Six inch proctor mold was modified with load cells on the side walls to measure horizontal stresses along with consolidation. This was used to calculate coefficient of lateral earth pressure, K (which is the ratio of horizontal to vertical effective stress). The results of the laboratory testing program found that K was relatively independent of the percentage of fines present in the SB mix. It also showed that backfill angle of internal friction and k of the backfill decreased with increased fines content. The results of the laboratory testing program were used to model the vertical stress distribution in deep walls. An analytical model (discrete model) and a coupled seepage stress-strain finite element model (FEM) were used to predict vertical stress changes with time and depth for the different backfill materials.

The primary conclusion of this research is that slurry wall backfill arching or “hang-up” significantly delays the magnitude and timing of vertical stress build-up in backfill. This loss of vertical stress results in backfill with lower density and higher hydraulic conductivity. The situation was found to be most critical for deep narrow slurry walls. Any advantage in using a coarser graded backfill was offset by higher backfill hydraulic

conductivity. The net result is that the upper portions of slurry walls may not be able to achieve their hydraulic conductivity objectives as soon as expected, if at all. In addition, the backfill in the upper portion of the trench may be susceptible to chemical attack and osmotic consolidation. Construction of a 2 m high surcharge berm over the slurry wall was found to increase vertical effective stress and result in significantly lower (2 to 8 times) hydraulic conductivity values in the top 5 metres of the trench. The final hydraulic conductivity (k) at a depth of 5 m was approximately 75 % lower with a surcharge berm. Thus, construction of a surcharge berm over the slurry wall helps to satisfy the k requirement for SB walls and lowers the risk of osmotic consolidation.

ACKNOWLEDGEMENTS

It is a pleasure to take this chance to thank those who made this thesis possible. First and foremost, I would like to show my deepest gratitude to God for giving me the opportunity to learn and for his presence and unspeakable generosity, patience, support, and love.

I proclaim my profound gratitude to Prof. Moir Dee Haug, my supervisor and mentor, for the invaluable time and effort he invested in this work. He provided freedom and a cordial and intellectually stimulating atmosphere while providing direction and critical advice to the successful completion of this research work. His advice spanned identification of the research problem, theory, conceptualization, modelling, and concise technical writing. I am thankful to my supervisor for being on my side and always understanding when I had difficulties. In the course of this thesis, my dad passed away with cancer. Prof Haug's support during this tragic time would be always remembered.

I am also profoundly grateful to Dr. Lal Samarasekera, who was Senior Geotechnical Engineer at SNC – Lavalin Environment, Saskatoon during this time, for his invaluable guidance and insights to this research work. His continuous encouragement and endless support during the modelling section of this thesis is sincerely appreciated.

Constructive feedback provided by the members of my Graduate Advisory Committee contributed to the successful completion and quality of this work. I am therefore grateful to Prof. Lee Barbour, Mr. Julian Gan, and Dr. Chris Hawkes, the Chairman of the committee.

I wish to thank the Saskatchewan Potash Producers Association (SPPA), MDH Engineered Solutions, Saskatoon, and the University of Saskatchewan for their financial support towards the successful completion of this work.

I owe a debt of gratitude to those who have provided me with laboratory assistance, including Doug Fisher, Alex Kozlow, Dale Pavier, and Brennen Pokoway. Special thanks to Jackie Hendrickx, clerical assistant Graduate Studies, Department of Civil and Geological Engineering, for all her help. I also wish to thank Mr. Gordon Pauls, Senior Geotechnical Engineer at SNC – Lavalin Environment, Saskatoon, for helping me with field data collection.

I am thankful to Prof. Jitendra Sharma for helping me during my initial days in Saskatoon.

I wish to thank my mentor, Dr. B.R Phanikumar, Professor, VIT University, Vellore, India, for his valuable input and suggestions over the phone. His encouragement and support brought me to Canada to do my Masters degree.

Most importantly, I wish to thank my parents, family members, friends, and my wife Sneha for their love, sacrifice, interest, and encouragement during the course of my study. I have been blessed with much in my life, for which I am grateful, but my family is truly the greatest of these gifts and will always be the centre of my world.

DEDICATION

This thesis and MSc is dedicated to my late father “Prof. Dilip Kumar Mukherjee” and my mother “Prof. Tapati Mukherjee”. My dad was my inspiration to come abroad to do research and pursue higher studies. My mom always stood by my side. Her encouragement and support helped me to come back from India and finish my thesis after my dad passed away in March 2011.

TABLE OF CONTENTS

LIST OF TABLES

LIST OF FIGURES

LIST OF SYMBOLS

D	Depth of the slurry wall [L]
E	Young's modulus [MLT^{-2}]
e	Void ratio [ ]
g	Acceleration due to gravity [LT^{-2}]
F	Frictional force [$ML^{-1}T^{-2}$]
FB	Field backfill
G	Specific gravity [ ]
h	Depth [L]
γ'	Effective unit weight [$ML^{-2}T^{-2}$]
K	Coefficient of lateral earth pressure [ ]
k	Hydraulic conductivity [LT^{-1}]
w	Width of the slurry wall [L]
SB	Soil bentonite
TM1	Trial mix1
TM2	Trial mix 2
TM3	Trial mix 3
ϕ'	Coefficient of friction [ ]
m_v	Coefficient of volume compressibility [ ]
C_C	Compression index [ ]
ρ	Density [ML^{3}]
σ'_h	Horizontal effective stress [$ML^{-1}T^{-2}$]
u	Horizontal displacement [L]
n	Porosity [ ]

υ	Poisson's ratio [ ]
v	Vertical displacement [L]
σ'_v	Vertical effective stress [$ML^{-1}T^{-2}$]
θ	Volumetric water content [ ]
q_y	Water flux in y direction [LT^{-1}]

CHAPTER 1 - INTRODUCTION

1.1 Background

Soil-bentonite (SB) slurry walls are one of the most common techniques to minimize the horizontal migration of contaminants. This technique involves excavation of a narrow trench in the presence of a bentonite slurry down through permeable strata and then backfilling the trench with a low hydraulic conductivity material. Backfill arching or “hang-up” of the backfill in the trench has the potential to significantly reduce the effectiveness of slurry walls.

A 47 m deep, 11,000 m long slurry wall is currently being constructed at the Potash Corporation of Saskatchewan (PCS)’s Potash mine in Rocanville, eastern Saskatchewan. This is the largest slurry wall ever constructed in Canada. This wall is being constructed through high clay content overconsolidated glacial till. The slurry wall is being keyed into a low hydraulic conductivity upper Cretaceous clay-shale. The purpose of this deep slurry wall is to cut off seepage of brine through sand pockets and stacked aquifers that are present in the till. These aquifers represent potential pathways for the migration of chloride contaminated fluids.

1.2 Need

One of the biggest concerns with narrow deep slurry walls is the potential for the development of more permeable soft zones or “gaps” in the backfill due to arching or “hang-up”. The hydraulic conductivity of trench backfill is highly dependent on backfill composition, weight of the overlying backfill, and trench geometry (Baxter 2001). As a result, backfill hydraulic conductivity usually decreases with depth as the slurry backfill consolidates under increasingly high loads. Laboratory model and field studies on slurry walls show that vertical stress does not increase linearly with depth (McCandless and Bodocsi 1987;Evans et al. 1995); rather friction at the interface between the backfill and the trench walls governs the consolidation behaviour of the backfill-slurry mix (Evans et al 1995; Filz 1996). This phenomenon has been explained as an arching mechanism.

Figure 1.1 shows the most probable vertical stress distribution in the slurry walls. The dashed line is the geostatic stress (ρgh) with depth. Where ρg is the unit weight of the soil and h is the depth. The solid line is the most probable stress distribution in the wall due to arching, which is less than the geostatic stress distribution.

The main design objective of these walls is to achieve a low hydraulic conductivity (k), which also depends on the stress state in the wall. Hence, accurate prediction of k requires knowledge of the vertical effective stress distribution with depth and time in these walls.

It is hypothesized that a change in the backfill gradation will result in less arching and will provide an acceptable and more stable hydraulic conductivity at depth (Yeo et al., 2005).

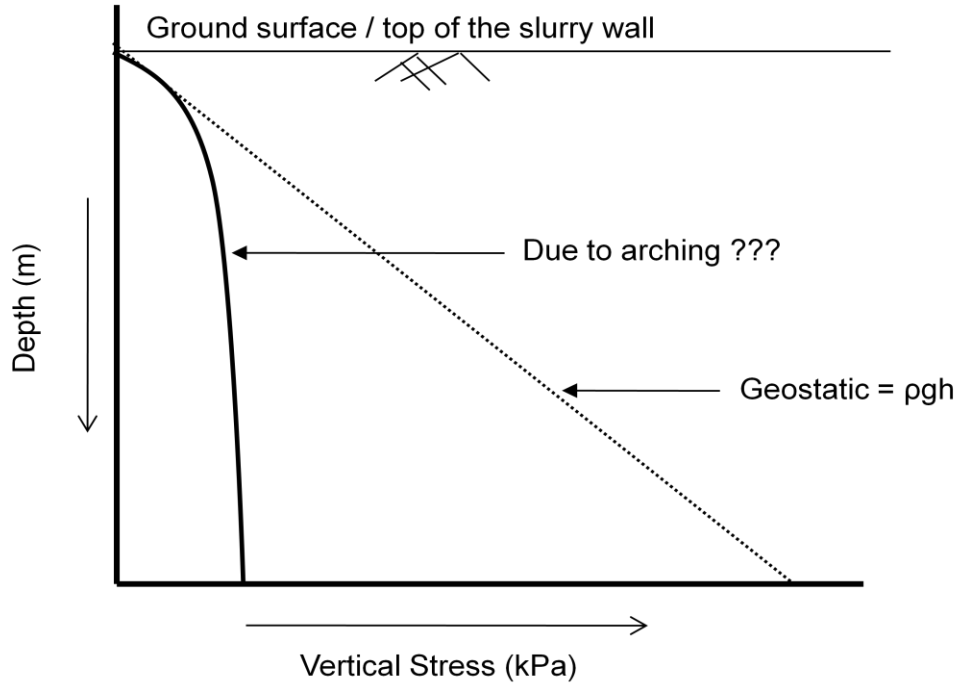

Figure 1.1. Backfill vertical stress distribution with depth for geostatic and arching conditions.

1.3 Research Objectives

The long-term performance of the slurry walls is dependent on their hydraulic conductivity. The key phenomenon that controls the hydraulic conductivity of a soil-bentonite (SB) wall is vertical effective stress distribution. This study had a global objective of developing an understanding of the performance of slurry walls with time and depth.

The specific objectives of this study were to:

1. Develop an understanding of the factors and their relative importance in controlling arching and hydraulic conductivity of slurry trench backfill.
2. Characterize the vertical effective stress distribution with depth and time in soil-bentonite walls.
3. Evaluate the change in hydraulic conductivity with depth and time for different backfill materials.

These objectives were achieved through the following tasks:

1. A literature review was conducted to examine the current state of knowledge on backfill arching.
2. Field excavation and backfilling of the PotashCorp Rocanville slurry wall was observed. Backfill samples were collected from the field.
3. An experimental setup was designed to measure lateral stress during large strain consolidation testing, in an effort to determine the coefficient of lateral earth pressure.
4. Tests were conducted to determine the geotechnical properties of soil-bentonite backfill materials containing different “fines” content.
5. Vertical stresses of these backfill materials in deep slurry walls were modelled. In addition, these stresses were modelled under different conditions (side wall hydraulic conductivity, intermediate aquifer, and presence of surcharge berm).

6. The modelled results were compared with values obtained from the field.

CHAPTER 2 - LITERATURE REVIEW

2.1 Introduction

This chapter presents background information about soil-bentonite (SB) cut-off walls with reference to their mechanical and engineering behaviour. The background includes information regarding the construction process and current design methods. The design method considers the hydraulic conductivity of the backfill, stability of the trench during excavation, and stress distribution mechanisms in SB walls. The present work focuses on stress distribution and hydraulic conductivity in SB cut-off walls.

2.1.1 Cut-off walls

Slurry trench cut-off walls were first used as seepage barriers in the 1940's by the United States Army Corps of Engineers (Xanthakos 1979, Haug et al. 1983). Gradually, with the development of improved backfill mixture designs and construction techniques, the use of slurry trench SB cut-offs started gaining wide acceptance (Haug and Kozicki 1983). Today, they are used in several different applications, such as ((Xanthakos 1979) :

a. Under or through dams, dikes, levees, or cofferdams;
b. Control of seepage or leakage from ponds and lakes;
c. Dewatering of areas to be excavated;
d. Control of groundwater infiltration from waste disposal sites;
e. Groundwater reservoir and isolation or maintenance of water tables; and
f. Waste collection from chemical or oil storage facilities.

2.2 Construction process

The foremost task in the construction of the wall involves establishing its alignment and depth. This depends on the use of the wall, site geology, and hydrogeology.

A slurry trench method is employed for the construction of soil-bentonite cut-off walls. The width of the trench is typically between 0.6 and 1.5 m (Woodcock and Miller 1971,

D’Appolonia 1980). The selection of excavating equipment depends on the purpose of construction, the type of soil, and the excavation depth, among other factors (Xanthakos 1979). Excavation of trenches with depths less than 15 m is typically done using backhoes. For deep trenches, cable clamshell or hydraulic excavators are generally used. During excavation, the trench is kept full with a bentonite-water slurry suspension to prevent the collapse of the side walls. As the excavation proceeds longitudinally, a ramp is initially created using mixed backfill from the bottom of the trench to the ground surface. Soil-bentonite is then pushed into the trench and allowed to slide down along the slope of the ramp; being denser, it displaces the bentonite-water slurry and hence becomes the cut-off wall. The soil used in the backfill can be the soil excavated from the trench or soil imported from offsite, depending upon the project requirements. Figure 2.1 shows the construction process (after LaGrega et al. 1994).

The slurry typically consists of 4 to 7% bentonite by weight (D’Appolonia 1980, Henry et al. 1998). The slurry level in the trench is maintained above the adjacent water table. Due to the existence of a hydraulic gradient, the slurry flows into the trench walls, forming a thin layer of bentonite cake at the interface referred to as ‘filter cake’ (D’Appolonia 1980; Filz et al. 1997; Henry et al. 1998). D’Appolonia (1980) recommends a slurry with and Marsh funnel velocity of 40 seconds for good cake formation. The porosity of filter cake ranges from 0.65 to 0.96. Due to the low hydraulic conductivity of the cake, the pressure difference between the slurry and the adjacent water table is dissipated across the filter cake and, hence, creates a stabilizing effect on the excavation face. The hydrostatic pressure from the slurry also acts against the filter cake and provides a stabilizing force.

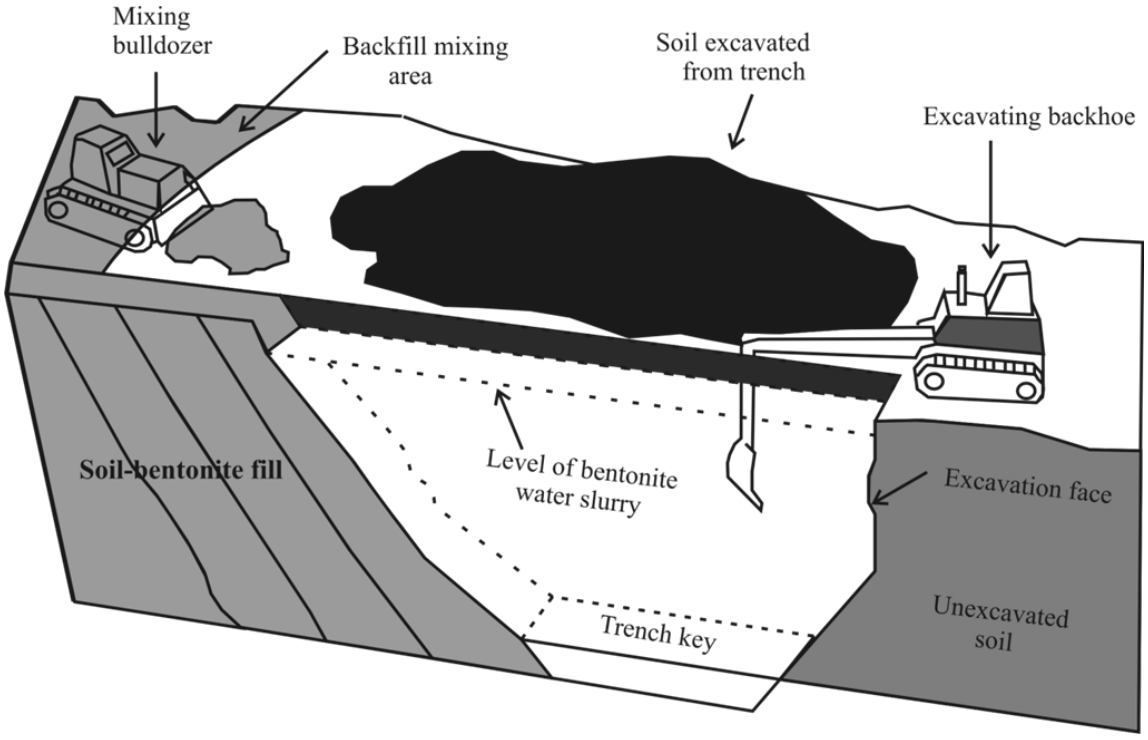

Figure 2.1 Construction process (after LaGrega et al. 1994).

2.3 Engineering behaviour of backfill material

This section presents a review of the literature regarding the engineering behaviour of SB backfill to date, with a primary focus on the strength and deformability of SB walls. It is difficult to characterize these walls in general, as they vary significantly from place to place. One of the main reasons for the variation is that the soil-bentonite is typically made by mixing materials excavated from the trench with the bentonite-water slurry. These excavated materials vary greatly from site to site or sometimes even within the same site.

2.3.1 Grain size distribution and consistency

Grain size distribution helps in achieving the required SB mix in terms of consolidation and hydraulic conductivity requirements for SB walls. Sufficient granular material with grain to grain contact helps with respect to achieving low compressibility. A well-graded

mix for the SB helps in achieving low hydraulic conductivity and low compressibility (Xanthakos 1979; D'Appolonia 1980; Yeo et al. 2005). A mix with 20-50% plastic fines and a minimum of 1% dry bentonite is recommended (D'Appolonia 1980, Evans 1991). Well-graded material similar to glacial till with 10 to 20% fines and 2 to 5% dry bentonite has been recommended by Millet et al. (1999). Successful use of other gradations, such as fine sands and clays, has also been reported in the literature. Yeo et al. (2005) recommend approximately 40% fines (particles less than 0.075 μm) in the SB mix to achieve a hydraulic conductivity of 10^{-9} m/s.

Consistency of the SB mix is important for proper placement of the mix in the trench. A standard concrete slump cone device is used for controlling the slump of the mix in the field. A slump of about 100-150 mm has been recommended for SB mix (D'Appolonia 1980, Millet et al. 1999). This slump value helps to control the slope of the backfill and to ensure that no liquid slurry is trapped in the backfill. If the slump value is greater than 150 mm, a flat backfill slope forms that can pose problems with reference to the efficiency of excavation. If the slump value is less than 100 mm, honeycomb-voids and entrapment of previous materials may result, and this can cause breaches in the cut-off walls.

2.3.2 Compressibility

A decrease in the volume of soil in response to static load is termed "soil compression", and the amount of volume decrease per unit load increment is an index of soil compressibility, known as the "coefficient of compressibility". Generally, compressibility is measured in terms of a compression ratio defined as:

$$\frac{C_c}{1+e_o} \qquad [2.1]$$

where C_c = compression index; and

e_o = initial void ratio.

Compressibility is generally not an important criterion in the design of SB cut-offs. However, when structures such as dams are to be built over a cut-off, compressibility criteria are considered in the design to avoid differential settlement of the cut-off with respect to the adjacent ground. To fulfill these requirements, the backfill material should have strength and compressibility properties compatible with the surrounding ground in addition to low hydraulic conductivity criteria (Pandian et al. 1995).

Although low compressibility and low hydraulic conductivity are contradictory requirements, overconsolidated clays do possess these traits (D'Appolonia 1980, Pandian et al. 1995). Bentonite soil mix, if properly proportioned, satisfies this requirement. Compressibility of the mix can be reduced by reducing its liquid limit and plasticity index (Skempton, 1944). Figure 2.2 is a plot of the compression ratio versus fines content for different SB mixtures for stresses ranging from 50 to 200 kPa (D'Appolonia, 1980). It shows that compressibility increases with an increase in fines content. A summary of the results obtained by Khoury et al. (1992) from a SB cut-off wall constructed in an earth dam is presented in Table 2.1. Several different SB mixtures were tested with various grain size distributions to represent the range of onsite backfill materials. Similar results have been reported by Yeo et al. (2005), who tested different soil-bentonite mixtures by varying their fines content.

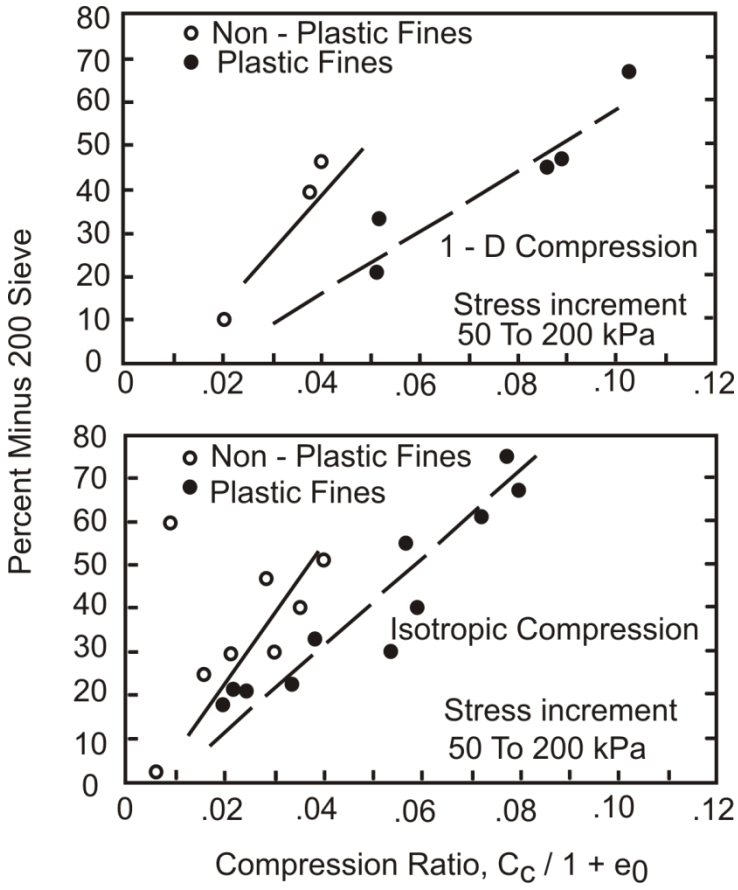

Figure 2.2 Compression ratios versus fines content for SB backfill (redrawn; after D'Appolonia 1980).

Table 2.1 Laboratory test data on various SB mixtures (Khoury et al. 1992).

Soil-Bentonite Mix Characteristics	Mix 1	Mix 2	Mix 3	Mix 4	Mix 5
Slump (cm)	12.7	13.3	12.1	12.7	12.7
% of bentonite by dry weight	1.08	0.87	1.05	1.18	1.65
% passing No. 200 sieve	8.7	23.4	30.5	37.6	72.5
Water content (%)	23.8	32.5	31.0	39.0	62.1
Compression ratio, $C_C/1+e_0$	-	-	0.077	0.091	0.137

2.3.3 Consolidation behaviour of backfill material

The concept of consolidation first entered the field of engineering practice when Terzaghi (1943) published his one dimensional consolidation equation. In the same year, he also designed the “oedometer”, the apparatus used for measuring the consolidation behaviour of soils (Leonards and Ramiah 1959). Terzaghi (1943) stated that “a decrease of water content of a saturated soil without replacement of water by air is the process of consolidation”. Consolidation can be defined as a phenomenon wherein gradual reduction in volume of a completely saturated soil takes place under sustained loading, principally due to expulsion of water from the voids and accompanied by transfer of stress from the water to solid soil grains as an increase in effective stress (Das, 2008).

2.3.3.1 Compression index

Compression index (C_C) is an important consolidation parameter that can be used to assess the response of the soil to the applied load. C_C is defined as

$$C_C = \frac{\Delta e}{\log\left(\frac{\sigma_f}{\sigma_o}\right)} \qquad [2.2]$$

where Δe = change in void ratio;

σ_o = initial stress on the soil (kPa); and

σ_f = final stress on the soil (kPa).

These parameters generally depend on the applied load and also on the amount of fines added to the soil. Yeo et al. (2005) and Evans and Ryan (2005) show that the value of C_C increases with increasing amount of fines in the soil. Similar results have been reported by Khoury et al. (1992). Results from Yeo et al. (2005) are summarized in Table 2.2 below.

Table 2.2 Compression index values (after Yeo et al. 2005).

Backfill composition

Constituent soil	Fines content (%)	Compression index C_C (10^{-1})
Clay and Sand	20	0.58
	40	1.4
	60	1.9
	75	2.4
	89	2.7
Bentonite and Sand	2	0.53
	3	0.77
	4	1.9
	5	2.1

2.3.3.2 Coefficient of consolidation

The coefficient of consolidation (C_V) is a factor that governs the rate at which compression can occur in a particular soil. C_V can be obtained from an e-log p curve using various well known graphical and analytical methods. The rate and amount of compression in soils varies with the rate at which pore water is lost and, therefore, depends on the hydraulic conductivity of the soil (Ranjan and Rao, 2002). C_V (m^2/s) is defined as

$$C_v = \frac{k}{m_v * \gamma_W} \qquad [2.3]$$

where k = hydraulic conductivity of the soil (m/s);

m_v = coefficient of volume compressibility; and

γ_w = unit weight of water (kN/m^3).

The coefficient of consolidation decreases with increasing in fines content due to the decrease in the coefficient of permeability (k) (equation 2.3). For a given fines content, C_V increases with an increase in effective stress (σ') (Ryan, 1987; Duncan, 1993; Yeo et al., 2005). This is because C_V is inversely proportional to the coefficient of volume compressibility $m_{v,}$ which also decreases with increasing σ'. Thus, if the decrease in m_v that occurs upon an increase in σ' is greater relative to k, then an overall increase in C_V with σ' is expected.

2.3.4 Strength parameter

Published information regarding the strength of SB cut-off walls is limited, as their strength is not the primary concern when designing containment cut-offs. The angle of internal friction for a SB cut-off is reported to be between 30 and 35 degrees (D'Appolonia, 1980; Filz et al., 1997).

Evans and Ryan (2005) published data from field vane shear measurements. Vane shear measures total stress in the soil. According to their study, there is no significant variation in undrained shear strength with depth. The shear strength measured 6 and 12 months after backfill placement is almost identical. This result is consistent with long-term data reported by Evans et al. (1995), where backfill was still soft after 10 years and the undrained strength almost the same. Strength gain depends upon the consolidation, creep, and thixotropic behaviour of the backfill material.

2.3.5 Hydraulic conductivity (k)

Hydraulic conductivity (k) plays an important role in the performance of SB cut-offs, which act as low k barriers against groundwater flow and subsurface contaminant migration (D'Appolonia, 1980). Hydraulic conductivity of SB cut-offs generally ranges between 10^{-7} and 10^{-11} m/s depending upon the quality of the backfill (Xanthakos, 1979; Yeo et al. 2005). It is a function of both the backfill inside the trench and the filter cake

formed at the wall of the trench. Thickness and hydraulic conductivity of individual components determines their relative contribution.

The contribution of filter cake and the backfill to the overall k of the SB wall is shown in Figure 2.3. The cut-off k of the wall is controlled by the backfill when the backfill k is low and by the filter cake when the backfill k is high. The hydraulic conductivity of the remolded material used for the backfill is directly related to fines content, particle fabric, and void ratio of the soil matrix (Tang, 1987; Evans et al., 1995).

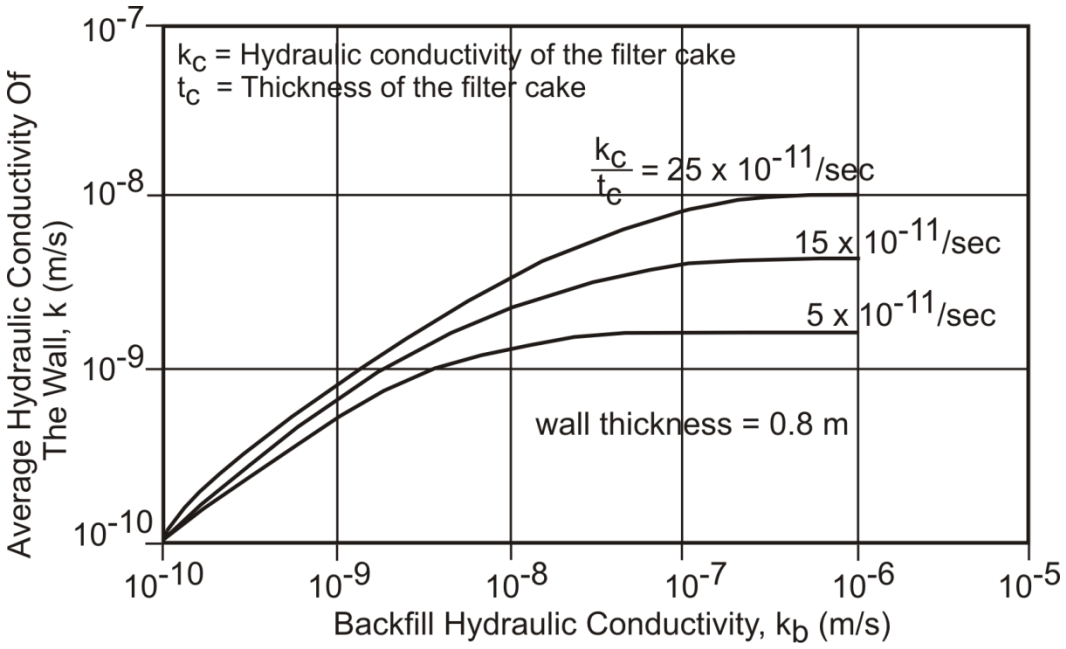

Figure 2.3 Theoretical relationships between wall, filter cake, and backfill hydraulic conductivity (redrawn; after D'Appolonia, 1980).

2.3.5.1 Fines content and gradation

Well graded soil consisting of a blend of gravel, sand, silt, and clays results in a backfill of low hydraulic conductivity (Evans, 1994). The hydraulic conductivity of the backfill decreases with increasing fines content. To minimize hydraulic conductivity and compressibility, the backfill should be granular material with 20-40% fines; moreover,

much lower hydraulic conductivity is achieved by addition of plastic fines to the blend (D'Appolonia, 1980).

The main function of the fines is to block the voids of the aggregate fraction and prevent segregation or displacement of soil particles (Xanthakos, 1979). By filling the pores between larger particles and by contributing to swelling, viscosity, gelation, and cation exchange capacity of the backfill, fine particles, particularly clays, contribute to low hydraulic conductivity (D'Appolonia, 1980). The increase in the bentonite content in the backfill helps to decrease the hydraulic conductivity of the mixture; however, the decreasing trend tapers off at bentonite contents beyond 2% (Tang, 1987; Figure 2.4). Similar results were found by D'Appolonia (1980) for clayey silted sand and poorly graded silted sand with 30 to 50% fines. Yeo et al. (2005) have also reported the effect of fines in controlling the hydraulic performance of backfills (see Figure 2.5).

A relationship between k and backfill fines content (%) for different applied vertical stresses is shown in Figure 2.5. Falling head k tests were run at the end of each loading increment. The hydraulic conductivity of the backfill decreased significantly up to 40% fines content and was constant thereafter. This is true for all applied vertical stress.

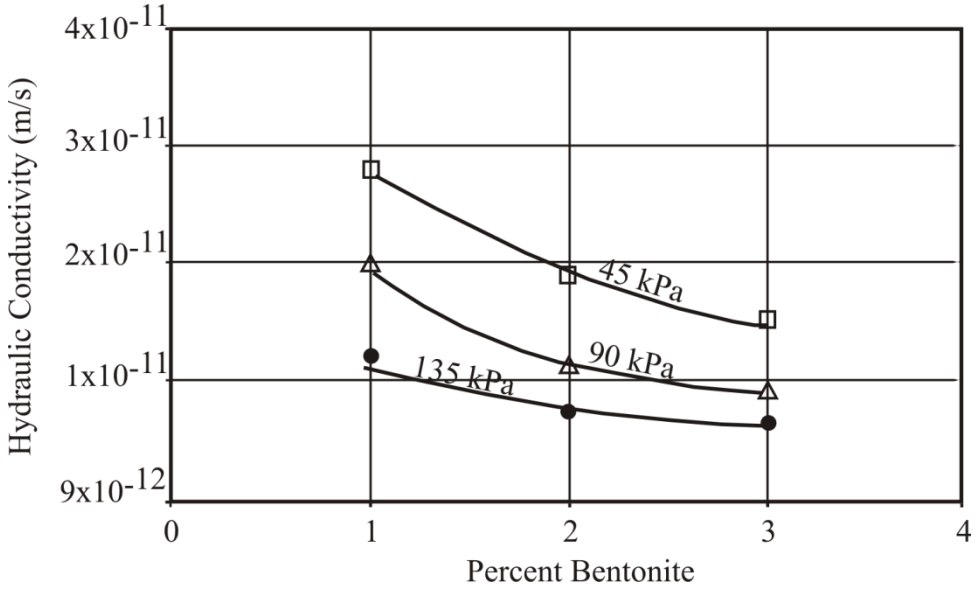

Figure 2.4 Variation of hydraulic conductivity with bentonite content (%) in backfill mix for different average vertical stresses (redrawn; after Tang, 1987).

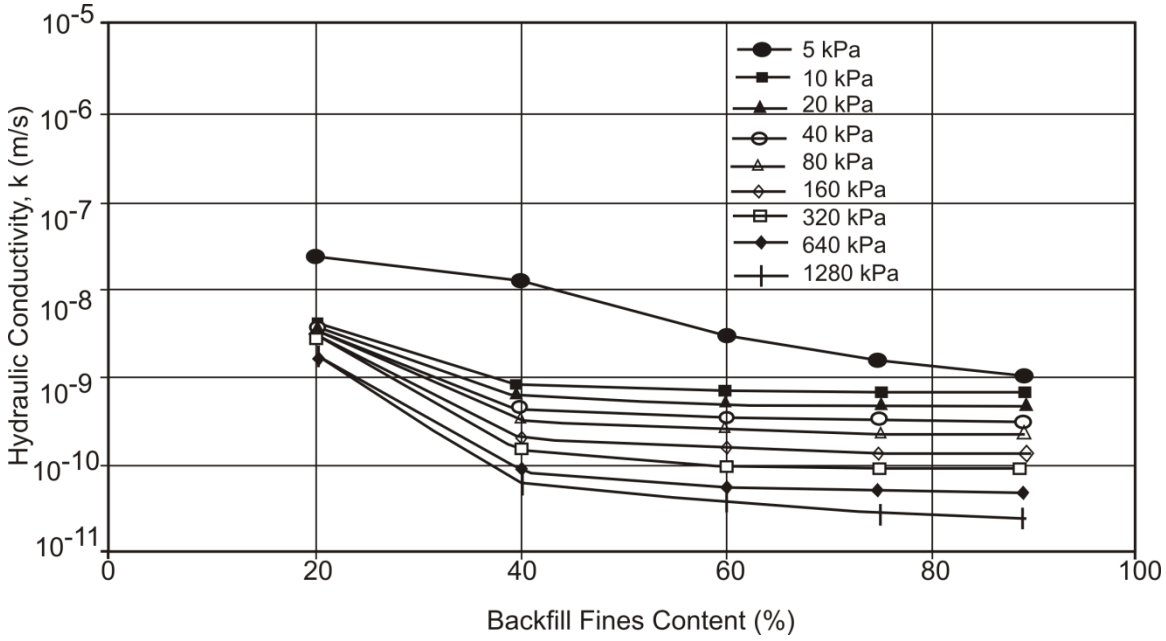

Figure 2.5 Measured hydraulic conductivity as a function of backfill fines (redrawn; after Yeo et al., 2005).

2.3.5.2 Effect of void ratio

The method of compaction and the remolding water content affects the structure of the compacted soil. Soils compacted when wetter than optimum possess dispersed structure and hence have lower hydraulic conductivity. A flocculated structure is generally observed in the case of soils compacted when dryer than optimum, and hence these soils possess higher hydraulic conductivity. Soils remolded from slurries are always saturated. Saturated hydraulic conductivity of the material depends on the void ratio which, in turn, depends on the remolding or consolidating pressure (Tang, 1987; Yeo et al., 2005).

According to Mesri and Olson (1971), application of pressure, under fully drained conditions and without lateral strains, results in the orientation of platy particles normal to the direction of maximum principal stress. This leads to an increasingly tortuous flow path in the direction of the applied pressure. Particle orientation, or tortuosity effect, is larger for particles with larger diameter to thickness ratios. Moreover, particle orientation

increases with increasing consolidation pressure. Hence, the hydraulic conductivity of the backfill decreases with the increasing consolidating pressure, which, in turn, decreases the void ratio (Figure 2.6). Figure 2.6 shows that an increase in effective confining stress of 100 kPa can decrease the measured hydraulic conductivity by an order of magnitude.

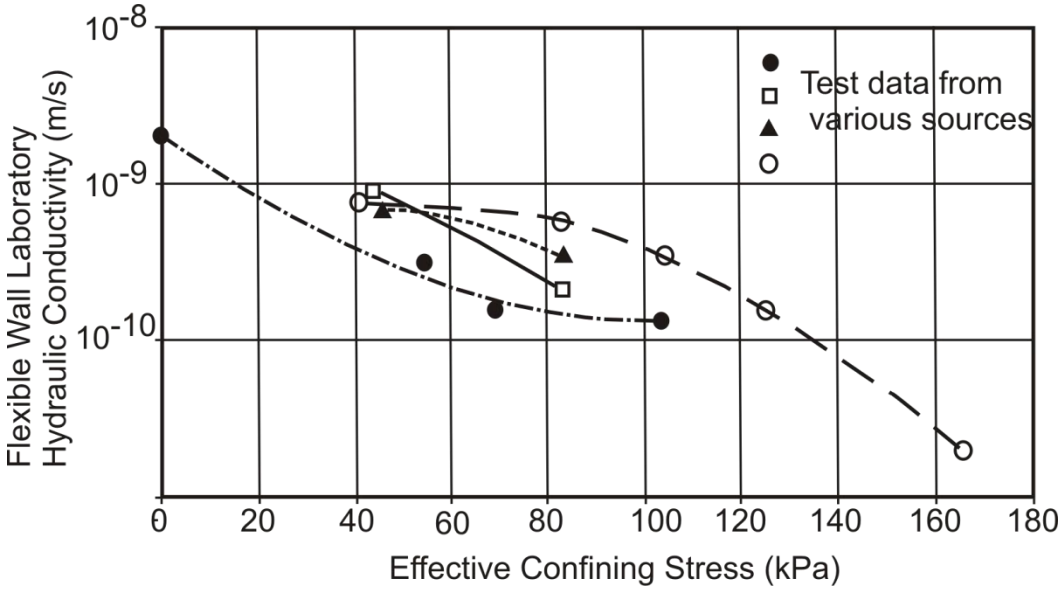

Figure 2.6 Effect of confining stress to hydraulic conductivity of the wall (redrawn; after McCandless and Bodocsi 1988, as taken from Baxter, 2001).

The selection and use of an appropriate confining stress for hydraulic conductivity tests on SB mix is an unresolved issue. This is because there are no guidelines for estimating the stresses in SB walls. Most researchers and engineers recommend the use of a confining stress that corresponds to the middle of the wall and assumes geostatic conditions. The stress distribution in the SB wall with depth is less than the geostatic condition (Evans, 2005); hence, it is important to understand the stress distribution pattern in SB walls.

2.3.6 Coefficient of lateral earth pressure at rest (K_o)

The coefficient of lateral earth pressure at rest (K_o) is considered to be a fundamental parameter in soil mechanics. Solving geotechnical problems often requires that the initial stress state in the soil be known. The coefficient of earth pressure at rest is frequently used to determine the stress state if geologic information is available about both the load history and the soil type. The concept of “the stationary pressure of unlimited ground” was first defined by Donath in 1891. The co-efficient of lateral earth pressure at rest, K_o is the ratio of horizontal effective stress (σ'_h) to vertical effective stress (σ'_v) in a soil that currently exists under the condition of zero horizontal deformation, with principal planes that are horizontal and vertical:

$$K_o = \frac{\sigma'_h}{\sigma'_v} \qquad [2.4]$$

The fraction of the force of gravity that is transmitted to the vertical planes is a function of the angle of internal friction that is mobilized under the laterally constrained deformation condition decreases with an increase in the mobilized angle of internal friction.

The next significant work on K_o was conducted by Terzaghi in 1920 at Robert College. Using a friction tape method, he reported values of K_o for a coarse sand to be 0.42. Later in 1923 Terzaghi presented a relation between coefficient of lateral earth pressure at rest and mobilized angle of internal friction (ϕ'_{mob}), which then has been discussed by Rowe (1954).

$$K_o = \frac{1-\sin\phi'_{mob}}{1+\sin\phi'_{mob}} = \tan^2(45^\circ - \frac{\phi'_{mob}}{2}) \qquad [2.5]$$

Although the mobilized friction angle ϕ'_{mob} cannot be directly measured, it can be correlated with the ultimate effective stress fiction angle ϕ' of soils. Several correlations for estimating ϕ'_{mob} using many experimental data have been reported in the literature.

$\phi'_{mob} = \frac{3}{4}\phi_e$ (Rowe1958) where ϕ_e is equal to the Hvorslev angle of true friction [2.6]

$\phi'_{mob} = \phi_e = 1.15(\phi' - 9^\circ)$ (Abdelhamid and Krizek, 1976) [2.7]

$\phi'_{mob} = \phi' - 11.5^\circ$ for ϕ' varying in the range 30º to 45º (Bolton, 1991) [2.8]

$\phi'_{mob} = 0.69\phi'$ for ϕ' varying in the range 20º to 35º (Simpson, 1992) [2.9]

Jaky in 1944 arrived at a relationship between K_o and maximum available angle of internal friction (ϕ') by analyzing a talus of granular soil freestanding at the angle of repose. He assumed that the angle of repose is equal to the angle of internal friction ϕ'. He proposed the following equation

$$K_o = \frac{(1-\sin\phi')}{(1+\sin\phi')}(1+\frac{2}{3}\sin\phi') \quad [2.10]$$

However Jaky in 1948 without any further explanation, adopted the following equation

$$K_o = 1-\sin\phi' \quad [2.11]$$

Recently, in the year 2008 Federico et al presented a new empirical expression for the mobilized angle of internal friction. This equation was determined from statistical analysis of experimental data found in the literature.

$$K_o = \tan^2(45^\circ - \frac{\phi'}{3}) \quad [2.12]$$

The corresponding equation of K_o has been obtained and its predictive capability has been tested by the authors. For a full range of ϕ' the values of Ko predicted by this new equation, although rather close to the ones determined by Jaky's equation have a better agreement with the experimental data.

2.4 Stress distribution in soil bentonite cut-off walls

Many authors have agreed upon the need to understand the final state of stress in SB walls (Khoury et al., 1992; Filz, 1996; Tien, 1996). Knowing the “final” state of stress helps to design the walls as it governs the “final” hydraulic conductivity.

When SB mix is placed in the trench, the water content of the mix is high and it almost flows as a liquid. It takes time for the mix to consolidate under its own weight before the effective stress due to the material above it and the adjacent ground acts upon it. The final stress in the wall influences the ultimate deformation in the wall and the adjacent ground. Engineers and researchers believe that the final stress in SB walls is less than the geostatic stress (Evans et al 1995; Filz 1996 and Baxter 2001), but by how much is not known. At present, two primary theories describe the state of stress in soil bentonite walls.

2.4.1 Arching theory

Terzaghi (1943) described arching as a “transfer of stress from a yielding mass of a soil onto adjoining stationary parts”. The shearing resistance tends to keep the yielding mass in its original position, resulting in a change in pressure on both the yielding parts and the adjoining soil. If the yielding part moves downward, shearing resistance acts upward to keep the mass in the same position and, hence, reduces the stress at the base of the yielding section and vice versa.

Depending upon the relative stiffness of the adjoining soil, arching can be classified as:

a. Active arching, where the structure in the soil is more compressible than the surrounding soil (Figure 2.7); or
b. Passive arching, where the surrounding soil is more compressible than the structure (Figure 2.8).

Figure 2.7 and Figure 2.8 shows the stress distribution in the soil for active and passive arching.

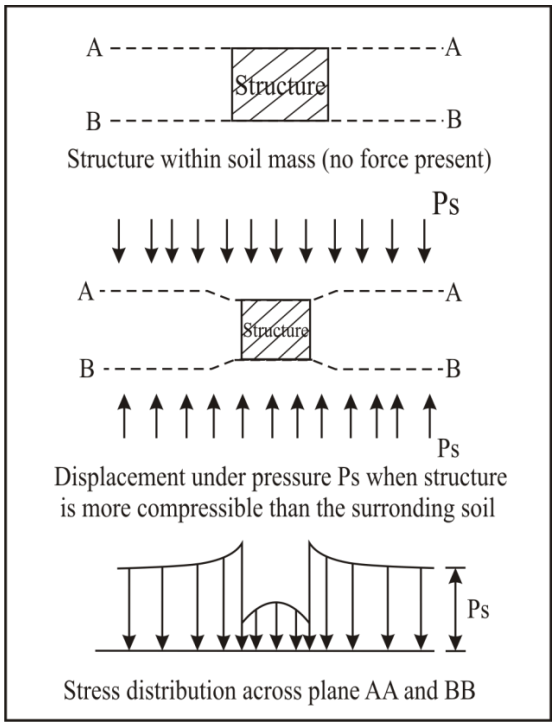

Figure 2.7 Active arching (after Evans.1984).

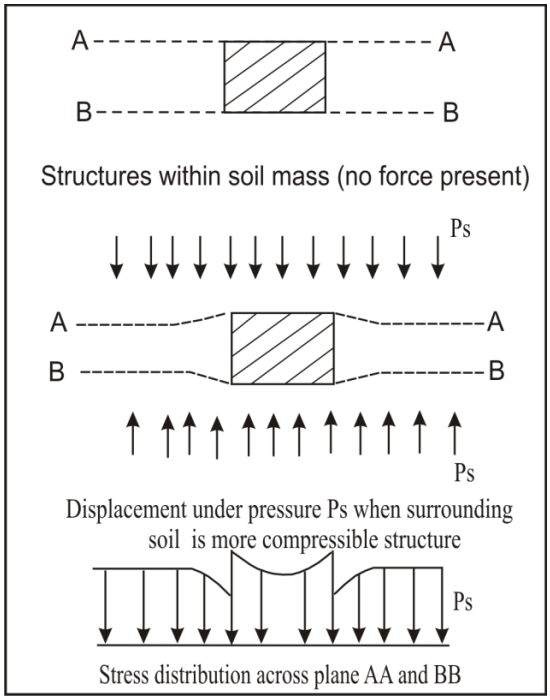

Figure 2.8 Passive arching (after Evans.1984).

An extensive experimental and theoretical investigation of arching has been conducted by Terzaghi (1943). In addition, an analysis of loads on buried conduits (Marston and Anderson, 1913; Spangler and Handy, 1973) based on the silo theory (Jacobson, 1958) has also been carried out to understand the concept of arching.

2.4.1.1 Design of buried conduits (Marston and Anderson 1913)

This theory was first described by Marston and Anderson in 1913 to show the state of stress on pipes in ditches, which was further described by Terzaghi in 1943. The assumptions of the Marston theory are:

a. Loads on the conduit are equal to the overburden, if no relative motion occurs within the soil or between the soil and the conduit;
b. Sufficient movement occurs to mobilize shearing resistance on a sliding plane; and
c. Cohesion between the backfill material and sides of the ditch is negligible. This assumption yields the maximum probable load on the conduit and offers a safe estimate for design purposes.

Figure 2.9 shows the force mobilization due to arching around a small element of thickness “dh” in a trench of width B. According to the Marston theory, the trench walls are considered rigid and the backfill material is considered compressible. Consolidation and settlement of backfill with time cause shear stresses to be mobilized along the trench walls (Figure 2.10), which act as a partial support for the backfill and hence reduce the effective vertical stress in the trench below the overburden pressure. If considering the vertical force equilibrium ($\sum F_{Y=}0$) of the horizontal slice in Figure 2.10, then according to statics

$$d\sigma_v + 2K_a \frac{\sigma_v}{B} dh = Bdh \qquad [2.13]$$

where μ’ = tan δ = sliding friction coefficient between the fill and the sidewalls (δ is the wall friction angle, generally assumed to be between ϕ/3 and 2ϕ/3);

ϕ = fill internal friction angle (degrees); and

$K_a = \tan^2 (45^\circ - \phi/2)$ or the co-efficient of lateral earth pressure (ratio of horizontal stress to vertical stress).

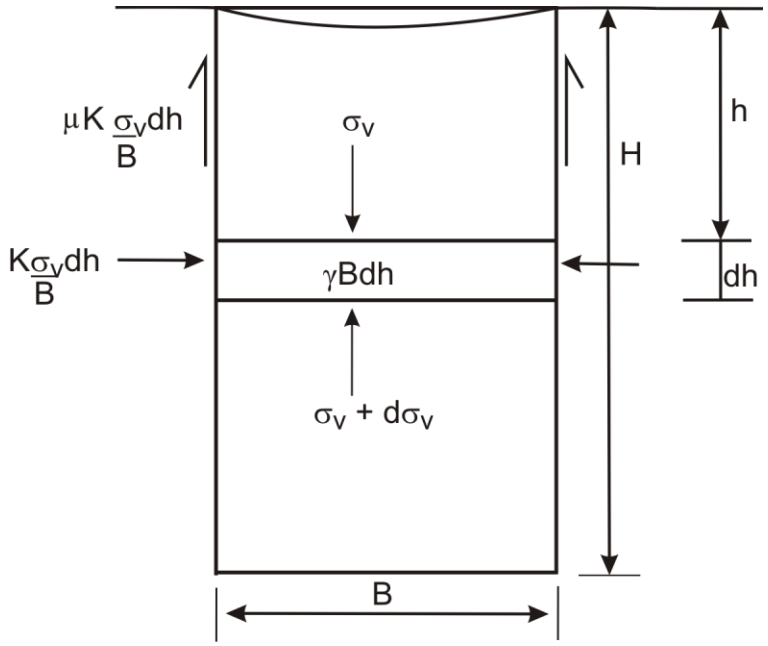

Figure 2.9 Arching mechanisms

(redrawn; after Marston and Anderson, 1913).

Solving the linear differential equation in (2.13), we get

$$.\boldsymbol{\sigma_v} = \frac{\gamma \mathbf{B}^2}{\mathbf{2K_a\,\mu}} \left(\mathbf{1} - \mathbf{e}^{\frac{-\mathbf{2K_a\,h}}{\mathbf{B}}}\right) \qquad [2.14]$$

2.4.1.2 Trap door experiment (Terzaghi, 1945)

In 1936, Terzaghi for the first time conducted a “trap door” experiment to study the arching phenomenon in sands. He concluded that arching does not require the crushing of soil particles to support the arch formation, but it is a temporary circumstance dependent on the shear stress in the soil. He included cohesion of the material in his work. Figure 2.10 shows a schematic diagram of sand in a trap door experiment.

Assumptions for Terzaghi’s trap door experiment were as follows:

a. Normal stress is uniform across horizontal sections;

b. Coefficient of lateral stress (k) is a constant;
c. Cohesion is assumed to exist along the sliding surface;
d. The trap door or the yielding surface is assumed rigid; and
e. The assumed sliding surfaces are not true (assumed straight, but in the real world are curved).

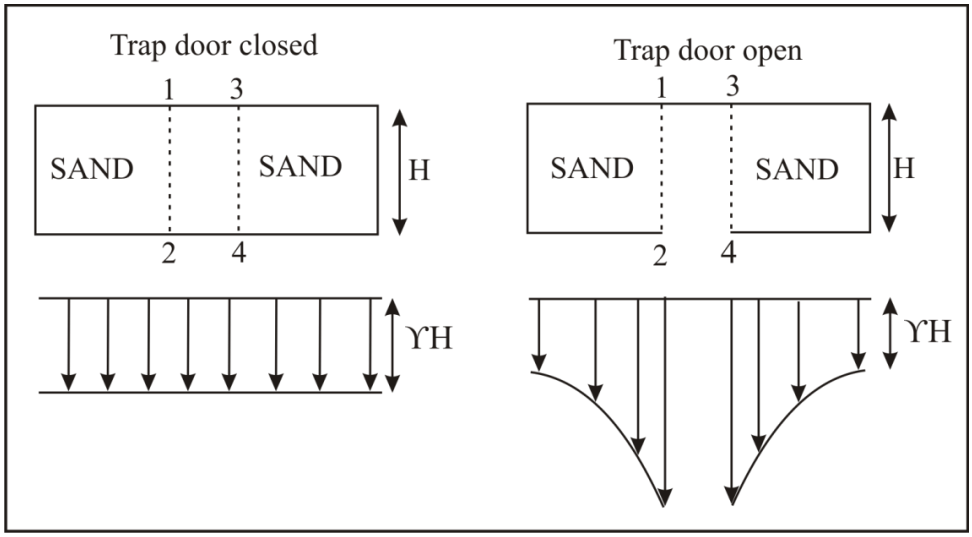

Figure 2.10 Schematic diagram of sand in a trap door experiment (redrawn; after Terzaghi, 1943).

According to his formulation, vertical stress σ_{av} (in the soil sample due to arching) is given by

$$\sigma_{av} = \frac{(B\gamma - 2c)}{2K\tan\phi}(1 - e^{-2\frac{K\tan\phi h}{B)}}) \quad [2.15]$$

,

where c = cohesion between the soil and sliding surface;

tan ϕ = fill internal friction coefficient;

γ = unit weight of soil (kN/m^2);

$K = \frac{1+\sin^2\phi}{\cos^2\phi + 4\tan^2\phi}$ or the coefficient of lateral earth pressure; and

for cohesionless soil, c = 0.

2.4.1.3 Modified Marston's cohesionless model (Aubertin et al., 2003)

Aubertin et al. (2003) proposed a modified version of Martson's two dimensional arch solution, originally defined using only the active earth pressure coefficient and the sliding friction between the wall and the fill. The modified version predicts effective vertical pressure using an earth pressure coefficient corresponding to three different states: ka (active), k_p (passive), and k_o (at rest). The vertical effective stress at a depth H is given by

$$\sigma'_v = \frac{\gamma B}{2\tan\phi'}(1-e^{-2\frac{KH\tan\phi'}{B}}), \qquad [2.16]$$

where ϕ' = fill effective internal friction angle (degrees);

K = at rest = K_o = 1- sinϕ'; and

K = active earth pressure = $K_a = \tan^2(45^\circ - \phi'/2)$.

2.4.2 Lateral squeezing theory

An alternative method for predicting stresses in SB walls was proposed by Filz in 1996. It is assumed that trench walls can deform and that the amount and direction of movement influences the stresses in the SB wall. The theory predicts stresses lower than the geostatic condition but higher than arching theory for most depths. According to lateral squeezing theory, the larger of the consolidation stresses predicted should be considered for SB wall design.

Figure 2.11 shows the ground movement adjacent to the SB wall. As illustrated in the figure, the trench wall moves inward during excavation under the bentonite-water slurry. This may cause settlement in the adjacent ground, which in turn may cause settlement in the adjacent buildings. When the trench is backfilled, the bentonite slurry is replaced by SB backfill, which has a higher unit weight. This could cause the trench wall to move

outwards. During the consolidation of the SB backfill, the trench wall may again move inward, which may cause further settlement of the adjacent ground.

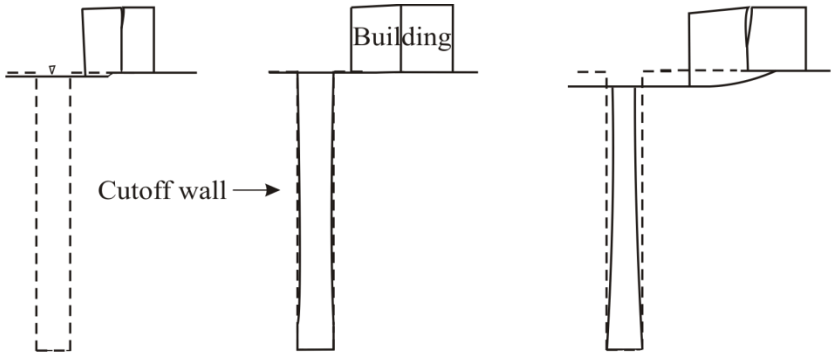

Figure 2.11 Ground movements adjacent to a soil-bentonite cut-off wall (redrawn; after Filz 1996).

Assumptions of this theory are as follows:

a. The trench walls can deform and the amount and direction of movement govern the stress state in the SB walls;
b. Long and narrow trench walls are assumed to move inward due to consolidation of the backfill;
c. The column is treated as a 1-D consolidation cell turned at 90°. The horizontal stress (σ'_h) is the major principal stress and the vertical stress (σ'_v) is the minor principal stress; and
d. The shear stress developed along the wall is sufficient to support the weight of the overlying soil-bentonite.

The constraint modulus (M), which is inversely proportional to the coefficient of volume compressibility m_v, is used to relate horizontal stress (σ'_h) to horizontal strain. Horizontal stress (σ'_h) in the adjacent ground is determined between the lateral movement (Δ) and coefficient of lateral earth pressure (k_h) using the Clough and Duncan (1991) relationship. The horizontal stresses in the adjacent wall and in the SB wall are equated

to solve for the horizontal stresses. The vertical stress in the soil-bentonite can be calculated using K_o conditions.

2.5 Deformation in SB walls – Case studies

Several field-measured data have been reported for SB wall performance over time. It can be concluded from the results that the stress in the SB wall is always less than geostatic stress.

Engemoen and Hensley (1986) present data from electronic cone penetration testing (ECPT) done on recently constructed SB walls at Calamus Dam, Nebraska. On the right abutment of the dam, the wall is 1.5 m wide and 34 m deep. Continuing onto the left abutment, the wall is 0.9 m wide and 14 m deep. The SB wall underwent 0.1% vertical strain, which occurred in one month. The tip resistance measured was generally less than 1000 kN/m^2. In several tests, large horizontal deviations of the tip of the cone resulted in higher tip resistances, which are attributed to the high probability of the tip hitting the side of the trench. There was no significant increase in the value of tip resistance with depth. This is an indication of low confining pressures maintained in the trench.

Khoury et al. (1992) report in situ data from an SB wall installed within Manasquan Dam, New Jersey. The wall was constructed in two phases. The lower stage was built when the dam reached a maximum height of 14 m; the upper stage was implemented when the dam was 17 m high. To accommodate the excess hydraulic head in the dam, the upper stage SB wall has a width of 1.5 m as compared to 0.9 m for the lower stage wall. The upper portion of the SB wall was keyed a minimum of 0.9 m into the lower portion of the wall. Total stress cells and piezometers were installed in the wall to monitor its performance after construction. The total stress cells were installed in two directions, i.e., parallel to and perpendicular to the dam axis. Settlement plates were also installed in both walls. The lower portion of the wall underwent total settlement in 1-2 months, whereas the upper potion underwent most of its settlement in about 2 weeks.

The 0.9 m width wall experienced a total strain of 3-4%, compared to the 1.5 m width wall that experienced a total strain of 7-9%.

Using the measured pore pressure and total horizontal stress, the total vertical stress at three different depths was calculated using

$$\sigma_h = K (\sigma_v - u) + u \qquad [2.17]$$

where σ_h = total horizontal stress from stress cells in the SB wall parallel to the dam axis (kPa);

σ_v = estimated total vertical stress (kPa);

u = pore pressure from piezometers in the SB wall; and

K = co-efficient of lateral earth pressure.

The authors assumed K_o was 0.5. From the field measurements, the authors concluded that the estimated total vertical stress values were lower than the overburden pressures, based on geostatic conditions at the corresponding depths (Figure 2.12).

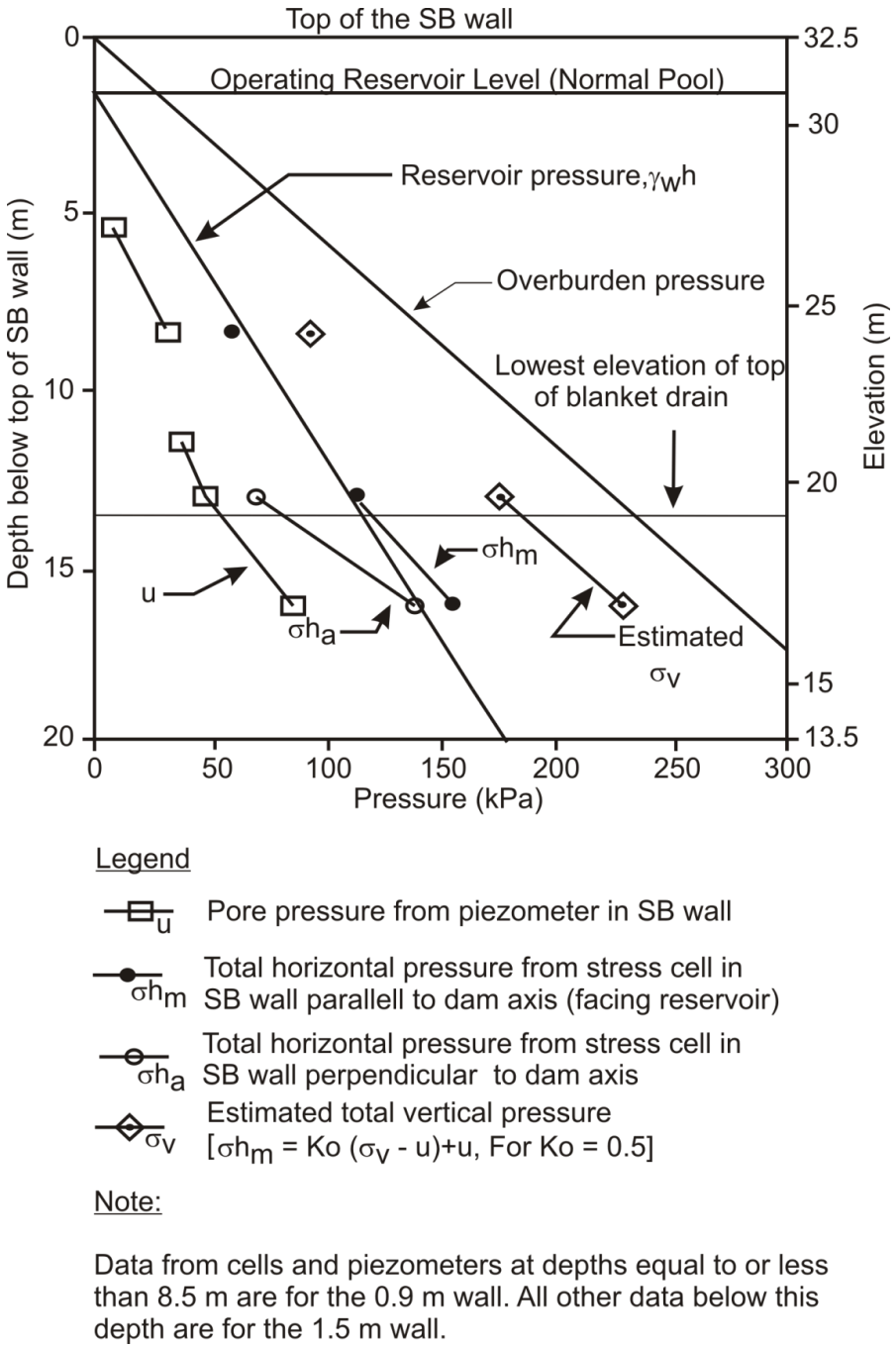

Figure 2.12 Total pressures in the SB wall

(redrawn; after Khoury et al. 1992).

Figure 2.12 presents a summary plot of the variation with depth of the total piezometric heads and total horizontal stresses in the SB wall. The data in the figure suggest that

the measured horizontal stresses from cells facing the reservoir are approximately equal to or slightly greater than the normal pool reservoir pressure.

Due to the elevations of the cells, direct comparison of horizontal stresses at similar depths could not be made between the 1.5 and 0.9 m wide walls. However, the smaller magnitude of the total settlements observed in the 0.9 m wall suggest that the transfer of total vertical stress with depth could be less than observed in the wider wall. This is consistent with analyses conducted using arching theory.

The total vertical stresses in the wall were estimated from the measured piezometric heads and horizontal stresses assuming the coefficient of lateral earth pressure K is equal to 0.5. These estimated vertical stresses are shown in Figure 2.12, and indicate values greater than the reservoir pressure and less than the total overburden pressure. However, the value of 0.5 for K is assumed; the actual value may be lower, which can lead to lower vertical stress values than shown in Figure 2.12.

Evans et al. (1995) presents data from laboratory and field tests conducted on a 10 year old wall, a 4 year old wall, and a wall constructed immediately prior to testing. Field testing included the standard penetration test (SPT) to provide information on the geotechnical engineering properties of soil, Marchetti flat plate dilatometer to estimate the in-situ lateral stress and lateral soil stiffness, vane shear to provide an indication of in-situ undrained shear strength and in situ hydraulic fracture testing. The following conclusions were drawn from the testing:

a. SPT tests indicated that the sampler was advanced by the “weight of the hammer” throughout the entire depth of the wall; hence, no conclusion were drawn from the data;
b. Dilatometer tests showed an increase in the vertical effective stress (σ'_v) with depth, which was less than geostatic stress;
c. Vane shear test results indicated that the shear strength of the backfill material is constant with depth;

d. Constant water content was observed at all depths below the water table. For a geostatic increase in stress, water content should have decreased with depth in response of increasing effective stress and decreasing void ratio; and
e. Preconsolidation pressures, calculated from consolidation test results of 26 field samples procured from different depths, showed that the stress in the SB wall is always less than the calculated geostatic stress.

Evans and Ryan (2005) present test results from an SB wall located in Delaware City, Delaware. They conducted field vane shear testing on freshly placed backfill and on both one month old and six month old SB walls. It was impossible to measure the strength of the freshly prepared wall as it was highly viscous at the time. There was no significant shear strength gain of the backfill aged one month vs. six months. Shear strength of the wall was constant with depth. This finding is consistent with the results reported by Evans et al. (1995).

2.6 Finite element modelling of slurry walls

It is a quite difficult to estimate the exact stress distribution with time and depth in soil-bentonite walls using the available analytical equations. Moreover, the analytical equations do not predict the pore pressure distribution in the walls. Hence, coupled finite element modelling of soil-bentonite walls plays an important role in accurately predicting their long-term behaviour.

Clark (1994) presents a finite element model study of a soil-bentonite cut-off wall. The objective of the study was to understand the stress transfer during soil-bentonite consolidation and the potential for hydraulic fracturing, due to construction of a levee on the top of the cut-off wall. All materials were modelled using the elastic-plastic Mohr-Coulomb model. Steps involved in the finite element analysis were as follows:

a. Initial stresses of the existing soil were established using gravity forces and K_0 = 0.5;

b. Trench excavation was modelled by changing the properties of the native soil to those of the bentonite-water slurry;
c. Filter cake at the trench wall was modelled by changing the properties of the frictional interface; and
d. Backfilling with soil-bentonite was modelled by incrementally changing the properties of the slurry to properties of the soil-bentonite mixture.

The analysis indicates that the construction of the trench should result in negligible settlement or lateral deformation of the adjacent soil. “Weak arches” develop in the first 5 m of the trench, which will break down with time upon consolidation of soil-bentonite wall. The author concludes that there is no significant stress reduction in the wall due to arching.

Baxter (2001) presents a sequential modelling of soil-bentonite walls using a finite element package “Sage”, which was developed at Virginia Tech University. Sage has a fully coupled formulation for fluid flow and deformation, and is capable of modelling consolidation of the soil-bentonite as well as the other phases of construction. The RS model developed by Kutter and Sathialingam (1992) is used to represent soil-bentonite. Steps involved in analysis were:

a. Establishment of initial site conditions, using the unit weights of the material and assuming geostatic conditions;
b. Excavation of a trench under the bentonite-water slurry. Application of stress distributions along the sides and bottom of the trench are used to represent the fluid pressure;
c. Backfilling of the trench with soil-bentonite, followed by row by row placing of soil-bentonite elements starting from the bottom of the trench. Stress-distribution representing the bentonite-water slurry was also adjusted to reflect the replacement of the bentonite-water slurry with soil-bentonite backfill; and
d. Consolidation of the soil-bentonite, specifically
    i. Deformation / settlement of the ground; and
    ii. Pore pressure variation.

The broad conclusions of the analysis were as follows:

a. To predict the stress distribution in SB walls accurately and confidently, it is necessary to sequentially simulate the construction process;
b. The hydraulic conductivity of the adjacent elements should be reduced to reflect the lower conductivity of the filter cake;
c. Proper selection of properties of the interface element at the trench wall would produce more accurate results; and
d. SB cut-off walls in the field should be well instrumented to calibrate the model accurately and to predict the results more confidentially.

Fahey et al. (2009) presents a numerical model study of aspects of the arching phenomenon using Plaxis-2D finite element software. The salient features of this study are as follows:

a. 50 m deep and 20 m wide backfilled stopes were modelled;
b. The backfilled material was modelled using the elastic-perfectly plastic Mohr Coulomb model;
c. A large spectrum of parameters was studied by modelling dry cohesionless as well as completely saturated backfill materials; and
d. A parametric study was carried out to understand the importance of material parameters, such as Young's modulus E, Poisson's ratio, and the angle of dilation.

The authors conclude the work by stating that:

a. The degree of arching depends heavily on the angle of internal friction ϕ of the backfill material and, hence, this should be carefully chosen;
b. Fully coupled finite element analysis is required to accurately and confidently predict the stress distribution in a partially or fully saturated backfill; and
c. Knowledge of the stress state with the backfill stope is crucial for safe design of dew point barricades and for other operational purposes.

CHAPTER 3 - EXPERIMENTAL INVESTIGATIONS AND TEST RESULTS

3.1 Introduction

A review of the literature indicates very little published information on vertical effective stress distribution and hydraulic conductivity distribution with depth and time in soil-bentonite (SB) trenches. Consequently, a laboratory testing program was conducted with the following objectives: 1) to add to the body of knowledge on properties of soil-bentonite mixtures and 2) to provide information required for predicting vertical effective stress distribution and hydraulic conductivity distribution with respect to wall depth.

This chapter describes the establishment and setup of the laboratory testing program. The detailed procedures explaining the laboratory tests conducted on the backfill mixes are described in the following sections. Four different backfill mixes were tested in the laboratory: three trial mixes (TM1, TM2, and TM3) were prepared in the laboratory and a field backfill (FB) sample was brought from the slurry wall construction site at Rocanville, Saskatchewan.

Tests were conducted to study the effect of the percentage of fine material (particle size < 75 μm) present in the backfill mixes. 1-D consolidation and shear box tests were conducted to characterize the backfill mixes. The experimental setup developed to measure the lateral earth pressure coefficient (K) is also described in the following sections.

This chapter aims to describe the tests conducted and test procedures followed in the present study. All tests were conducted according to ASTM codes.

3.2 Material Properties

3.2.1 Host soil

A glacial till from Rocanville, Saskatchewan, was used as a host soil for preparing the backfill mixes. The index properties of the host soil are shown in Table 3.1. The gravimetric water content of the till was about 6-8%. The soil was light brown in colour and had particle sizes ranging from 425 μm to 75 mm. Based on the liquid limit and

plasticity index, the till can be classified as soil of low plasticity (CL) according to USCS classifications (ASTM D2487). Air-dried and pulverized till passing through a 4.75 mm sieve was used for preparing the trial backfill mixes. The in situ hydraulic conductivity of the till was about 1×10^{-8} m/s. The preconsolidation pressure of the host soil ranged from 1200 to 1500 kPa (M.D. Haug and Associates Ltd. 1998).

Table 3.1 Index properties of the test materials.

Property	Till	FB	TM1	TM2	TM3
Liquid limit (%)	42.5	37.5	38	50	57
Plastic limit (%)	24	20	22.62	23.12	23.48
Plasticity index (%)	18.5	17.5	15.38	26.88	33.52
% Gravel (6.20-4.75 mm)	30	35	N.A	N.A	N.A
% Sand (4.75-0.075 mm)	50	37	87.1	71.1	47.2
% Silt and clay (<0.002 mm)	20	28	12.9	28.9	52.8
USCS classification	CL	CL	CL	CH	CH

3.2.2 Backfill Mixes

A total of four different backfill mixes were examined in the testing program. Three backfill trial mixes (TM1, TM2, and TM3) were prepared in the laboratory by varying the fines content (particle size <75 μm); the fourth mix (FB) was collected in the field from the Potash Corp Rocanville slurry wall construction site. The trial mixes in the laboratory were prepared using dried and pulverised glacial till brought from Rocanville. All particles greater than 4.75 mm were removed from the till prior to preparing the trial mixes. The pulverized soil was turned into a plastic backfill material by mixing with a 5% bentonite (by dry weight) to 95% water slurry. The bentonite content used in the backfills considered in this study is consistent with practice (Section 2.3.1); Ryan (1987) presented data from 30 projects involving SB vertical cut-off walls that indicated the amount of dry bentonite added to SB backfill ranged from 0 to 5%.

The index properties of all four backfill mixes as well as the host soil (glacial till) are shown in Table 3.1. According to USCS classification (ASTM D2487), FB and TM1 are clays of low plasticity (CL), while TM2 and TM3 are clays of high plasticity (CH).

Table 3.2 describes the backfill mixes used in the study. The amount of fines without bentonite for the trial mixes ranged from 10 to 25 to 50% (Section 2.3.1) for TM1, TM2, and TM3, respectively. Hydrometer analysis of the trial mixes were done before and after addition of the bentonite slurry. The amount of bentonite in Table 3.2 was calculated from the fines present in the mix before and after slurry addition. The amount fines present in the field backfill (FB) prior to bentonite slurry addition was not known.

Table 3.2 Description of backfill mixtures.

Mix	Percent of fines without bentonite	Percent of fines with bentonite	Amount of bentonite in the mix
Trial Mix1 (TM1)	10	12.9	2.9
Trial Mix2 (TM2)	25	28.9	3.9
Trial Mix3 (TM3)	50	52.8	2.8
Field Backfill (FB)	N.A	28	N.A

The grain size distribution (ASTM D422) of all test materials used in the study is shown in Figure 3.1. The dashed line represents the grain size distribution of the glacial till and FB as brought from the field (“before”); particles as large as 75 mm were evident, and such sizes are generally used in the field. The solid line represents the grain size distributions of the test mixes (TM1, FB, TM2, and TM3) examined in this study, where FB (“after”) is the grain size distribution of the field backfill after particles bigger than 4.75 mm were removed.

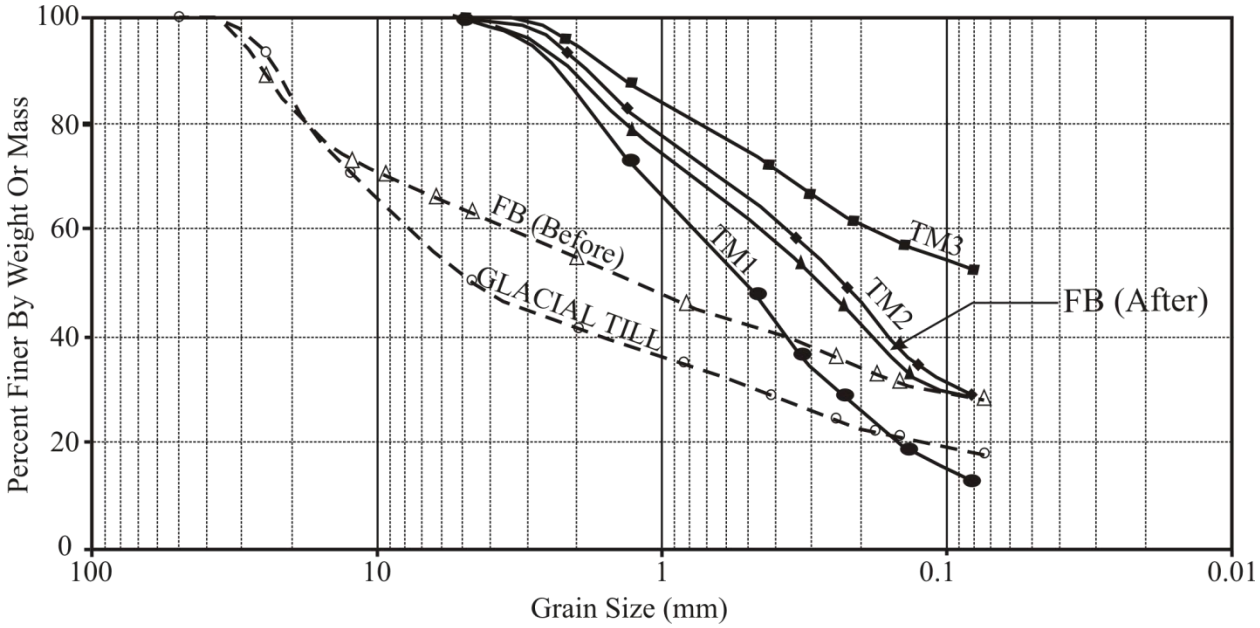

Figure 3.1 Grain size distribution curve.

3.2.3 Slurry

The bentonite slurry was prepared in the laboratory in the same proportions as used in the field. To simulate the properties of SB backfill slurries used in vertical cut-off walls, a 5% bentonite-water slurry, i.e., 5% bentonite (by dry weight) and 95% tap water by weight, was used as the admixture to the various backfills. The electrical conductivity (EC) and pH of the tap water used for the slurry were 400 to 450 micro Siemens per centimetre (mS/cm) and 8-8.3, respectively. Sodium bentonite was used for preparing the slurry. It is a hydrous silicate of alumina primarily consisting of the clay mineral montmorillonite, which swells several times its own volume when wetted. The free swell of the bentonite is 16 mL/2 g (Appendix A).

The bentonite was mixed with tap water using a high-speed colloidal shear mixer. The bentonite-water slurry was then allowed to sit for 48-72 h to properly hydrate the bentonite powder. The density of the slurry was 1860 kg/m^3 and the Marsh cone viscosity was 39 s (API 1990). The pH of the slurry was 9.20. The properties of the bentonite as supplied by the manufacturer are provided in Appendix A.

3.3 Experimental setup

3.3.1 Introduction

A test apparatus for measuring the coefficient of lateral earth pressure (K) during large strain consolidation was developed. This apparatus was based on an original design by Gan et al. (2011). A Proctor mold (150 mm diameter) was modified to measure the coefficient of lateral earth pressure and consolidation characteristics of the backfill mixtures under large strains. Hydraulic conductivity (k) values for the test mixes were also measured simultaneously. Button-type load cells (Figure 3.3) were installed in the Proctor mold to measure the lateral pressure exerted on the wall of the mold by the backfill mixes during consolidation. The whole setup was then loaded using a Conbel and was connected to a data acquisition system.

3.3.2 Mold modification

The Proctor mold was modified to have eight ports for measuring hydraulic heads at eight different depths in the soil. The bottom outlet of the mold was connected to a Marriotte bottle setup to run a constant head hydraulic conductivity test along with consolidation. Figure 3.2 shows a schematic diagram of the modified large-strain consolidation mold used in this study. Table 3.3 shows the loading sequence simulating various depths used for the consolidation test.

Two stainless steel, button-type design load cells were attached to the sides of the mold as shown in Figure 3.2. Initially, a load cell was also attached to the base of the mold from inside; it was later removed because water seeped into the circuit of the sensor and destroyed it. The load cells can measure compressive loads to a maximum of 4500 kg. They were purchased from Honeywell. Figure 3.3 shows the top view and the cross-section of the load cell; the diameters D1 and D2 as well as L and H values of the load cell are 38.1, 10.16, 2.03, and 16.0 mm, respectively. The load cells were calibrated before each experiment in the lab to account for any offsets. Figure 3.4 shows a picture of a load cell being calibrated in a Universal testing machine.

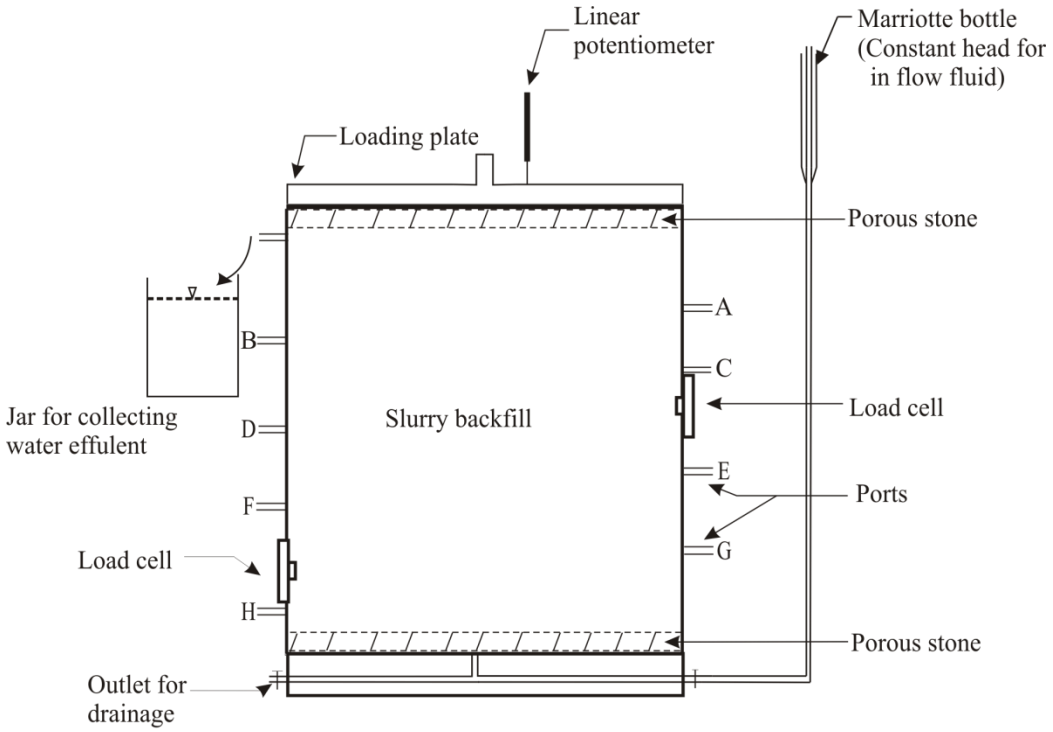

Figure 3.2 Schematic diagram of the modified large strain consolidation test mold.

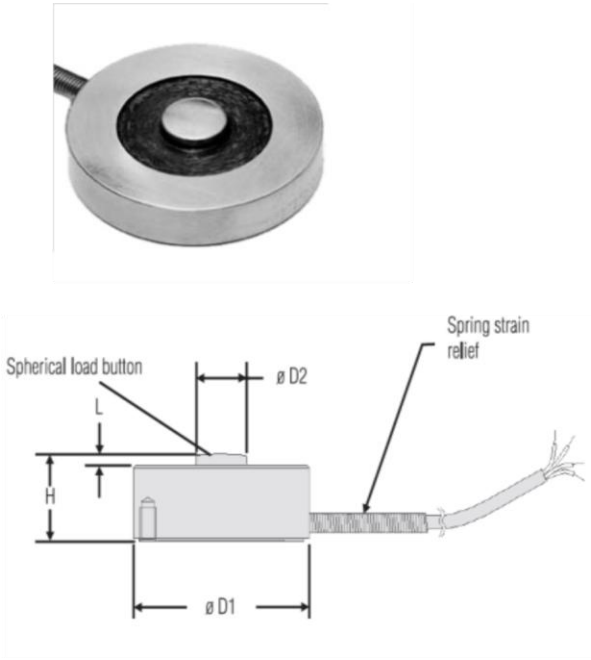

Figure 3.3. Top view and cross-section of button type load cells.

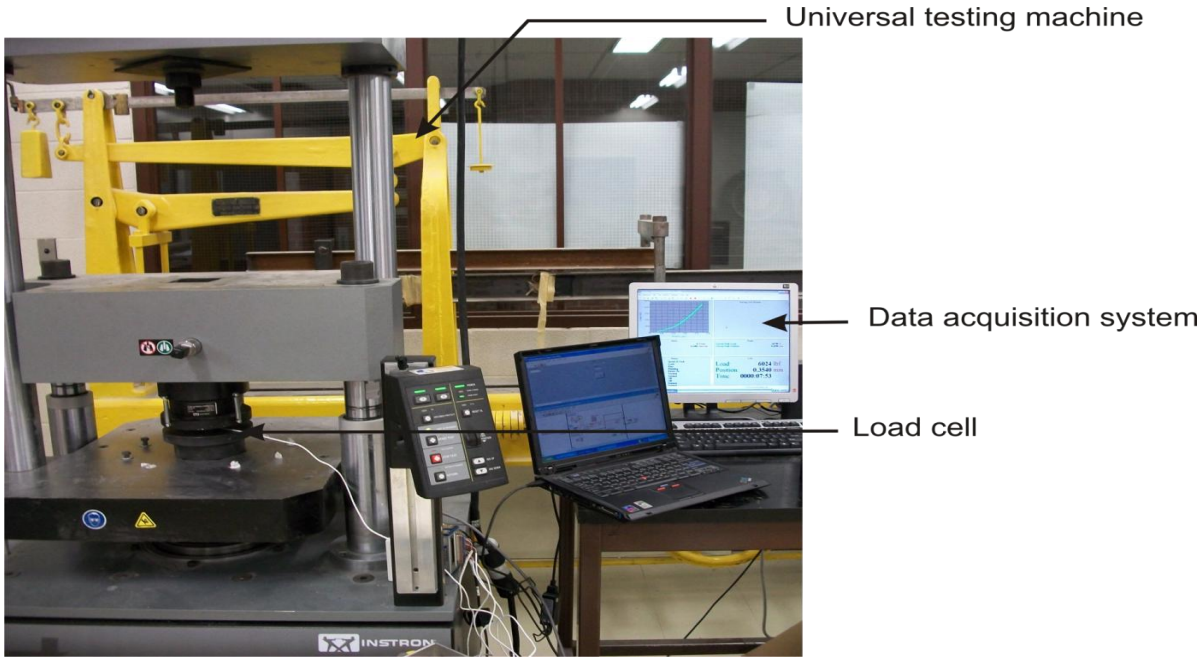

Figure 3.4 Calibration of load cell.

3.3.3 Large strain consolidation setup

Figure 3.5 is a schematic diagram of the experimental setup in the laboratory. The modified mold (Figure 3.2) was loaded by a Karol-Warner Conbel up to 900 kPa. Two load cells and the linear potentiometer were connected to the computer by a National Instruments (NI) data logging system. LabVIEW was used to communicate with the NI data logging system to record the raw data automatically on the computer.

A Marriott bottle was connected to the bottom outlet of the mold to simultaneously run the constant head hydraulic conductivity (k) test along with consolidation. All eight ports in the mold were connected to a piezometer to enable head readings at different heights in the sample. Figure 3.6 is a picture of the test in progress.

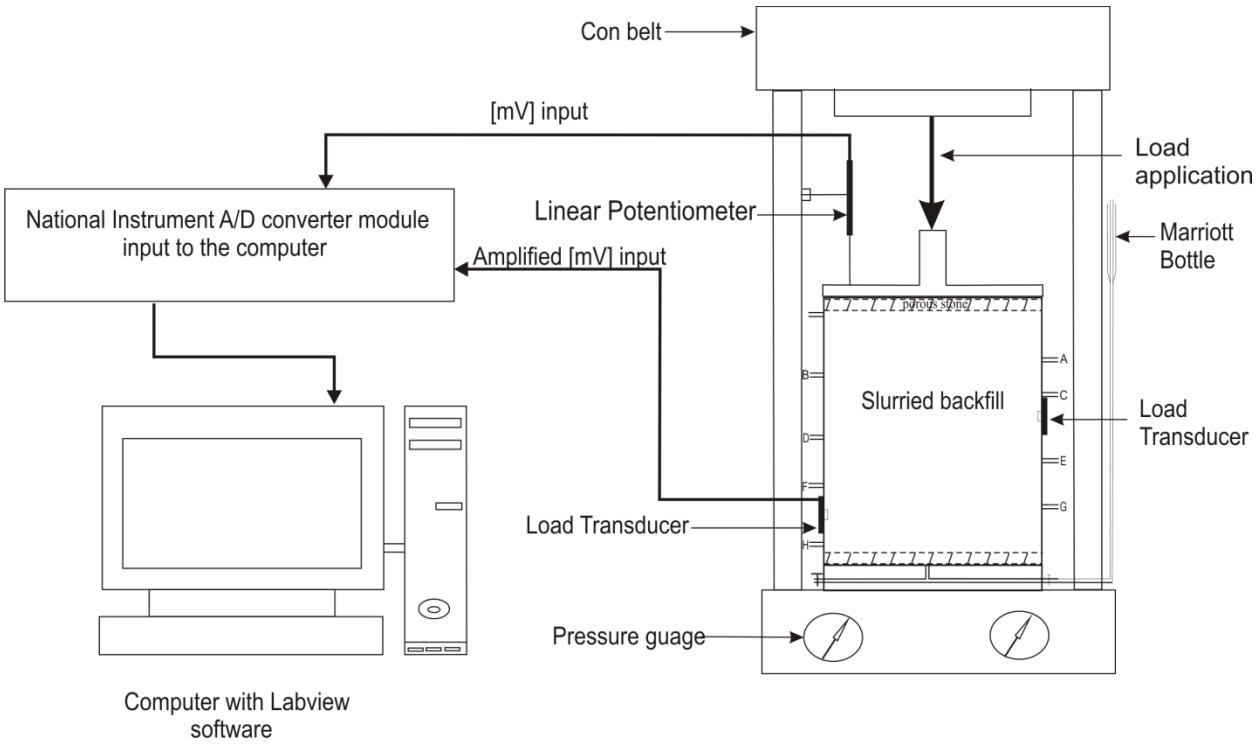

Figure 3.5 Schematic diagram of lab setup.

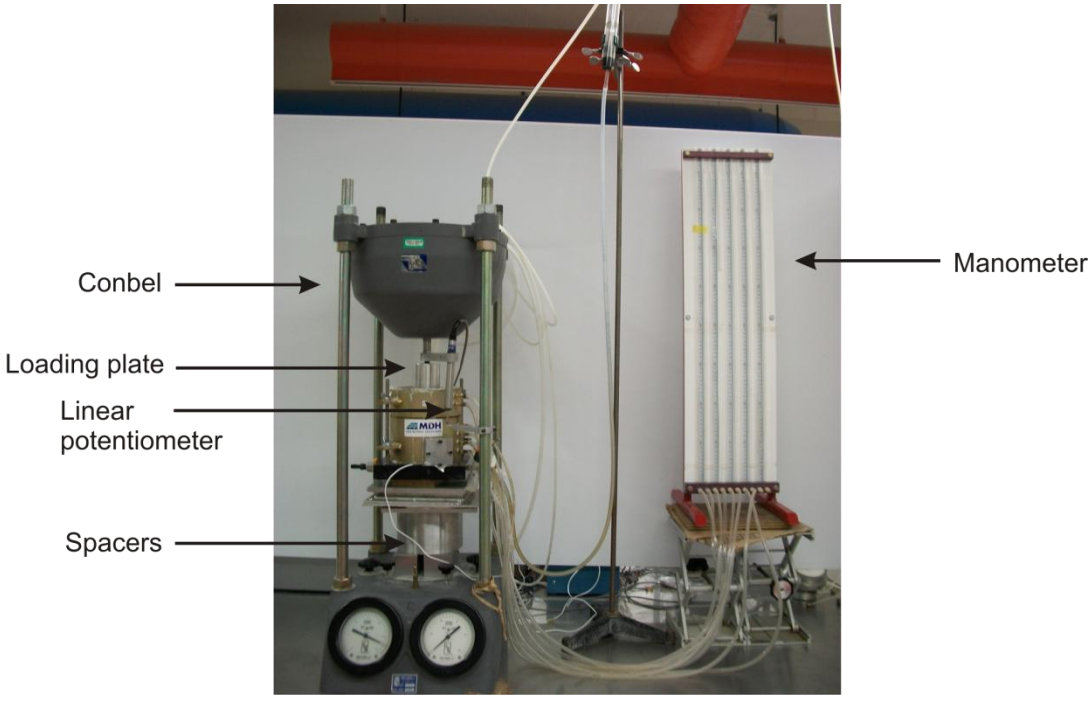

Figure 3.6 Picture of the test setup.

3.4 Test Procedure

The following section describes the procedures for the tests conducted in the laboratory as part of present work. This includes preliminary tests, such as Atterberg limits, slump tests for SB backfill, 1-D consolidation tests, and measurement of the coefficient of lateral earth pressure (K). All test procedures comply with those proposed by the American Society of Civil Engineers (ASTM).

3.4.1 Preliminary tests

Preliminary tests, such as the determination of Atterberg limits, were performed on all soils used in the test program, namely the glacial till obtained from the field, the field backfill (FB), TM1 (10% fines ≤ 75 μm), TM2 (25 % fines ≤ 75 μm), and TM3 (50% fines ≤ 75 μm).

The various tests performed to study material index properties were liquid limit, plastic limit, specific gravity, and grain size analysis. Liquid and plastic limits were determined according to ASTM D4318-00. Specific gravity (G) of the materials was determined according to ASTM D854-02. Grain size distribution of the materials was determined according to ASTM D422-63 (1998). Table 3.1 shows the index properties of all test materials and the mixture classifications according to ASTM D2487.

3.4.2 Slump cone test

The slump cone test helps in determining the consistency of the SB mix. This is an indirect way of measuring the flowability of the mix. The amount of bentonite that ends up in the backfill as a result of mixing in the slurry can vary depending on the properties and moisture content of the base soil used to prepare the backfill-slurry mixtures (Table 3.2).

In the present work, each backfill mix was mixed with a 5% bentonite-water slurry (Section 3.2.3) in various proportions to evaluate the relationship between the gravimetric water content of the resulting backfill-slurry mixture and the resulting slump. The slump was measured according to ASTM C143, and the slump tests performed for

each specimen at a given water content were repeated two to three times to account for variability in the measured values.

The amount of slurry mixed with the backfill was varied to provide a slump of 120 mm. A slump value of 100-150 mm is generally recommended, as this helps to control the slope of the backfill during filling. This also ensures that no liquid slurry is trapped in the backfill (Section 2.3.1, Page 4). Figure 3.7 is a picture of the slump cone test and apparatus taken in the laboratory. Figure 3.7a shows the cone, tamping rod, and base plate used for slump cone test. Figure 3.7b is a picture of a slump cone test in progress in the laboratory.

3.4.3 1-D consolidation test

The consolidation properties of each backfill-slurry mixture were studied using a fixed-ring consolidometer. A filter paper and a porous stone were placed at each end of the sample. The consolidation test procedures conformed to ASTM D2435.

Specimens of backfill slurry mixes were mixed using a high speed mixer and placed in the consolidometer in the remolded state at a constant dry density of 1.22 gm/cc (i.e., the initial void ratio for all the samples was kept constant). The backfill-slurry mixing ratios for the test specimens corresponded to those required to provide a 120-mm slump. After the specimens were kept in the consolidation cell (27 mm thickness and 64 mm diameter), they were allowed to equilibrate under a token seating load of 5 kPa for at least 24 h. The samples were then loaded slowly according to the loading sequence shown in Table 3.3. Each load increment was applied on the specimen for
24 to 48 h before the next increment was applied. Figure 3.8 shows the total settlement undergone by a sample at the end of a consolidation test.

(a) Slump cone apparatus

(b) Slump cone test in progress

Figure 3.7 Slump cone test.

Table 3.3 Loading sequence simulating various depths (for γ =18 kN/m^3).

Simulated depth (m)	Pressure (kPa) (corresponding to total stress)
0.5	9
1	18
2	36
4	72
8	144
15	270
30	540
40	720
50	900

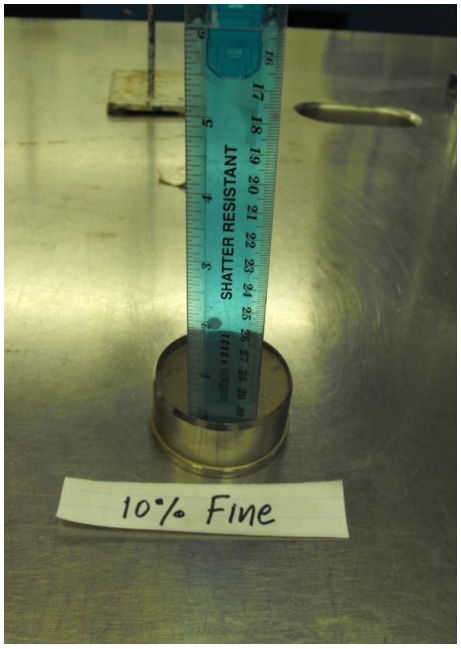

Figure 3.8 Sample settlement at the end of test.

3.4.4 Shear box test

Consolidated drained (CD) shear box tests were conducted to study the shear strength parameters of the backfill mixes. All samples were sheared under increasing normal pressures of 54.7, 163.2, and 316 kPa. In total, 12 samples were tested. The shear box test was performed at a constant rate. A linear potentiometer was used to measure the

horizontal and vertical displacements. The shear box setup was connected to a data logger system to record the displacements. Remolded samples from different backfill mixes were allowed to consolidate in large consolidation molds at different specified normal loads prior to placement in the shear box mold. They were left in these molds for 7-14 d for consolidation depending on the normal load. The samples were extruded and trimmed to fit into a 60 $\times$ 60 mm box after consolidation. Care was taken not to disturb the consolidated samples during the trimming process. The samples were then left in the shear box for 1-3 d depending upon the normal load being applied. The normal loads were applied in small amounts so as to prevent the mix from squeezing out of the box. The shear box test was then carried according to ASTM D-3080-04.

3.4.5 Large strain consolidation and hydraulic conductivity tests

The six-inch modified Proctor mold as described in Section 3.3.2 was used to conduct large strain consolidation tests. The consolidation test conformed to typical 1-D consolidation test procedures, except that load cells were attached to measure the lateral load exerted on the wall of the mold and a constant head hydraulic conductivity test was run simultaneously.

Remolded saturated samples were placed in the mold at a water content corresponding to a slump of 120 mm and at a constant dry density (γ_d = 1.22 gm/cc, same as the 1-D consolidation test). Porous stones and filter papers were placed on both ends of the sample. A linear potentiometer was used to measure the vertical settlement in the sample during consolidation. Once the samples were placed, they were left to consolidate under the weight of the loading plate until the load cell and potentiometer readings stabilized.

The test apparatus was loaded using a Karol-Warner Conbel (Figure 3.5). Load cell and deflection readings were recorded and monitored continuously. A constant head hydraulic conductivity test was run simultaneously using a Marriott bottle arrangement. Tap water was injected into the sample from the bottom, as distilled water is not recommended for hydraulic conductivity testing (Daniel 1994; Dunn and Mitchell 1984).

The water was collected in a sealed bottle. The test was repeated three times to account for any variability in results.

Once the load cell and the potentiometer reading stabilized (7-14 d, depending upon the load being applied) and equilibrium was attained, a new load was applied to the sample in accordance with the loading sequence in Table 3.3.

CHAPTER 4 - DISCUSSION OF TEST RESULTS

The following section discusses the results obtained from the tests conducted on different soil mixes in the laboratory. The test procedures, conducted as per ASTM codes, were discussed in the previous chapter.

4.1 Slump cone test

A slump cone test was performed (ASTM C143) on TM1, TM2, TM3, and FB samples for a prefixed slump value of 120 mm, as a slump value of 100-150 mm has been recommended for SB mix (Section 2.3.1). The prefixed value of 120 mm was chosen as a midpoint between 100 and 150 mm and to keep slump as a constant parameter for all mixes. The fines content was 12, 28, 31, and 53% (upon adding bentonite) for the TM1, FB, TM2, and TM3 test materials, respectively. The water content was continuously increased in the material until the prefixed slump value of 120 mm was obtained.

The variation of water content (%), corresponding to the prefixed slump of 120 mm with the varied fines content in the materials, in shown in Figure 4.1. The figure shows that water content increased with increasing fines content of the materials. The surface area of the fine particles is high and, therefore, fines require greater water content to reach a given degree of saturation. Hence, the test water content increased with fines content in the material. In the present work, the slump test was performed at a 100 % degree of saturation for all materials.

For comparison, the figure also shows the data presented by Khoury et al. (1992) and Yeo et al. (2005) for different values of slump (Figure 4.1). The properties of the mixes used by Khoury et al. (2005) in their study are shown in Table 2.1. Yeo et al. (2005) used clay with various proportions of silica sand to provide backfills with total fines contents of 20, 40, 60, and 75% by dry weight. In these data shown for comparison, water content also increased with fines content. While the data presented by Khoury et al. (1992) lie below the present laboratory test data in the figure, those presented by Yeo et al. (2005) lie above. It can be inferred from this disparity in the water contents

that the clay content of the material used by Khoury et al. (1992) was lower and used by Yeo et al. (2005) was higher, respectively, than the material used in the present work.

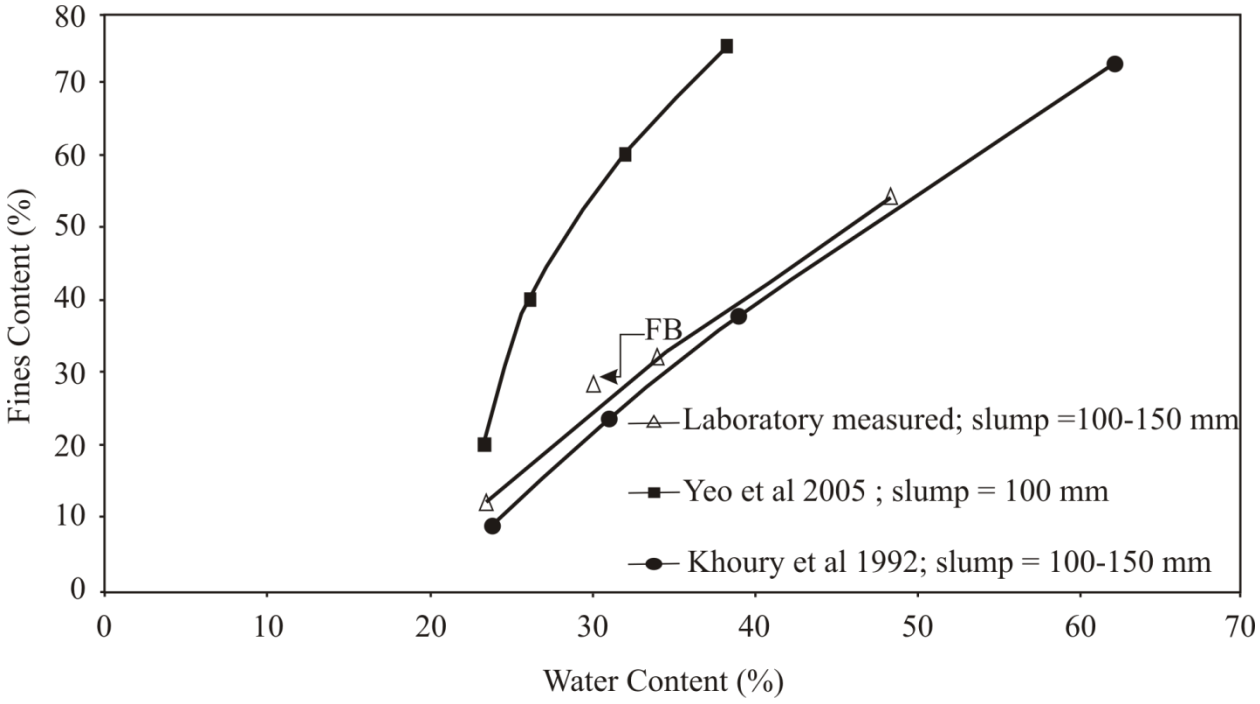

Figure 4.1 Variation of water content (%) vs. variation of fines content (%).

4.2 Shear strength test data

Failure envelopes of TM1, TM2, TM3, and FB obtained from the shear box test data are presented in Figure 4.2. The effective angles of internal friction (ϕ') measured from the failure envelope were 32, 29, 26, and 23° for TM1, FB, TM2, and TM3, respectively. This was due to sand contents in TM1, TM2, and TM3 of 87, 71, and 47.2% respectively. Although from literature ϕ' for SB mix lies between 30 to 35º, no explanation on the type of mix is given (section 2.3.4). Table 3.1 shows the percent gravel and sand in the test materials. The amount of fines present in the mix (Table 3.2) also justifies the ϕ' values. These results were used as an input for modelling consolidation of the SB wall, as described in the next chapter. The raw data for all the tests is presented in Appendix B.

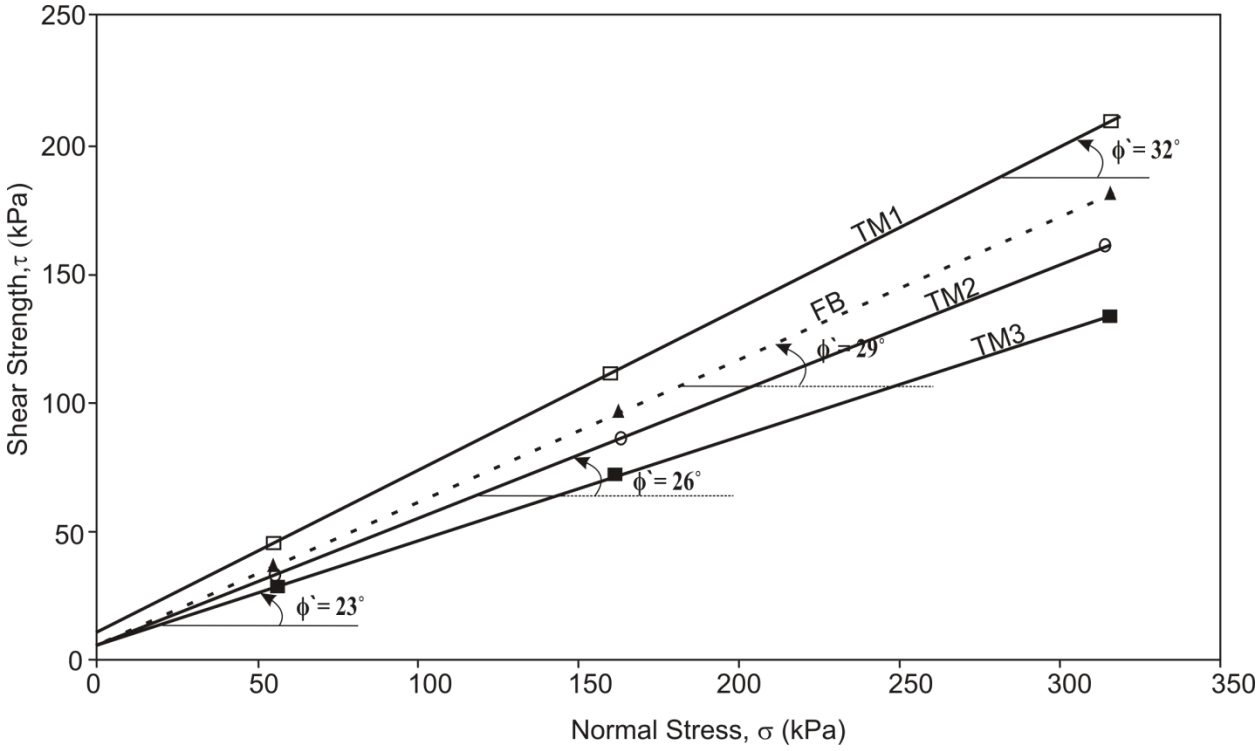

Figure 4.2 Failure envelopes for different types of backfill mix.

4.3 1 - D consolidation test

Figure 4.3 shows e-log σ'_v curves of different test materials. The data shown were obtained from 1-dimensional consolidation tests performed in an oedometer. The tests were performed on all materials compacted in the oedometer at a constant γ_d = 1.22 gm/cc.The e-log σ'_v curve shows that TM3 was the most compressible of all of the materials. The compressibility then decreased in the order TM2 > FB > TM1. This conclusion can be arrived at based on the position of the e-log σ'_v curve in the graphical data, where the TM3 curve is at the bottom and the curves of TM2, FB, and TM1 above. TM3 had the maximum compressibility, as its fines content was also the highest. The compressibility of TM2, FB, and TM1 also decreased according to fines content (Table 2.1, Page 10). The compression index (Cc) values of the different materials are shown in Table 4.1.

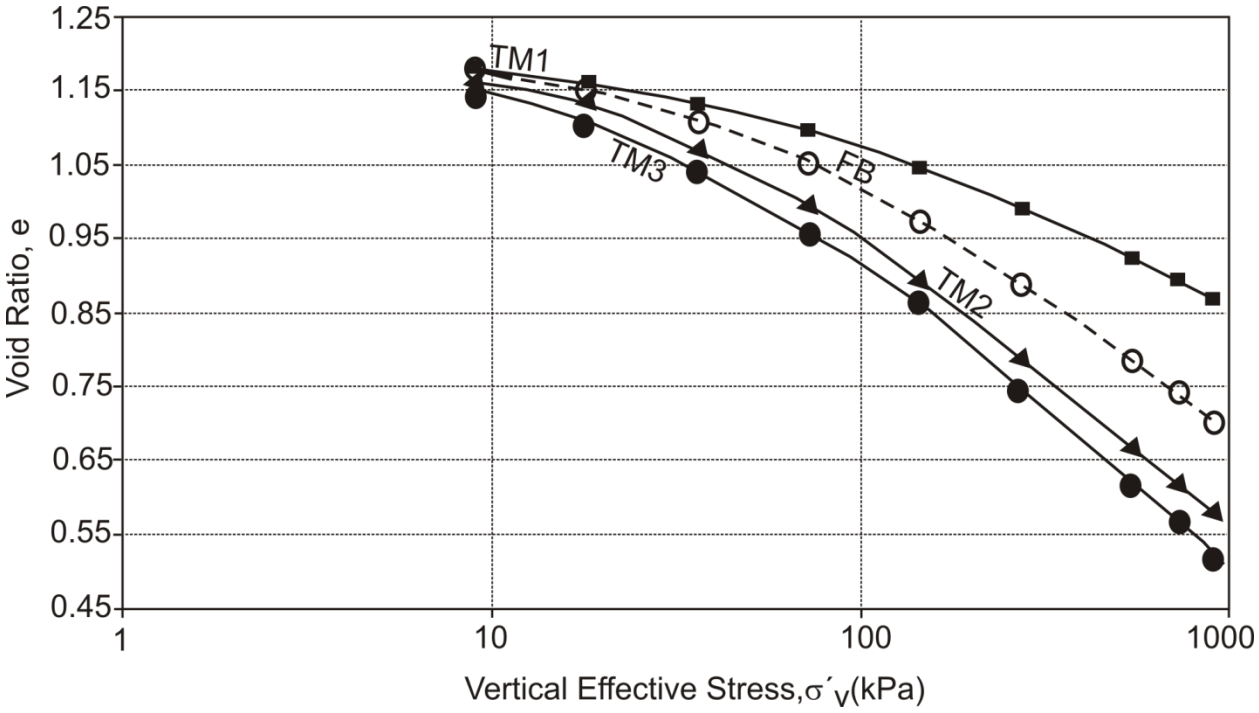

Figure 4.3 e-log σ'_v curves from 1-D consolidation testing.

Table 4.1 Compression index for different backfill mixes.

Test Mix	Compression Index, Cc
TM1	0.2221
FB	0.3389
TM2	0.3979
TM3	0.4274

Figure 4.4 shows the variation of settlement (%) with vertical effective stress (kPa). Settlement (%) is defined as ((δl/l)*100), where δl is the change in sample thickness at the end of each load and l is the initial sample thickness (27 mm, Section 3.4.3). The data shown in the figure reflect behaviour similar to that indicated in Figure 4.3. For all materials, the total settlement increased with greater vertical effective stress. TM3 is the most compressible of all of the materials, because it resulted in the highest amount of settlement under a given vertical effective stress. The compressibility of the other

materials under a given vertical effective stress decreased in the order TM2 > FB > TM1.

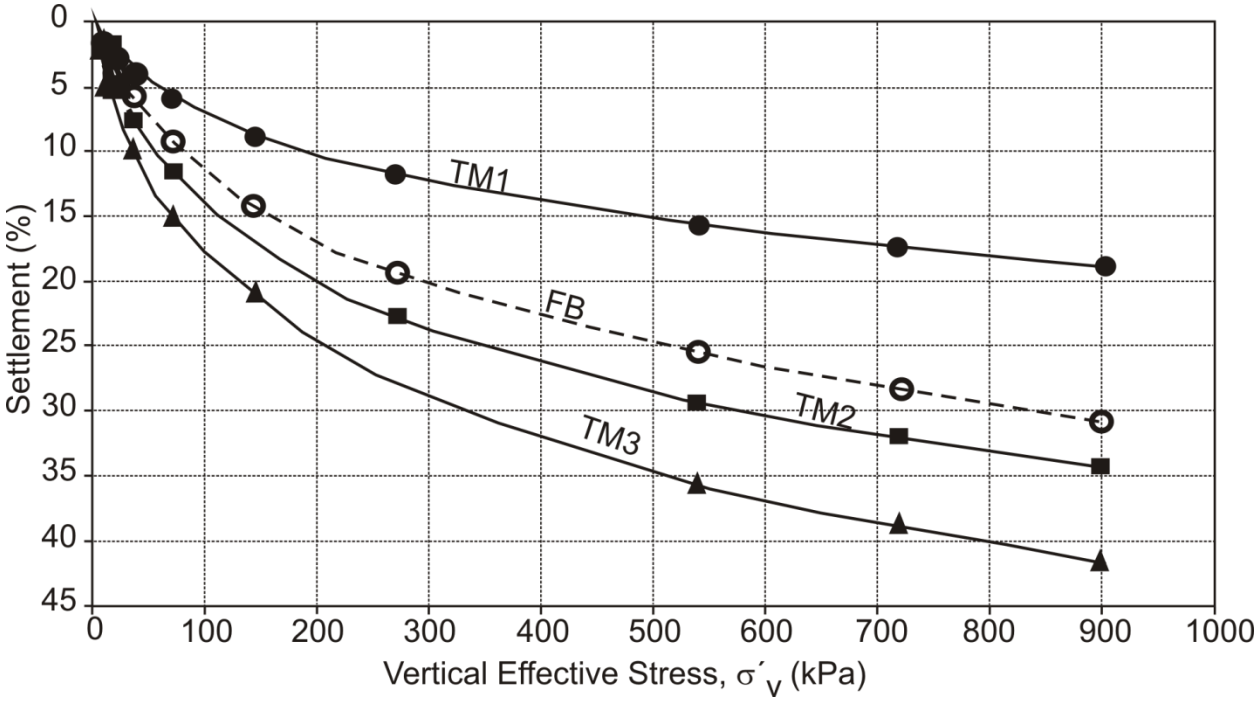

Figure 4.4 Total settlement measured at the end of consolidation.

4.4 Large strain consolidation tests

Six-inch Proctor molds were modified to test all of the backfill mixes. They were modified to house load cells to measure horizontal load, as well to measure hydraulic conductivity of the SB mix simultaneously with consolidation (Section 3.4.5). This section presents the results of the tests conducted in these modified molds.

Figure 4.5 shows the e-log σ'_v curves for all of the test materials tested for compressibility in the modified mold (Section 3.3.2), the diameter of which was 150 mm. The sample thickness was 160 mm. Consolidation tests were performed by applying air pressure to the sample and monitoring settlement. The equilibrium void ratio corresponding to the vertical effective stress was plotted against the log of vertical effective stress, as shown in Figure 4.5. The data reflect a similar behaviour as shown in Figure 4.3. TM3 showed the highest compressibility because it had the highest fines

content; the lower fines content of the other materials, namely TM2, FB, and TM1, resulted in less compressibility.

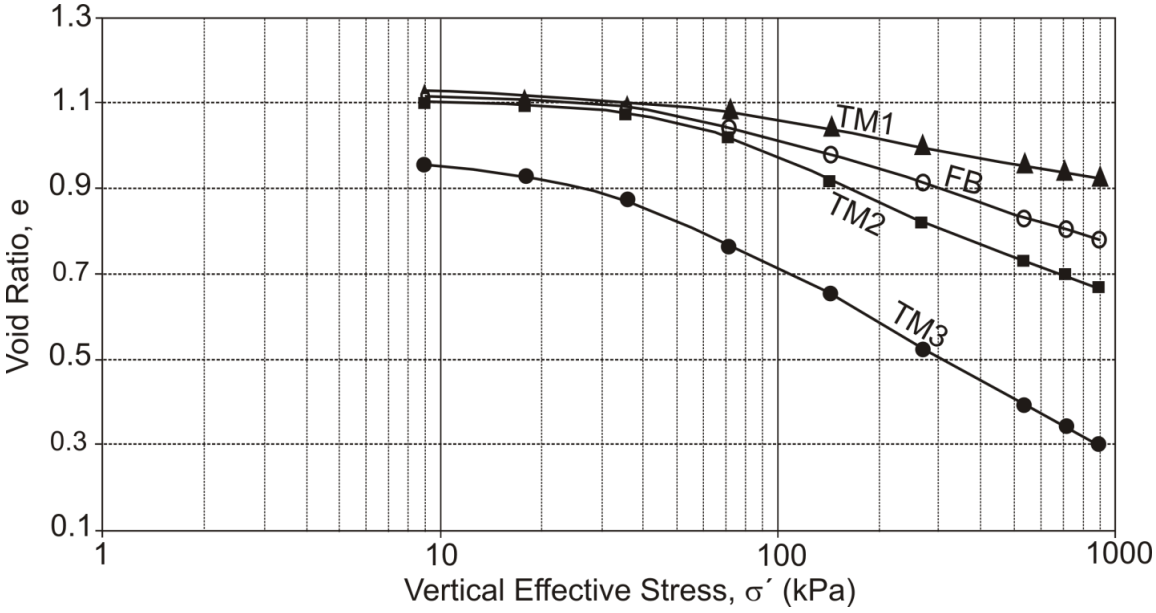

Figure 4.5 e-log σ'_v curves from large strain consolidation tests.

Figure 4.6 shows the variation of measured hydraulic conductivity, k (m/s), with the vertical effective stress. These k tests were run simultaneously with consolidation. This was done using a Marriott bottle arrangement as described in Chapter 3. All tests were run three times to account for variability in results. The data show that hydraulic conductivity (k) decreased with increasing total vertical stress (i.e., decrease in equilibrium void ratio, Figure 4.7). This was true for all materials tested. The data also show that the hydraulic conductivity value of TM3, which had highest fines content of all of the materials (Table 3.2), was lower than other materials. The vertical effective stress-hydraulic conductivity relation for FB and TM2 was similar because the fines content (silt and clay) in these materials was nearly equal (Table 3.1). TM1, which had the lowest fines content and highest amount of coarser materials, resulted in the highest value of hydraulic conductivity, corresponding to the equilibrium void ratio.

The hydraulic conductivity (k) for TM1 decreased from 1×10^{-4} to 2.5×10^{-7} m/s and for TM3 decreased from 8×10^{-9} to 4×10^{-10} m/s as the vertical effective stress

increased from 9 to 900 kPa. Hence, the amount of fines present in the mix plays an important role in controlling k. Similar results have been reported in the literature by Yeo et al. (2005), where hydraulic conductivity for their test mixes also decreased with increasing fines content (Figure 2.6).

Hydraulic conductivity (k) from consolidation test results for each load increment has been calculated and compared with the measured k value obtained in the lab (Appendix G). Calculated hydraulic conductivity (k from consolidation results) at a stress of 900 kPa for TM1, FB, TM2 and TM3 is 4.33 x 10^{-10}, 7.33 x 10^{-11}, 4.03 x 10^{-11} and 2.21 x 10^{-12} m/s. These values are lower than the corresponding values measured in the lab at the same stress level. This is true for all load increment. The k values estimated using consolidation results are an underestimate of actual measured k values in lab. This is because the reduction in coefficient of consolidation (c_v) is much faster near the drainage boundary than in the middle of the specimen so that a nonhomogenous condition is created in the specimen. Hence the sample at the boundaries densifies more in comparison to the rest of the sample which in turn underestimates the k of the whole sample (Tavenas et al, 1983)

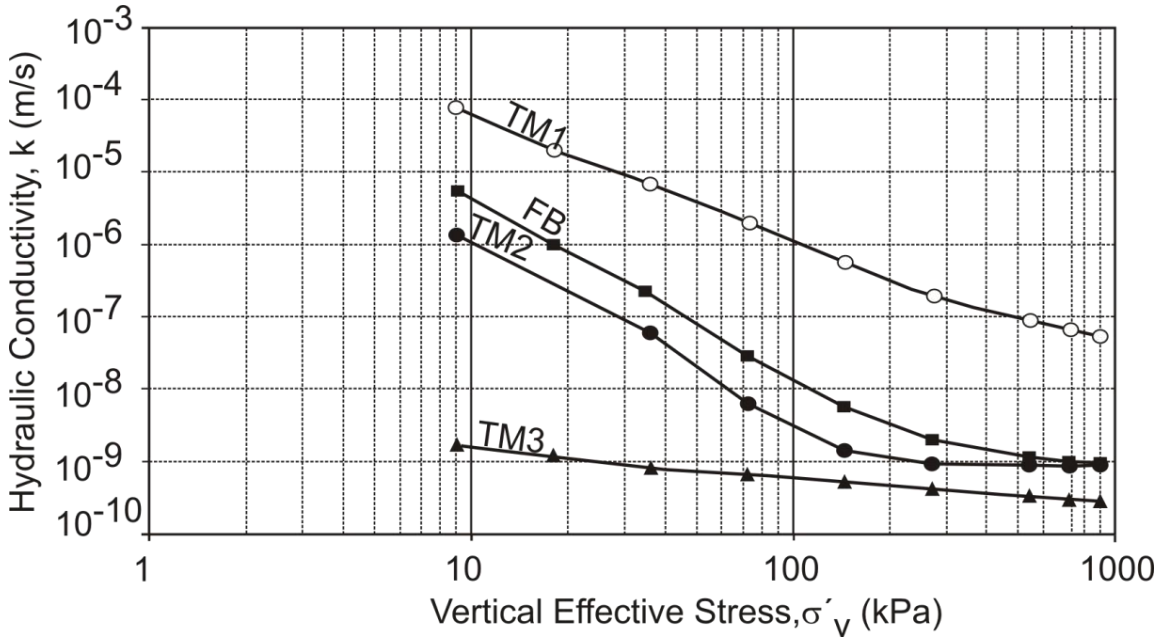

Figure 4.6 Hydraulic conductivity (k) plots for various backfill mix.

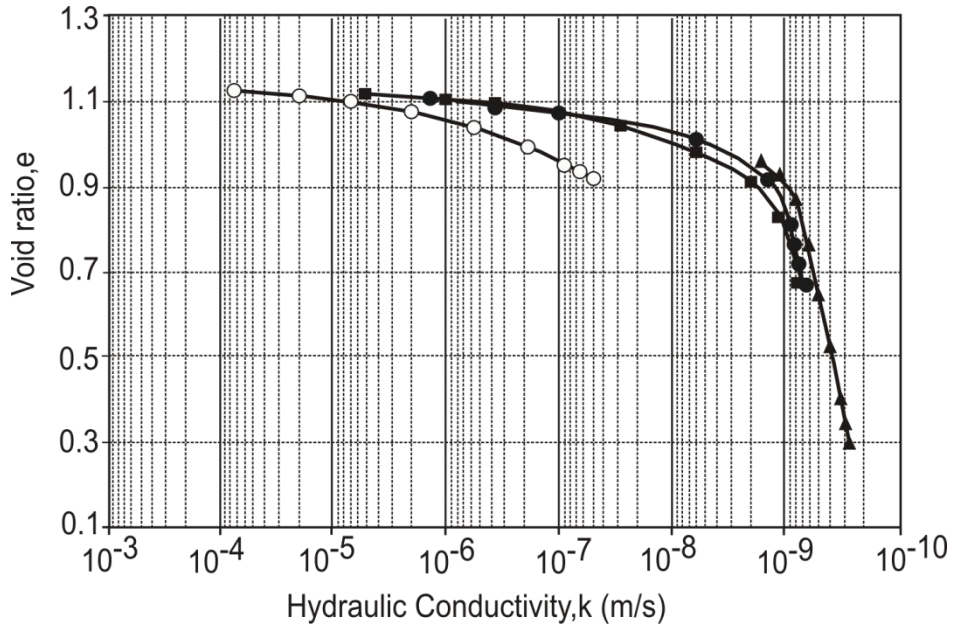

Figure 4.7 Hydraulic conductivity (k) plots for various backfill mix (e-k plots).

Variation in the coefficient of lateral earth pressure (K) with simulated depth (Table 3.3) is shown in Figure 4.8. K is the ratio of horizontal effective stress (σ'_h) to the vertical effective stress (σ'_v) measured at the end of consolidation (after more than 95% of the excess pore water pressure has dissipated). The figure shows that for all backfill mixes, K increased initially with simulated depth up to 10 m, and thereafter it became constant with depth. This is because the SB mix was initially in a slurry state. Therefore, the slightest increase in vertical stress resulted in a sharp increase in horizontal stress. However, excess pore pressure dissipates with increasing vertical stress and, as a result; the SB mix starts to gain strength and resists its lateral movement.

The K value for TM3 (maximum fines content) is 0.34 and for TM1 (least fines content) is 0.36; this difference is negligible. Therefore, it can be concluded that the amount of fines has no or little influence on the lateral coefficient of earth pressure.

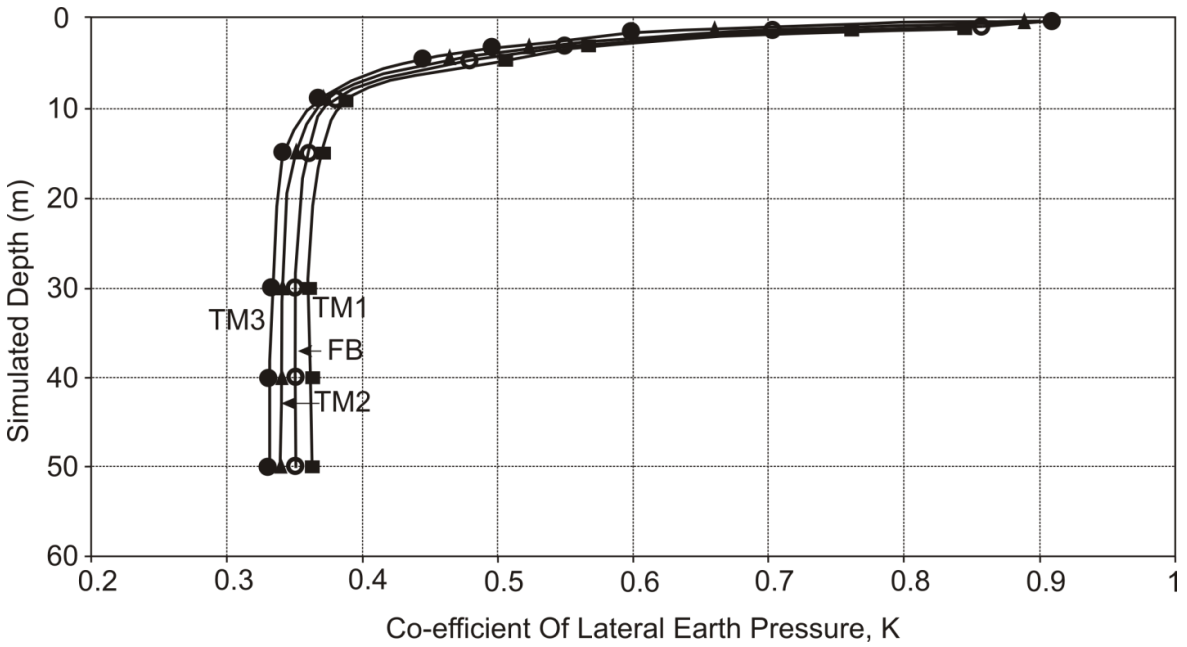

Figure 4.8 Coefficient of lateral earth pressure (K) with simulated depth.

Comparison of measured and estimated coefficient of lateral earth pressure using relation between K_o and ϕ' from literature (section 2.3.6) has been presented in Table 4.2. $K_{measured}$ refers to the K values obtained in the laboratory whereas $K_{estimated}$ refers to the K calculated using various equations from literature (section 2.3.6). For all the mix, the K values obtained in the laboratory are less than estimated K. This disparity in results could be explained due to the measurement of K values in the laboratory at higher final effective stresses which may not be the actual stress experienced by the soil due to development of shear stress (τ) between the soil and the mold boundary.

Table 4.2 Comparison of measured and estimated K

Mix	$K_{measured}$ (laboratory results)	$\phi'_{measured}$ (degrees) (laboratory results)	$K_{estimated}$		
			Terzaghi (1923)	Jaky (1948)	Federico et al (2008)
TM1	0.36	32	0.48	0.47	0.46
FB	0.35	29	0.49	0.52	0.50
TM2	0.345	26	0.53	0.54	0.54
TM3	0.34	23	0.57	0.56	0.58

The following algorithm describes the method used to correct the measured K ($K_{measured}$, Figure 4.8) in the laboratory.

1. Assuming that the angle of internal friction, ϕ' obtained from the laboratory test results (section 4.2) is correct.
2. Using Jaky's equation for K_o (section 2.3.6, equation 2.11) which is the most popular equation, k_o for ϕ' measured in the laboratory is determined.
3. Using equation 2.4 (section 2.3.6), horizontal stress is calculated for all effective stresses (figure 4.4).
4. Using calculated σ'_h and measured ϕ' in the relation shear stress, $\tau = \sigma'_h \tan\phi'$, shear stress ($\tau$) at given depth (in this case depth for τ calculation is equal to the location of the load cell) is calculated.
5. Actual vertical effective stress on the sample at any depth is equal to vertical effective stress at the end of load in the lab minus the shear stress at that depth.
6. Using the measured σ'_h in the lab and calculated actual σ'_v, corrected K value is calculated.

A plot between applied vertical effective stress (stress at the end of each load) and corrected co-efficient of lateral earth pressure is presented in Figure 4.9. The trend of the variation of K with depth (related to effective stress from Table 3.3) (Figure4.8) / effective stress is same. However, the K values in Figure 4.9 are very close to the ones presented in Table 4.2, which are the value based on the ϕ' for each mix. . A comparison of estimated K using Jaky's equation and corrected K has been [resented in Table 4.3.

Table 4.3.Comparision of estimated and final corrected K

Mix	$K_{estimated}$ (From Literature; Jaky, 1948)	Final Corrected K
TM1	0.47	0.54
FB	0.52	0.53
TM2	0.54	0.52
TM3	0.56	0.50

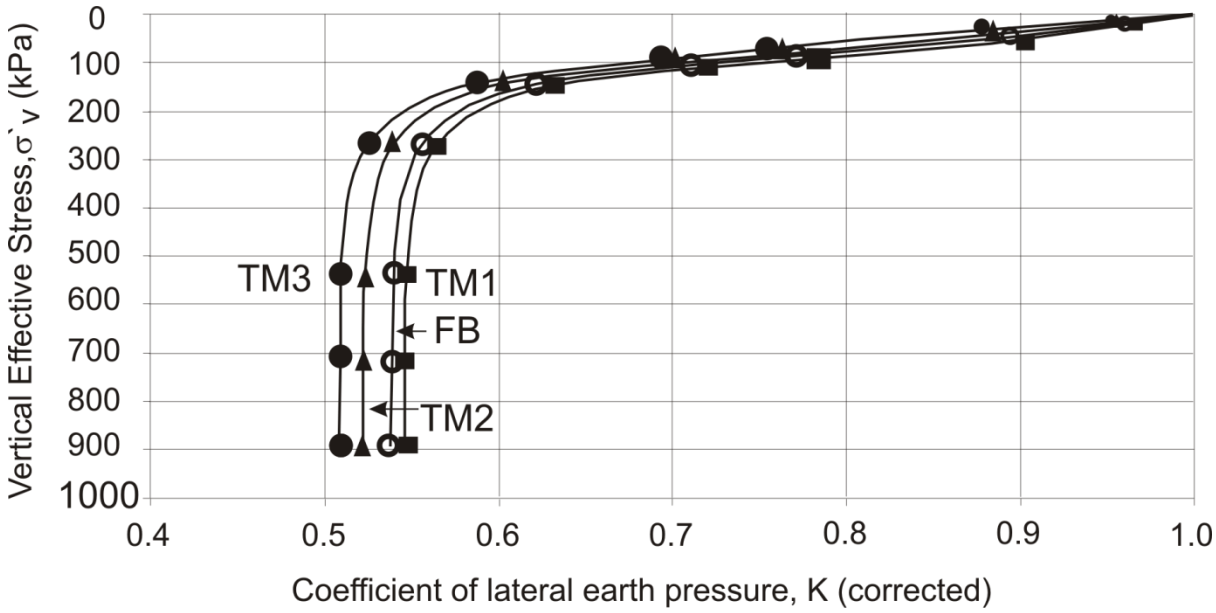

Figure 4.9 Coefficient of lateral earth pressure, K (corrected)

CHAPTER 5 – MODELING ARCHING OF STRESSES IN SOIL-BENTONITE WALLS

5.1 Introduction

This chapter presents detailed modeling of consolidation and arching in soil-bentonite (SB) walls. It describes two methods: first, a numerical method based on principles of statics (discrete model), and second, a finite element method. These methods do not consider time-dependent behaviour, such as secondary consolidation or creep. The results of modeling using both methods are discussed and comparisons drawn between them.

5.2 Solution based on statics

The discrete model is based on the principles of statics. A body is said to be in a state of "static equilibrium" if, and only if, all the forces acting on it are balanced (total forces acting on an object at rest add up to zero).

5.2.1 Assumptions in static models

1. The coefficient of lateral earth pressure $K = \sigma'_h / \sigma'_v$, where σ'_h and σ'_v are horizontal and vertical effective stresses (Figure 5.1). These are not necessarily principal stresses.
2. For a given trench width, at any depth σ'_v is uniform across the trench.
3. The coefficient of lateral earth pressure (K) is constant throughout the wall.
4. Friction is fully mobilized along the two vertical interfaces of the slurry wall.
5. More than 95% of the excess pore water pressure (PWP) has dissipated.

Note that this solution does not take into account stress-strain relations of the material.

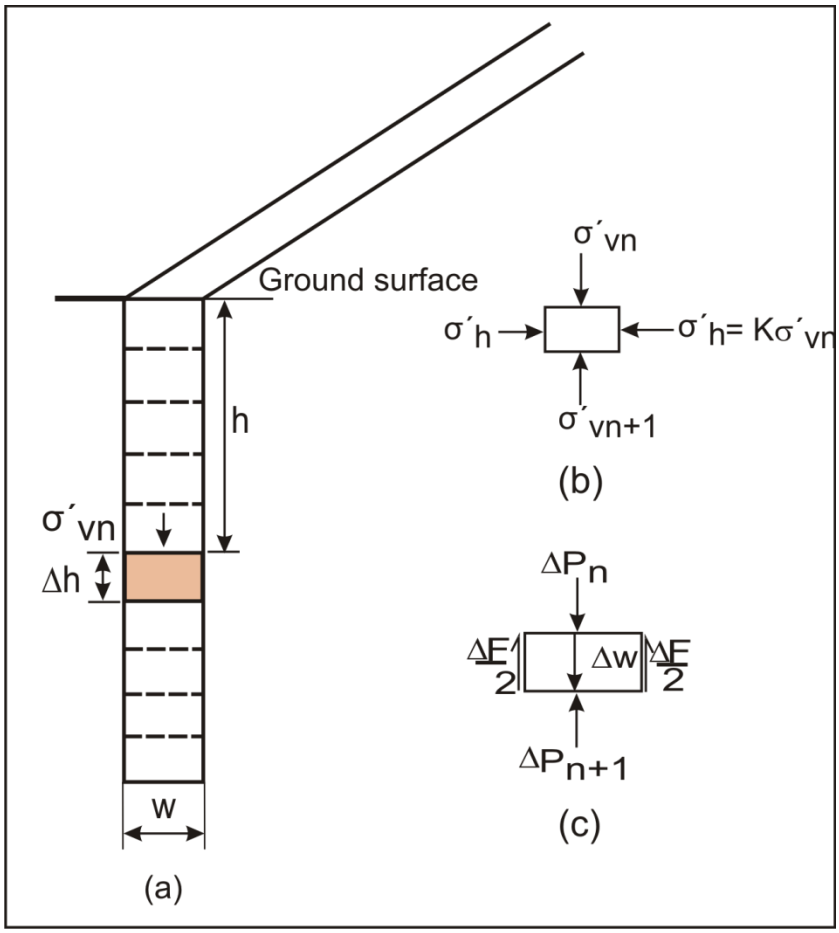

Figure 5.1 Discrete model.

5.2.2 Discrete model

In the discrete model, the equilibrium of forces in each and every element is considered to determine the vertical stress distribution with depth. The slurry wall under consideration is divided into smaller elements or segments of equal thickness (Δh) and weight (Δw), as shown in Figure 5.1. The greater the number of elements, the more accurate the stress prediction. Figure 5.1 shows a trench w units wide that has been discritized into small elements of thickness, Δh.

Consider an element of thickness Δh, at a depth h from the ground surface (Figure 5.1a). σ'_{vn} is the stress acting on the top of the element, which is the cumulative vertical

stress being transferred by the elements above it. Figure 5.1(c) shows the free body diagram of vertical forces for the shaded element under consideration.

Let ΔP_n (force acting downwards) be the force being transferred due to the normal stress to the top of the element under consideration by the elements above it. Δw is the self weight of the element. $\Delta F/2$ is the frictional force acting upwards on each side of the block. This frictional force is preventing the block from sliding downward. ΔP_{n+1} is the net force acting upward on the segment to keep it in static equilibrium. For vertical forces in equilibrium (Figure 5.1a):

$$\Delta P_o + \Delta W - \Delta P_1 - 2*\Delta F/2 = 0,$$

$$\Delta P_1 = \Delta Po + \Delta W - 2*\Delta F/2.$$

Writing the forces in terms of stresses,

$$\sigma_{vn+1} * w * 1 = (\sigma_{vn} * w * 1) + (\gamma * w * 1 * \Delta h) - 2*F/2$$

where, $F/2 = (\tan \phi)\, \sigma_h\, \Delta h = (\tan \phi)\, K\sigma'_v\, \Delta h$. Using the relation $\sigma = \sigma' + u$

$$\sigma'_{vn+1} * w * 1 = (\sigma'_{vn} * w * 1) + (\gamma' * w * 1 * \Delta h) - 2*F/2$$

$$\sigma'_{vn+1} = (\sigma'_{vn}) + (\gamma' * \Delta h) - 2*(\tan \phi' K\sigma'_{vn}/w)\, \Delta h. \qquad [5.1]$$

Hence, it is evident from equation 5.1 that the vertical stress on any element is a function of the coefficient of lateral earth pressure (K), the width of the wall (w), and the angle of internal friction (ϕ').

5.3 Parametric study using the discrete model

The parameters in equation 5.1 were varied to study the effect of their change on vertical stress distribution in the slurry wall with depth. This important part of the study helps to determine the optimum values for the width of the wall as well as the soil properties. Arching is defined as a phenomenon of “stress transfer from a yielding mass to an adjacent stationary solid body”. In the present study, arching is observed in the

stress distribution pattern in long narrow SB slurry walls. By properly selecting the above parameters, arching in the wall can be minimized.

The following parameters were varied:

1. Width (B) of the wall;
2. Coefficient of lateral earth pressure (K); and
3. Angle of internal friction (ϕ') of the backfilled material (note that K and ϕ' are not completely independent).

Figure 5.2 shows the variation of vertical effective stress in the wall, with depth, for different wall widths and for K = 0.35 and ϕ' = 29°. Values for the width (w) of the wall that were considered were 0.5, 1, 2, and 4 m. The dashed line (w = 1 m) represents the predicted stress distribution for the SB wall at Rocanville, Saskatchewan.

With increasing wall width, the vertical effective stress (σ'_v) distribution more closely aligns with the geostatic stress distribution.

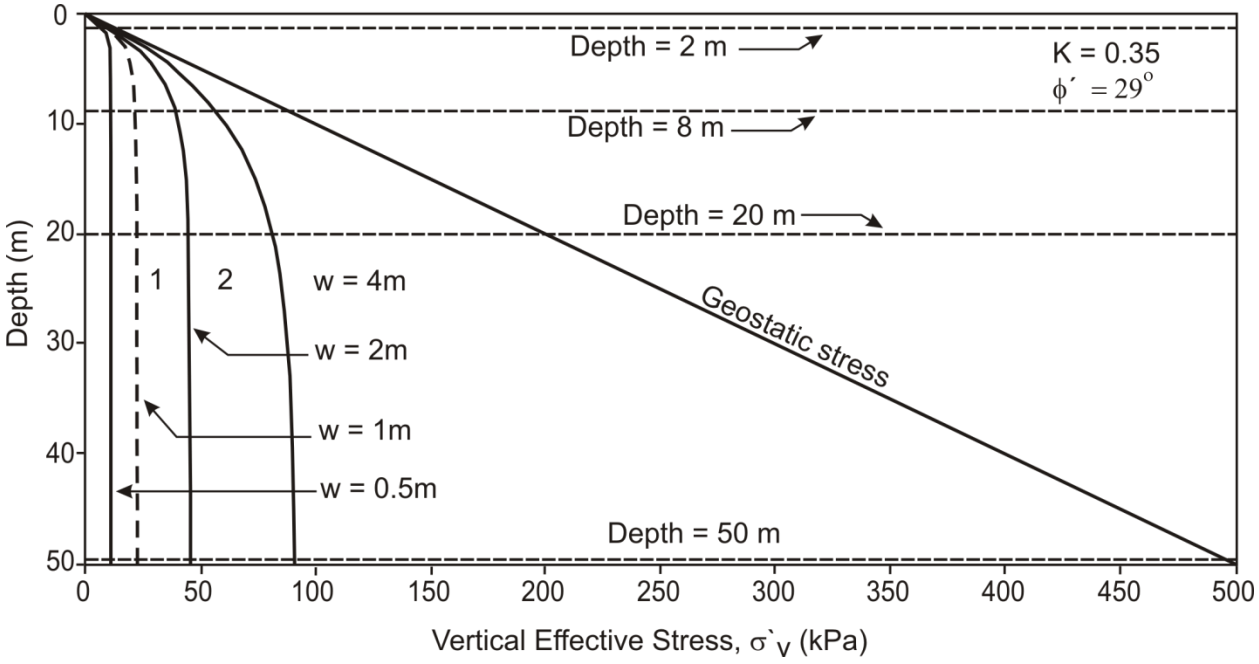

Figure 5.2. Variation in vertical effective stress (σ'_v) with depth for different wall widths.

From Figure 5.2, it is evident that, for all widths, the stress up to 2 m depth is approximately equal to the geostatic stress at the same depth. Thereafter, the vertical stress decreases and deviates significantly from the geostatic stress with depth for all widths. This is also evident from Figure 5.3, which is a cross plot for Figure 5.2 at depths D equal to 2, 8, 20, and 50 m.

At a depth of 8 m, the vertical effective stress (σ'_v) is 11 and 61 kPa for walls 0.5 and 4 m wide, respectively (Figure 5.3). This is about 89 and 40% less, respectively, than the geostatic stress at the same depth. The σ'_v at 50 m depth is 11.43 and 91 kPa for walls 0.5 and 4 m wide, respectively, which is about 97.5% and 80% less than the geostatic stress at same depth. Based on above discussion, arching in the SB walls decreases as the wall width increases.

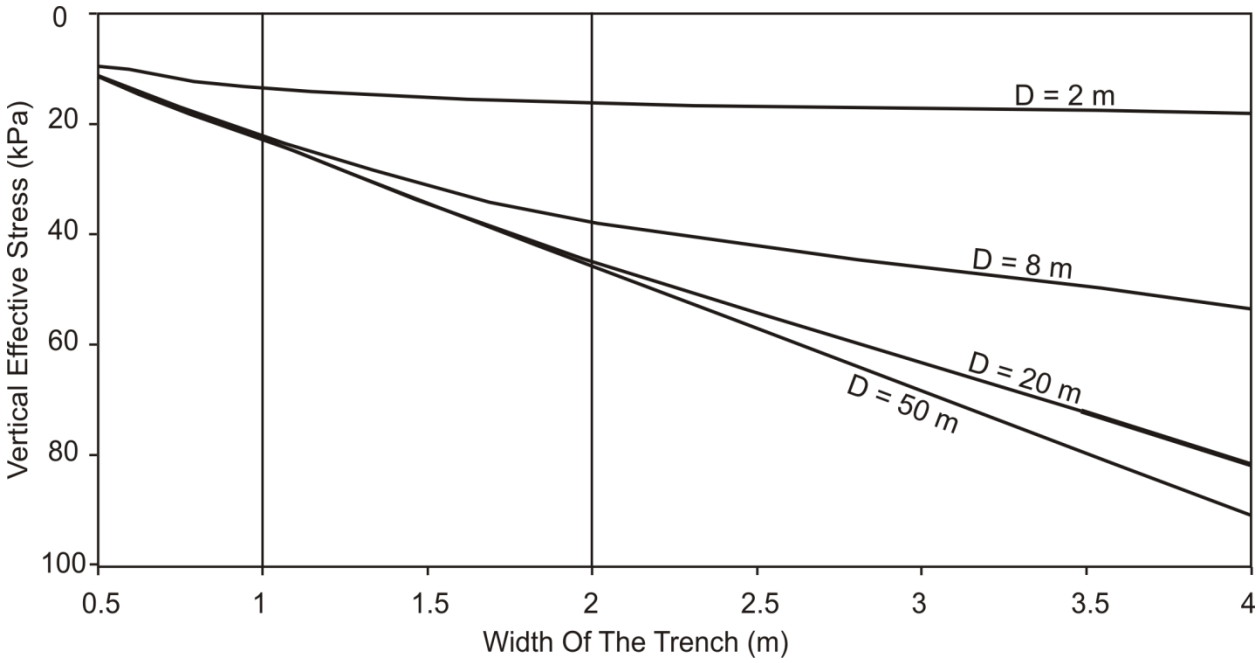

Figure 5.3 Cross plot of data from Figure 2 at different depths (D = 2, 8, 20, and 50 m).

The variation of vertical effective stress (σ'_v) with depth of the wall for different angles of internal friction (ϕ'), K = 0.35 m, and w = 1 m is shown in Figure 5.4. Based on Rankine's theory of active and passive earth pressure, K should lie between 0.35 and 3.25. These are the lowest and highest values of K, respectively, calculated using the ϕ' value shown

in the figure. The angle of internal friction, ϕ', for the SB mixes was varied between values of 23, 26, 29, and 32°. The dashed line in Figure 5.4 represents the properties of field backfill (FB) brought from the slurry wall construction site at Rocanville, SK.

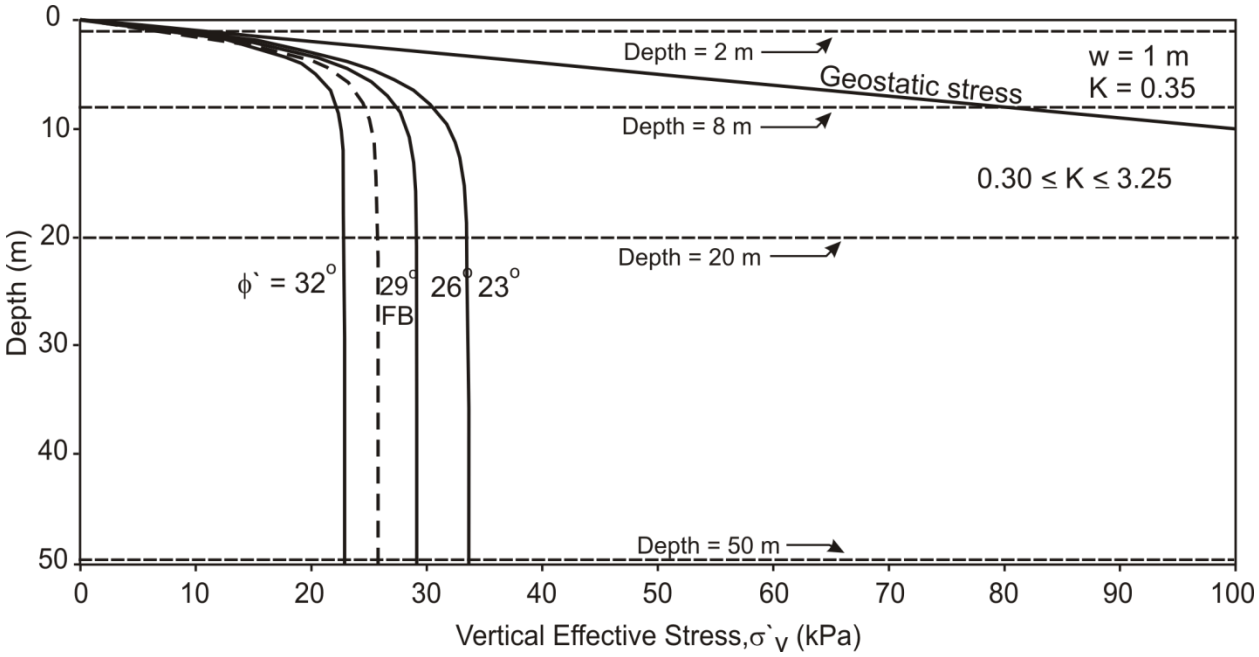

Figure 5.4 Variation of σ'_v with depth for different angles of internal friction (ϕ') of the SB mix.

Vertical stress in the wall moves away from the geostatic stress with the increase in ϕ'. For all values of ϕ', σ'_v in top 3 m is approximately equal to geostatic stress and thereafter starts to deviate to values less than geostatic stress. With the increase in ϕ, the vertical effective stress decreases. This is because friction along the side walls, which acts upward (Figure 5.3), is a function of ϕ'. Hence, the SB material resists settlement with increasing ϕ'. Although, σ'_v decreases with increasing ϕ', the effect of ϕ' is not overly significant (Table 5.1).

A comparison of σ'_v values for different values of ϕ' at depths of 2, 8, 20, and 50 m is presented in Table 5.1. From the table, the percent differences with geostatic stress and σ'_v at 2 m depth for ϕ' = 23 and 32° can be calculated as 24.2 and 32.9%, respectively; the corresponding percent differences at 50 m depth are 93.3 and 95.43%. Although the

σ'_v value moves towards the geostatic stress with decreasing ϕ' (Figure 5.4), the increase is not significant (Table 5.1). Hence, ϕ' alone has no significant effect on arching in SB walls.

Table 5.1 Comparison of σ'_v values for different ϕ' and depth.

Depth (m)	Effective geostatic stress, $\gamma' h$ (kPa)	Vertical effective stress, σ'_v (kPa) for different effective angle of internal friction ϕ' (degrees)			
		23	26	29	32
2	20.00	15.16	14.58	14.00	13.42
8	80.00	30.58	27.42	24.65	22.19
20	200.00	33.57	29.26	25.76	22.85
50	500.00	33.65	29.19	25.77	22.86

The coefficient of lateral pressure, K, is related to the vertical (σ'_v) and horizontal (σ'_h) effective stresses. Figure 5.5 shows the variation of vertical effective stress in the SB wall for different K values for w = 1 m and ϕ' = 29°. K values considered were 0.35, 0.40, 0.50, 0.60, and 0.70. With an increase in K, the stress distribution with the depth moves away from geostatic stress distribution. This is because the side friction increases with an increase in K.

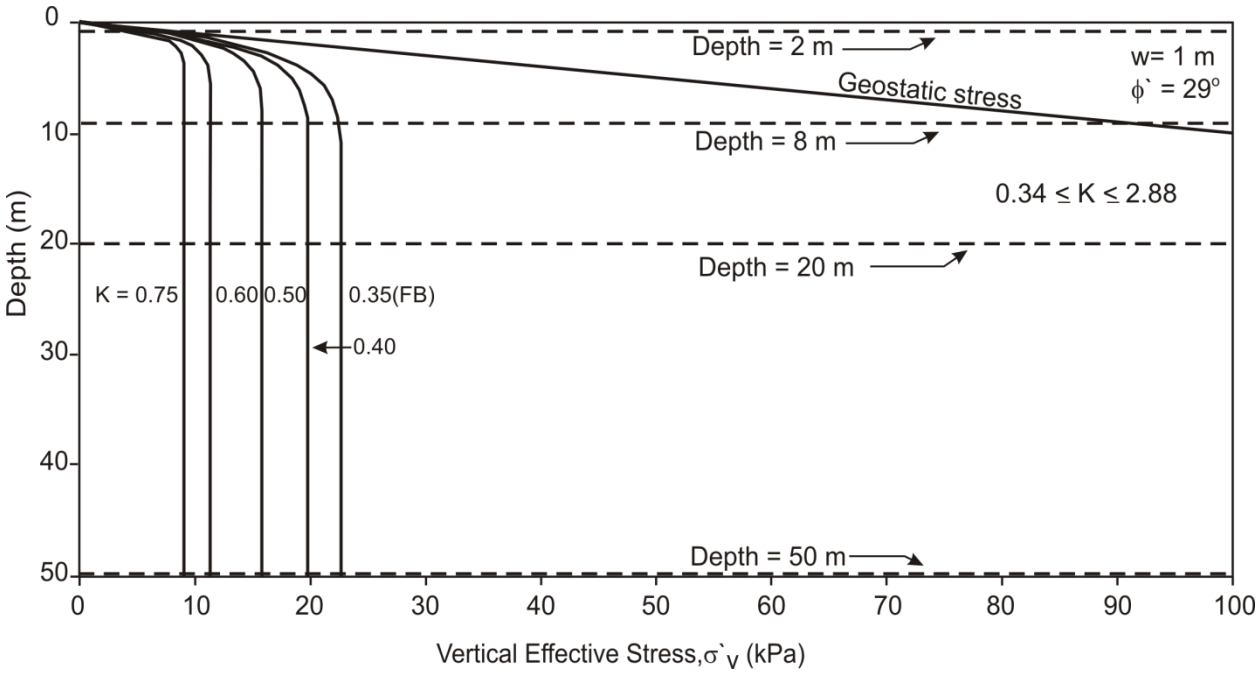

Figure 5.5 Variation of σ'_v with depth for different values of K.

The vertical effective stress in the top 2 m for all K is approximately same. The stress at D = 8, 20, and 50 m decreases as K increases from 0.25 to 0.75. Based on Rankine's earth pressure theory, for ϕ' = 29° the K should lie between 0.34 and 2.88. The percent difference between the geostatic stress and σ'_v at 50 m depth for K = 0.35 and 0.75 is 95.4 and 98%, respectively. This difference is not significant. Hence, K alone has no significant effect on arching in the SB walls.

Table 5.2 Comparison of σ'_v for different K at different depths.

Depth (m)	Effective geostatic stress, γ'_h (kPa)	Vertical effective stress, σ'_v (kPa) for different coefficient of lateral earth pressure, K (σ'_h/σ'_v)				
		0.35	0.40	0.50	0.60	0.75
2	20.00	13.42	12.73	11.50	9.54	8.20
8	80.00	21.19	19.05	14.90	11.46	9.17
20	200.00	22.35	20.00	14.55	11.47	9.18
50	500.00	22.86	20.50	16.00	11.47	9.18

The width of the wall plays a significant role in designing SB walls. If possible, the wall should be designed with larger widths (Figure 5.2). The stress distribution using trial mix 3 (TM3) would result in the least arching (Figure 5.6). The vertical effective stress at 50 m depth is 22, 25, 29, and 36 kPa for TM1, FB, TM2, and TM3, respectively. All of these stresses are approximately 90% less than the geostatic stress (γ'_h) at the same depth.

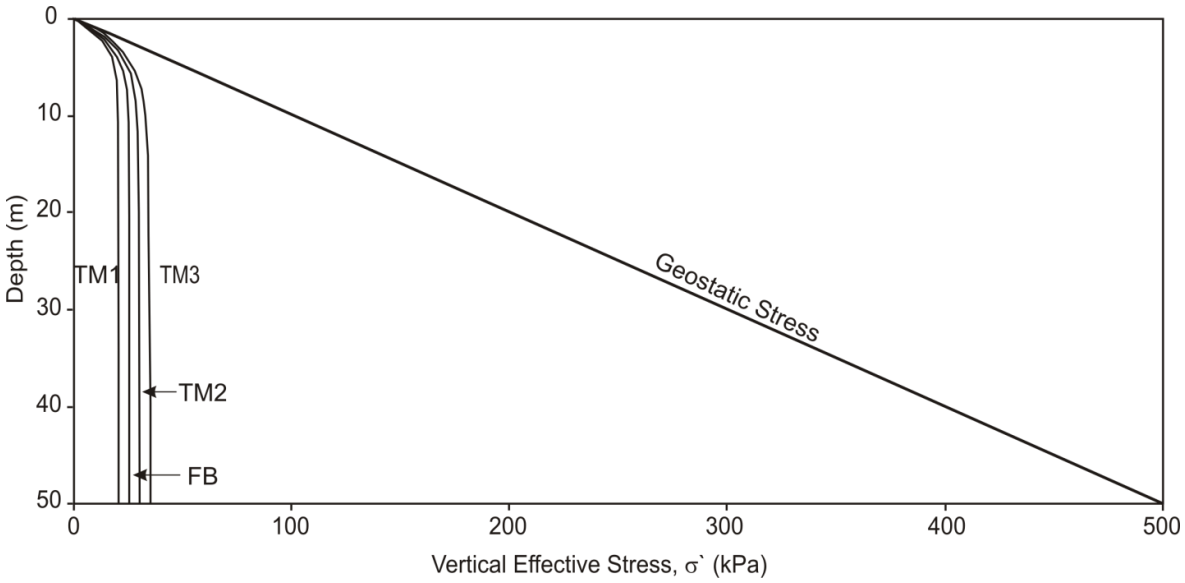

Figure 5.6 Vertical stress distribution for different SB mixes used in the present study.

5.4 Finite element model (FEM)

A finite element model (FEM) for soil-bentonite cut-off walls was developed for this research program. The model simulates the consolidation of the backfill material. Finite element software "GeoStudio 2010", developed by GEOSLOPE International, Calgary, was used for the analysis. Seep and Sigma packages in GeoStudio were coupled for this work to simulate fully coupled behaviour. The coupled analysis simultaneously solves two groups of nodal equations—equilibrium (stress-deformation) and continuity (flow) equations—across the finite element mesh (GEOSLOPE 2010). The basic material parameters required for such analyses on fully saturated systems are: Young's modulus, E'; Poisson's ratio, υ; unit weight of the material, γ'; and saturated hydraulic conductivity, k. However, the software does not take into account secondary consolidation and deformation due to creep.

5.4.1 Model applied to 1-D consolidation

Before proceeding to the analysis of the slurry wall, the methodology was used to model 1-D consolidation and compared with Terzaghi's analytical solution. A finite element model should be always validated before using it for new analyses. This task can be achieved by either validating the model with field values or by reproducing a well documented previous model. In the present work, a 1 m deep and 0.2 m wide trench is modelled using Terzaghi's one-dimensional consolidation theory (Figure D1, Appendix D). The results (Figure D2) are compared with the analytical solution obtained by hand calculations using isochrone curves. Although they do not exactly match, the shape of the curves are in agreement. While impossible to tell which solution is more correct, neither would likely exactly match the laboratory findings. However, the curves in Figure D2 are sufficient to indicate that the solution predicted by the numerical model agrees in principle with the consolidation solution.

5.4.2 Outline of finite element model

The model domain was delineated as a 1 m wide soil bentonite column from the top of the ground surface and keyed at a depth of 50 m into a stiff material, such as heavily consolidated clay or bedrock (shale, in this case). Simplified representation of the complex site geology at Rocanville, SK is shown in Figure 5.7. No intermediate aquifers were considered in this section (Figure 5.8). In a later section of this thesis (Appendix G), an aquifer was included to study the vertical stress distribution with depth in an SB wall. Here, only a fully saturated SB wall was modelled, with a water table present at the top. The hydraulic and stress boundary conditions used in the model are laid out in Table 5.3.

The key assumptions required for this simplification are as follows:

1. The filter cake (Section 2.2, Chapter 2) remains intact on the SB wall. It never falls apart, i.e., during filling or at any other time thereafter.
2. The stiffness of the heavily consolidated adjacent till is assumed to be several orders of magnitude higher than that of the SB backfill material.

3. The hydraulic and stiffness properties of the till are uniform throughout.
4. There is a lateral flow of water due to consolidation of the SB material into the till. A hydrostatic state is assumed in the till (except in Appendix F, where lateral flow of water is not allowed but drainage through the top of SB wall is allowed).

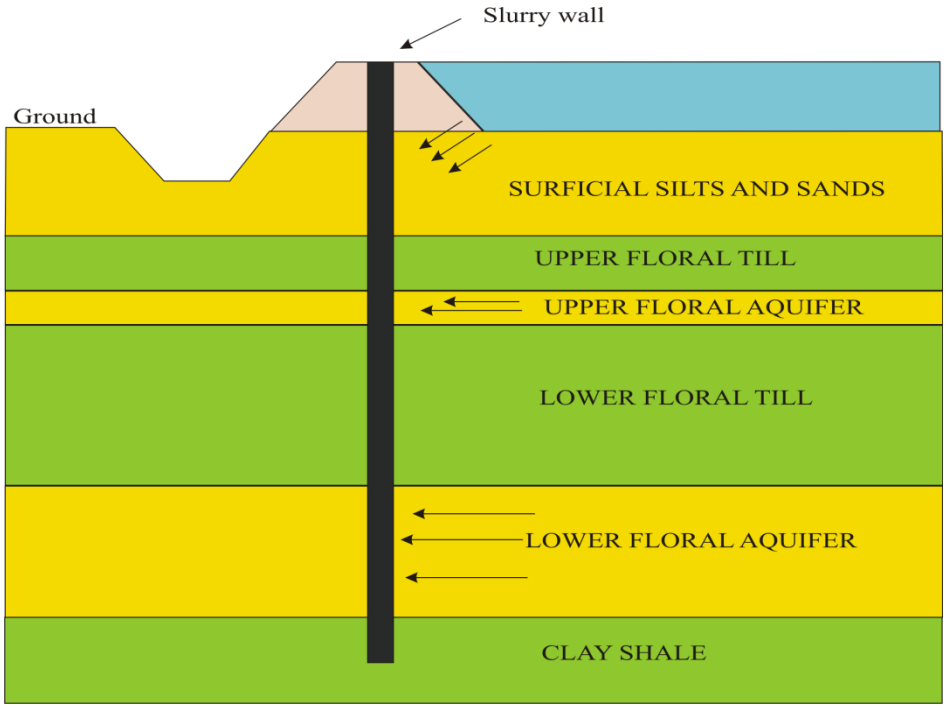

Figure 5.7 Schematic representation of complex site geology.

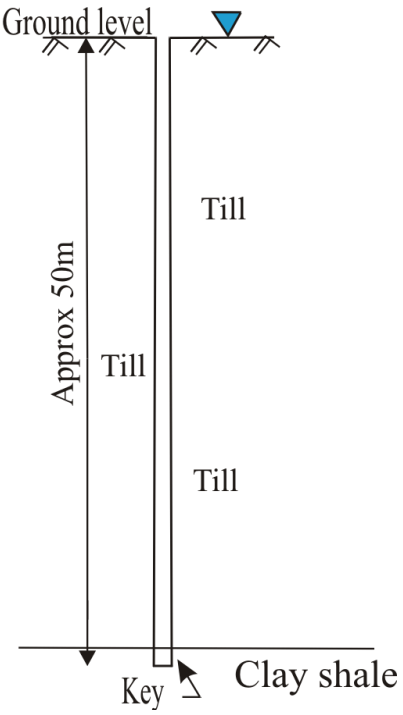

Figure 5.8. Cross-section of an SB wall without an intermediate aquifer.

Table 5.3 Boundary conditions used in the FEM analysis.

Type of analysis	Flow boundary	Displacement boundary
In situ	Water table at top	Sides: x direction fixed (∑x = 0) Bottom: x & y direction fixed (∑x and ∑y = 0)
Transient	Water table at top (Inherited from in situ analysis) Zero pressure at top Seepage into side walls (Hydrostatic condition in till outside trench)	Sides and bottom: fixed (∑x and ∑y = 0)

The full stratigraphic depth of the till was characterized by drilling. It was confirmed that the site has inter-bedded aquifers. These aquifers flow into the Qu'Appelle River, which flows adjacent to the site. The aquifers are located at 10 to 45 m depth at different locations along the wall. Thus, the adopted model has a depth of up to 50 m and is

keyed into the bedrock (higher stiffness and lower hydraulic conductivity) at the site. This assumes that the SB wall would prevent the transport of contaminants from the mine tailings site into the adjacent Qu'Appelle River. Figure 5.8 shows the simplified configuration of the SB slurry wall without an intermediate aquifer.

For in situ analysis, the SB material was assumed to be linear elastic. The initial pore water pressure (PWP) in the in situ analysis is established using a water table at the top of the fill. Initial excess pore water pressure for the transient analysis at a given depth is γH. The finite element program can also compute these values using "in situ" stress computations. The SB material in the transient analysis is assumed to be elastic-plastic and isotropic. Previous researchers (Fahey et al., 2009) have made similar assumptions (Section 2.6).

The elastic and hydraulic parameters of the glacial till were assumed to be constant for the entire period of simulation (i.e., until all of the excess pore pressure has dissipated). The parameters were assumed to be several orders higher in magnitude than the adjacent SB material. This assumption is based on the fact that the preconsolidation pressure of the glacial till is on the order of 1800 kPa (Sauer et al., 1993). In the model, this condition is achieved by restraining the movement of the trench walls in x and y directions and also assigning a no flow condition to the boundary, where the filter cake is assumed to be impermeable.

5.4.3 Defining material properties

The material parameters used for the model were obtained from the results of the laboratory tests conducted as a part of the present study (Chapter 3). Direct shear box tests were conducted on all of the samples to determine their frictional properties (ϕ') for the SB mixes (Section 3.4.4). The effective Young's modulus, E', and hydraulic conductivity, k, required as inputs to the model were obtained from the large strain consolidation experimental results. Constant head hydraulic conductivity (k) tests were conducted on all of the SB mixes as described in Chapter 3, Section 3.4.5. The effective

Poisson's ratio, υ, was calculated using the relation $\upsilon = \frac{K}{1+K}$, where, K is the measured coefficient of lateral earth pressure (Section 3.4.5).

Volumetric water content (θ) is the ratio of the volume of water present in the soil voids to the total volume of the soil. In geotechnical engineering practice, θ is defined as a product of the porosity of the soil and the degree of saturation (θ = nSr). In the present study, the SB mixes used were completely saturated (i.e., Sr = 1); hence, θ = n. Table 5.4 summarizes the various soil properties for SB mixes used in the present study. The composition of the various SB mixes was described in Table 3.2, Section 3.2.2. Trial mix 1 (TM1) had the least amount of fines and TM3 had the highest.

Table 5.4. Soil-bentonite (SB) mix properties as used in the modelling.

Mix	Saturated hydraulic conductivity, k_{sat} (m/s)	Porosity, n	Measured coefficient of lateral earth pressure, K	Poisson's ratio, υ	Calculated effective Young's modulus, E' (kPa)	Effective coefficient of friction, ϕ' (degrees)
TM1	1.88×10^{-7}	0.45	0.3618	0.266	0.95×10^{4}	32°
FB	1.98×10^{-9}	0.40	0.3514	0.260	0.57×10^{4}	29°
TM2	8.99×10^{-10}	0.38	0.3426	0.255	0.43×10^{4}	26°
TM3	3.99×10^{-10}	0.31	0.3416	0.254	0.32×10^{4}	23°

All of the soil properties listed in Table 5.4 decrease with an increase in fines content in the backfill mix. The k_{sat} values in the table are from laboratory measurements, after k became constant with increasing vertical pressure (form the straight line portion of Figure 4.6). These values simulate depths of 15 m below ground surface (Table 3.3, Section 3.3.3). Porosity, n, for the SB mixes was calculated using the relationship between porosity and the density of the soil, where $n = 1 - \frac{\text{Bulk density}}{\text{Particle density}}$. The effective Young's modulus, E', is calculated from the large strain consolidation curves. Appendix C shows the detailed procedure for calculation of Young's modulus for SB mixes.

Figure 5.9 shows the SB backfilled trench along with the boundary conditions used in the present analysis. A close view of the hydraulic boundary conditions used in the transient analysis is shown in Figure 5.10. Two different FEM models, varying the drainage boundary condition (top drainage only vs. top and side drainage) of the deep slurry trench were modeled. Because the preconsolidation pressure of the till is high (Section 3.4.2), the boundaries of the SB trench are constrained in both the x and y direction. To allow drainage through the vertical boundary, a total head condition (T_h = 50 m) is applied along the entire boundary. This is based on the assumption that the pore pressure regime in the till (adjacent soil) is hydrostatic. To simulate the interface elements (i.e., the elements at the boundary of the till and slurry wall), thin vertical strips (red strips in Figure 5.10(b)) were assigned k values similar to the adjacent till material ($k = 10^{-8}$ m/s).

For the transient analysis, the associated hydraulic and stress-strain boundary conditions mathematically required at the two ends, top (h = 0) and bottom ($h = h_{max}$), of the one-dimensional-response domain are:

1. Top boundary condition
   a. Stress-strain boundary
      - $\frac{d\sigma(0,t)}{dt}$ = 0, as there is no loading on the top; self weight consolidation.
   b. Hydraulic boundary
      - U(x,0,t) = constant, as the water table at the top is assumed to be constant; 0≤x≤B
2. Bottom boundary condition
   a. Displacement boundary condition (no displacement; fixed boundary)
      1. v (x, h, t) = 0; where v is the vertical displacement; 0≤x≤B
      2. u (x, h, t) = 0; where u is the horizontal displacement; 0≤x≤B
   b. Hydraulic boundary
      - q_y (x, h , t) = 0 ; impervious (zero water flux); 0≤x≤B

where q_y = water flux in the y direction (i.e., volume of water flowing through a unit cross-sectional area perpendicular to the y axis per unit time).

3. Side boundary condition
   a. Displacement boundary condition
      - u (0, y, t) = 0; v (0,y,t) = 0 ; 0≤y≤h
      - u (B, y, t) = 0; v (B, y, t) = 0; 0≤y≤h
   b. Hydraulic boundary

      For total head, T_h = 50 m
      - H(0,y,t) = T_h ; 0≤y≤h
      - H(B,y,t) = T_h ; 0≤y≤h

5.4.4 Numerical solution approach

The stress and transient flow problems (the governing equations) were simulated using the coupled load-deformation and seepage finite element numerical modelling packages, SIGMA/W and SEEP/W, respectively (GEOSLOPE 2010a,b). These packages were operated from a high speed personal computer using Microsoft's Windows XP operating system. The coupled stress and pore-pressure (coupled Sigma/W and Seep/W) mode is used for the analysis of consolidation type problems (all on Sigma/W interface) (GEOSLOPE 2010). The basic material parameters required for such analyses on fully saturated systems are the effective Young's modulus, E'; drained Poisson's ratio, υ; porosity, n; and saturated hydraulic conductivity, k. Numerical models can simulate two-dimensional or axi-symmetric domains and their corresponding element types (GEOSLOPE 2010). A two-dimensional model domain, one element wide, was used to represent the one-dimensional regime described by the governing equations. The model was constrained laterally (hydraulically and mechanically) with the appropriate boundary conditions to achieve the one-dimensional behaviour (e.g., Fahey et al. 2009, p.14). These included zero deflection in the stress-deformation analyses and zero water flux boundary conditions for the hydraulic analyses placed along base of the domain. The top boundary had specified stress and total head (hydraulic) boundary conditions. The model setup indicating most of the typical boundary conditions is shown in Figure 5.9.

5.4.5 Boundary conditions

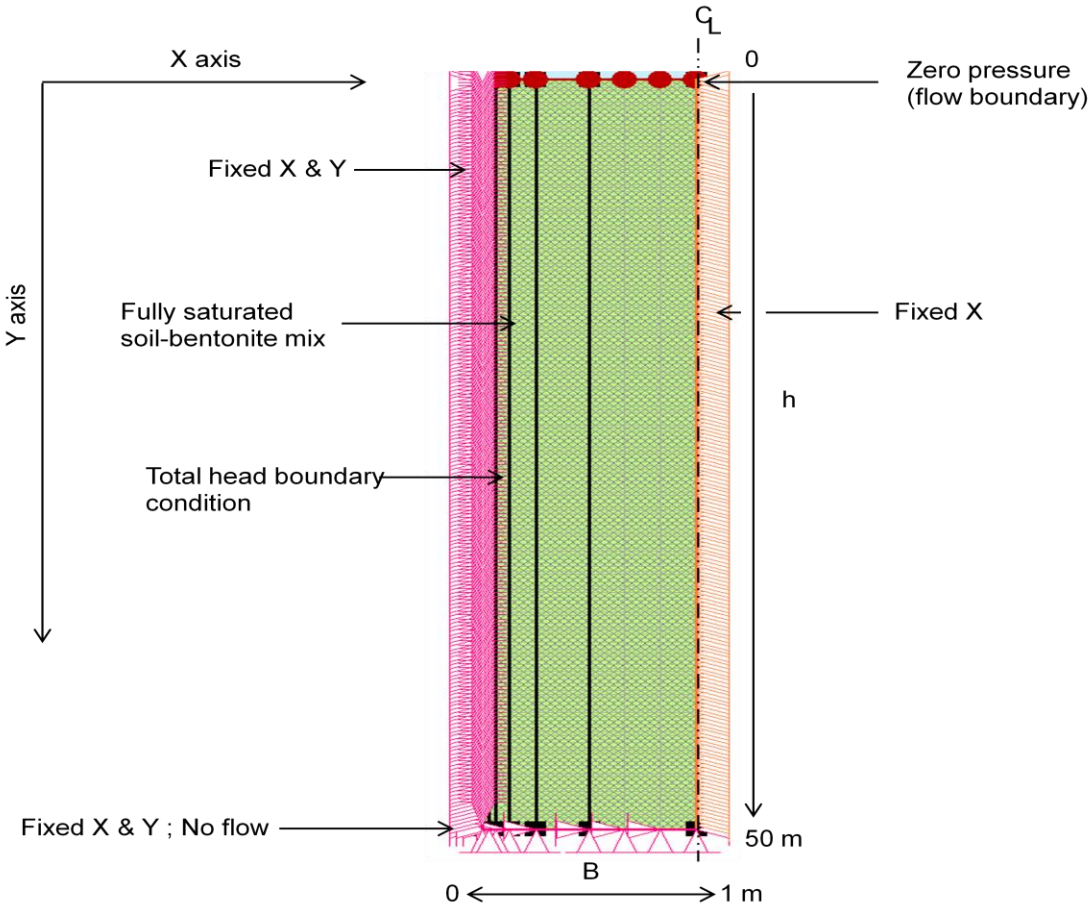

Figure 5.9. Fully saturated system showing boundary conditions.

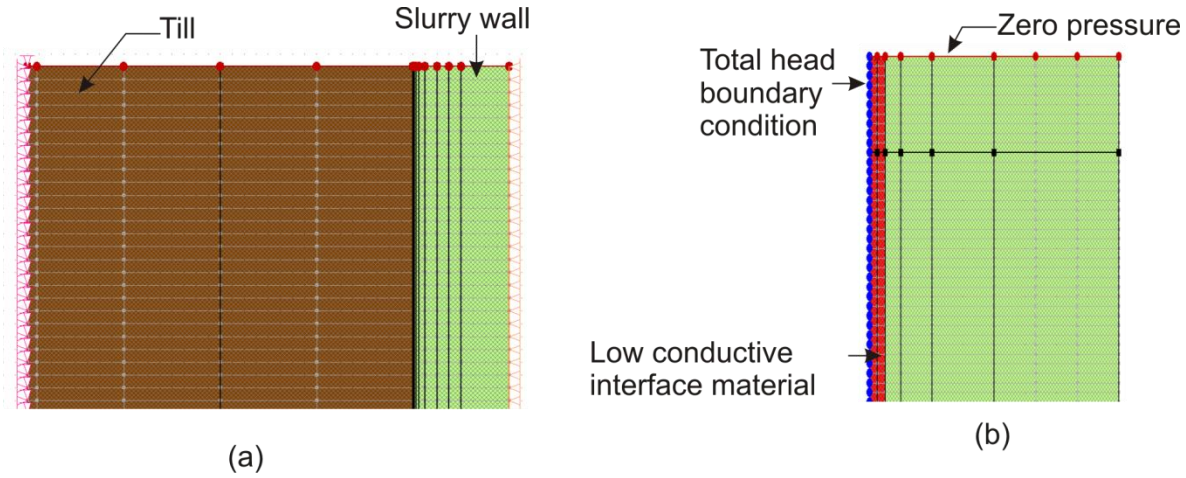

Figure 5.10. Closer view of hydraulic boundary conditions.

5.5 Discussion of results from the finite element method

5.5.1 Overview of the modelling process

Designing a SB wall without correctly understanding the vertical stress distribution may lead to failure of the walls in terms of function. Low hydraulic conductivity (k), which is the design requirement, is a function of vertical effective stress in these walls. Hence, it is important to correctly estimate the vertical stress distribution in SB walls as the vertical stresses in the field never reach geostatic stress conditions (Khoury et al., 1992; Baxter, 2001). This is attributed to “arching” (Section 5.3) in the narrow SB walls.

A parametric study using a discrete model was conducted to investigate the sensitivity of fines (particles less than 75 μm) to arching (reduction in vertical effective stress, σ'_v) in SB walls (Section 5.3). Arching decreases with increasing fines content (Figure 5.6). Although there is a decrease in arching with increasing fines content (i.e., stress moves towards geostatic stress), the vertical stress at any given depth is not significantly different for different mixes.

The following section presents the stress distribution pattern predicted using the finite element method and its comparison with discrete model predictions.

5.5.2 Arching of stresses in soil-bentonite walls

At any given time, pore pressure varies with the depth of the slurry wall, as shown in Figure 5.11. Dissipated pore pressure is the total amount of pore pressure dissipated (drained) due to consolidation of the SB material. Excess pore pressure is the amount of extra pore pressure in the system that should dissipate for the system to be at hydrostatic pressure, which is steady state in this case. According to Terzaghi’s 1-D consolidation theory, total stress in the system remains constant at any given depth and time. However, in the case of consolidation of SB walls, the total stress decreases with time (Figure 5.12). This change in total stress with time could be attributed to arching in SB walls.

In the finite element study, the properties of the field backfill (FB) were used (Table 5.4) to model the SB walls. Seepage of water into the adjacent stiff material was allowed in the FEM model.

It is important to wait for excess pore pressure to dissipate completely as it reflects the end of consolidation (primary consolidation). In the present case (Figure 5.13), it takes 1.75 years to dissipate more than 95% of the excess pore pressure. With the increase in fines content of the mix, the time required for this to occur increases (Appendix F). This is because the amount of void in the soil matrix decreases with increasing fines content of the mix.

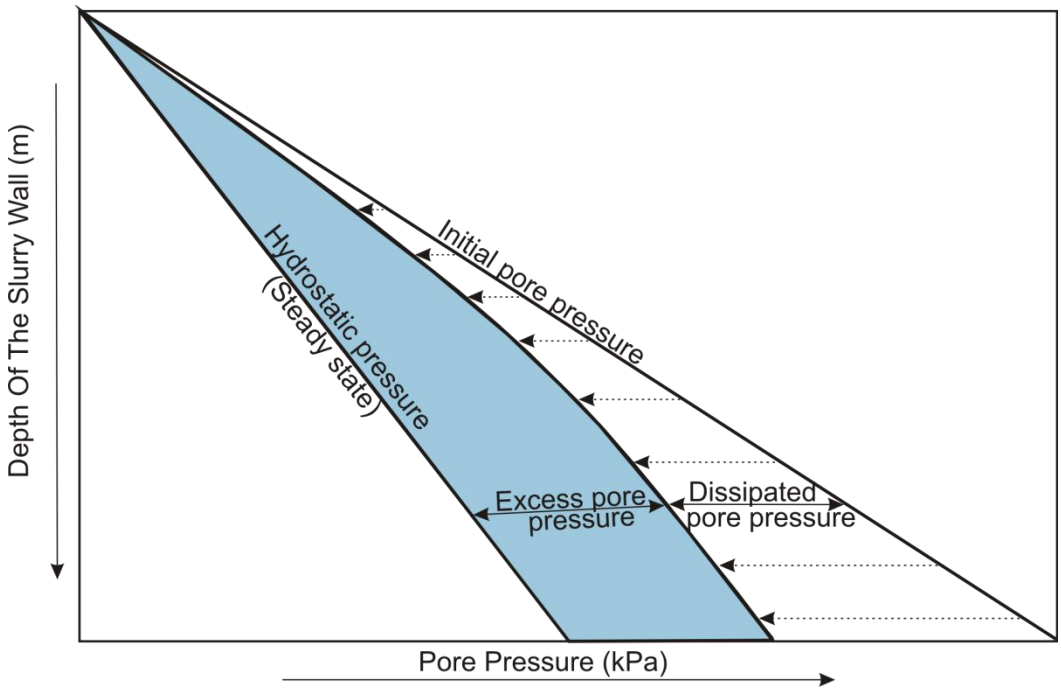

Figure 5.11 Pore pressure regime in the slurry walls.

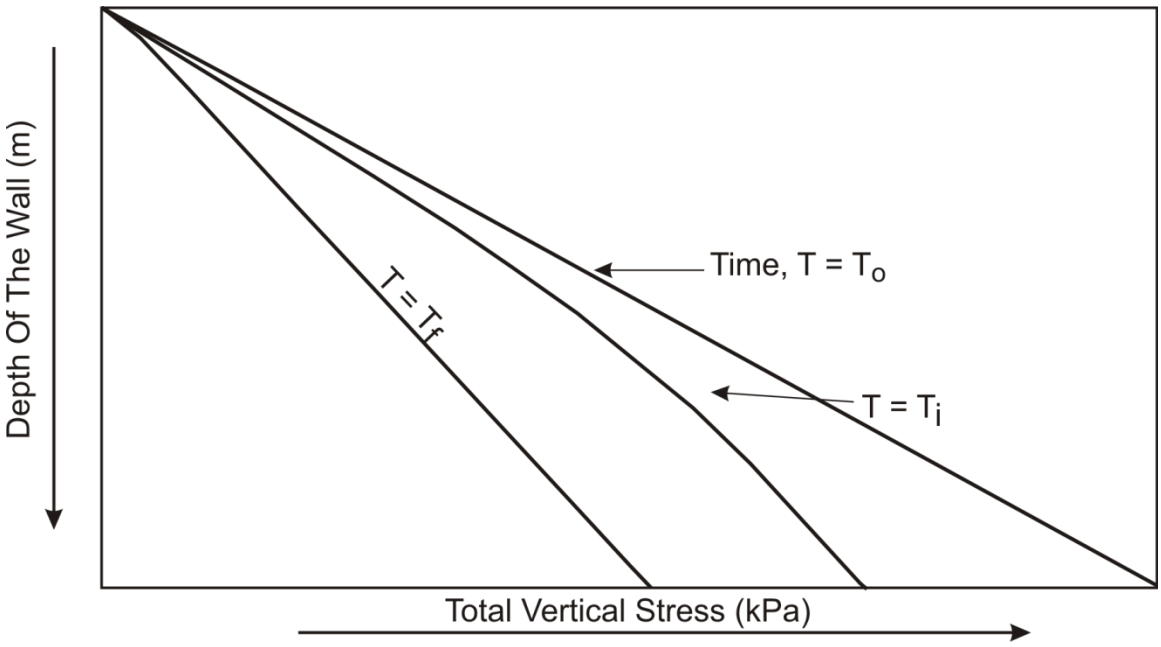

Figure 5.12. Variation of total vertical stress with depth of the wall and time.

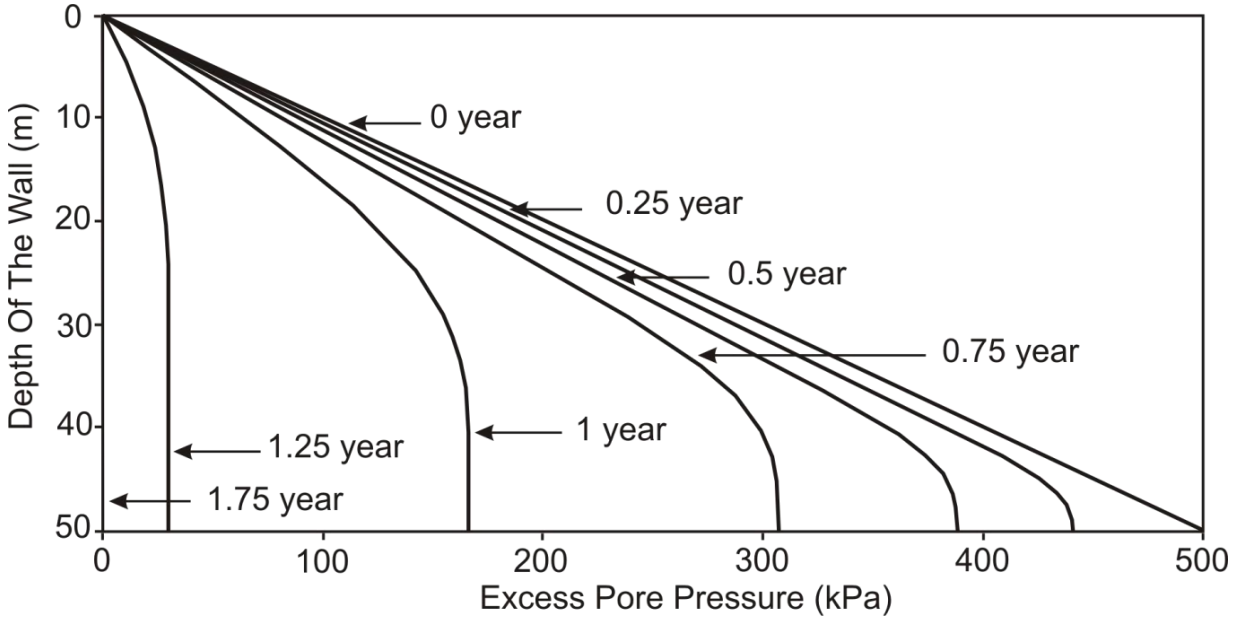

Figure 5.13. Dissipation of excess pore pressure with time.

Construction of SB slurry walls is a remediation technique to contain waste at contaminated sites. An 11 km long SB slurry wall is being constructed around a potash mine tailings management area (TMA) to retard and prevent the flow of brine into the

nearby aquifers and water channels. The top few metres of the wall are prone to attack by brine, which can cause osmotic consolidation; hence, it is important to understand the vertical effective stress distribution in SB walls with depth of the wall and with time. The variation of σ'_v with depth of the wall and with time for the FB mix is shown in Figure 5.14. Similar curves for the other trial mixes (TM1, TM2, and TM3) are shown in Appendix F. At any given depth along the wall, the time required for the vertical effective stress to build up increases with increasing fines content in the SB mix. For example, the vertical effective stress at time T = 0.5 years at 20 m depth for TM1 and TM3 is 6 and 2 kPa, respectively. This is approximately 65 and 95% less, respectively, than the effective stress at the same depth at the end of consolidation.

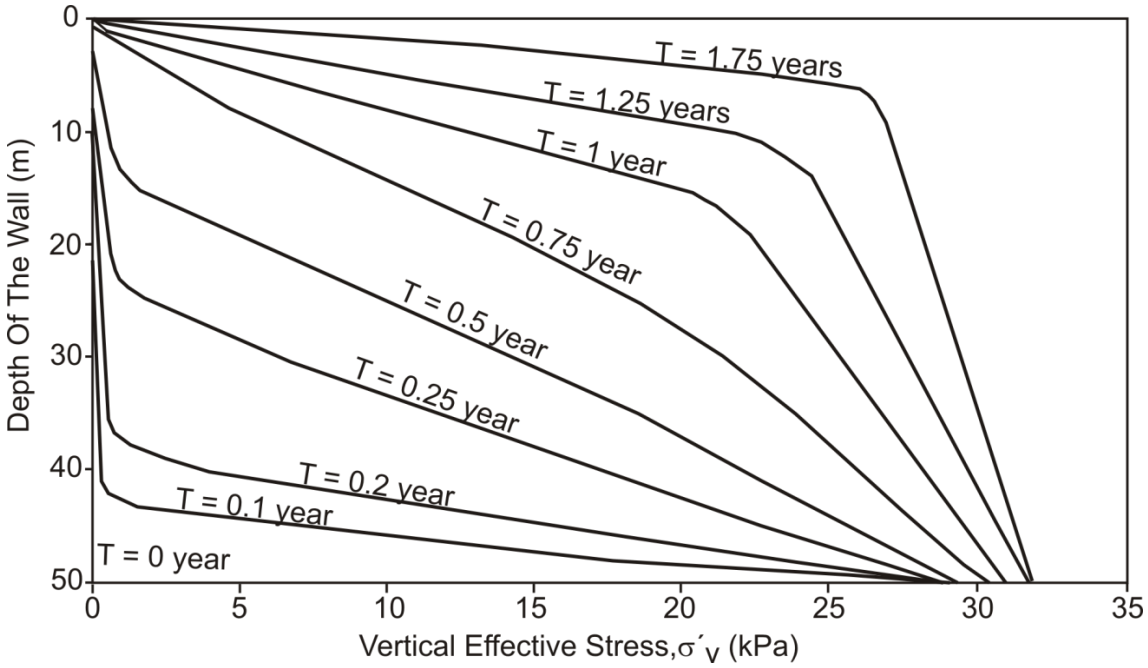

Figure 5.14 Variation of vertical effective stress (σ'_v) with time.

The vertical effective stress distribution shown in Figure 5.15 includes for comparison the "Final" σ'_v at the end of consolidation, i.e., when all of the excess pore pressure has dissipated. In the case of the FB mix, it took 1.75 years (Figure 5.13) for the excess pore pressure to dissipate completely and for a hydrostatic state (steady state in this case) to be reached.

The dashed line in Figure 5.15 shows the vertical stress distribution as predicted by the discrete model. It shows that after a depth of about 5 m from the top, the stress becomes approximately constant with depth. The solid line representing the FEM prediction shows an increasing trend of stress from the top to the bottom of the wall. This is because the self weight of the material adds from the top as the depth of the trench increases.

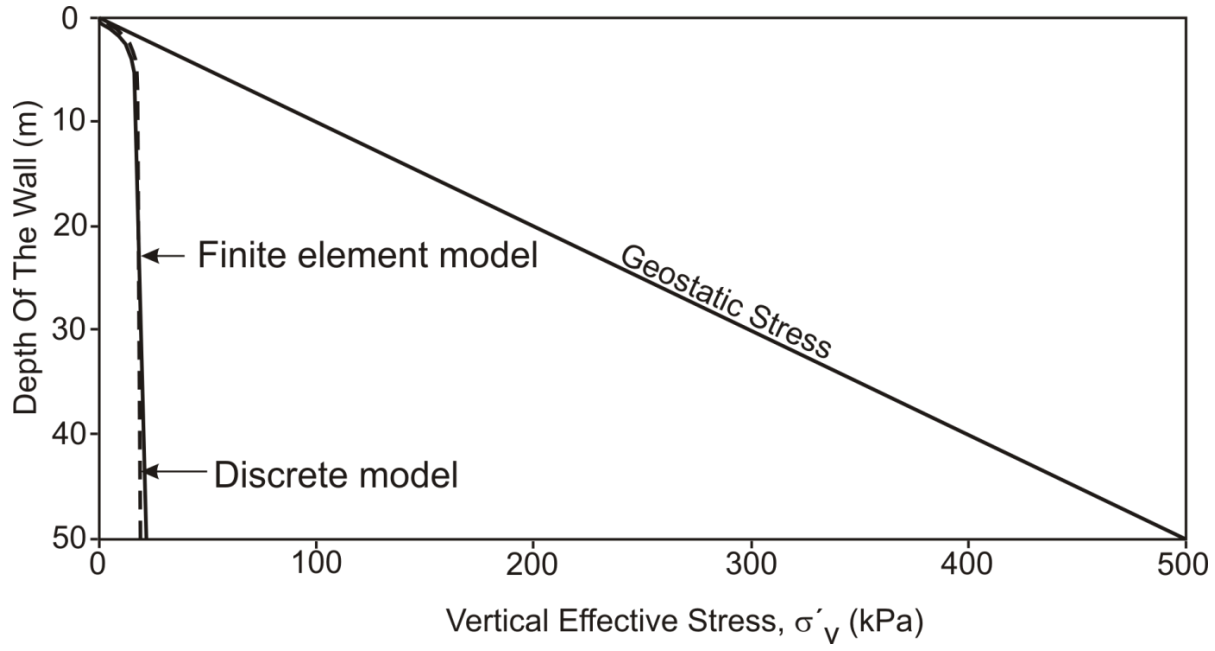

Figure 5.15 Comparison of "final" vertical effective stress, σ'_v, with depth of the wall as predicted by the two models.

The FEM and discrete model predictions seem to match over the entire depth of the wall. As predicted by the FEM and discrete models, the stress at a depth of 5 m from the ground surface is 65.0 and 62.0% less than the geostatic stress, respectively; corresponding values at 50 m depth (at the bottom of the trench) are 96.5 and 95.5% less than the geostatic stress.

A study using FEM was conducted to evaluate the sensitivity of the σ'_v distribution in the walls with depth and fines content. Arching in deep and narrow SB walls decreases with an increase in fines content in the mix (Figure 5.16). This is because the ϕ' of the SB

mix decreases with the increasing amount of fines (Table 5.4). Again, the "Final" σ'_v is the vertical effective stress distribution in the wall after more than 95% of the excess pore pressure has dissipated. The σ'_v values at the bottom of the trench are 20, 31, 33, and 39 kPa for TM1, FB, TM2, and TM3, respectively.

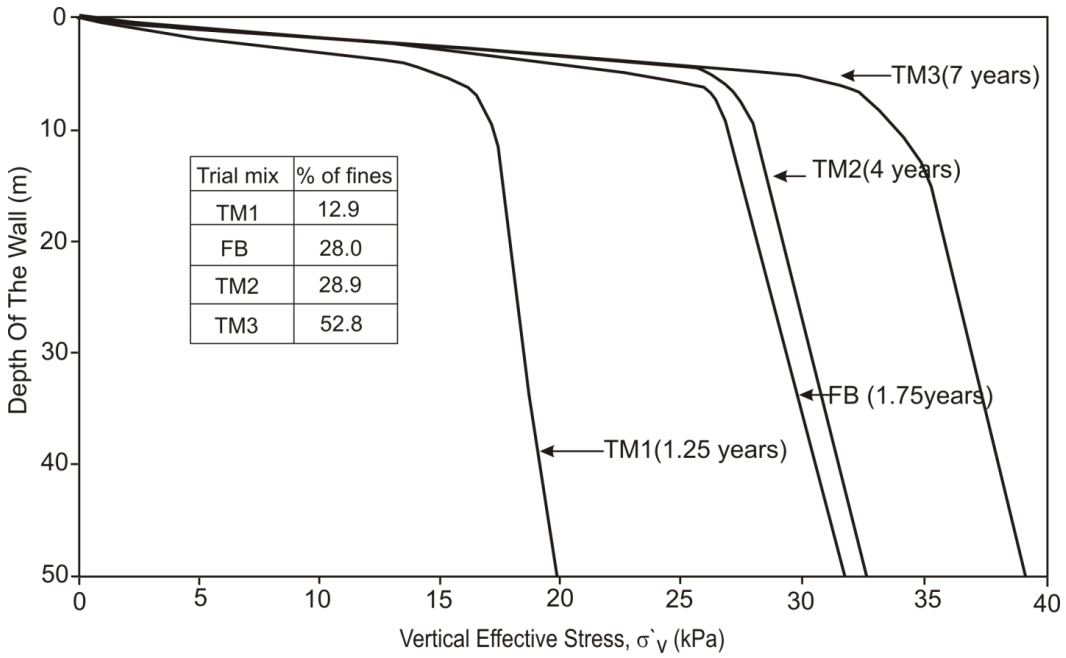

Figure 5.16 "Final" vertical effective stress, σ'_v with depth of the wall.

5.5.3 Estimation of hydraulic conductivity of SB walls

SB slurry walls act as a barrier that prevents the migration of contaminants (brine in this case) from a contaminated site into the regional groundwater regime. They are designed to have low hydraulic conductivity (k) to retard the flow. Hydraulic conductivity of these walls is dependent on the stress state in the wall. In the present study, k with depth and time is estimated using the vertical effective stress (σ'_v) distribution (Figure 5.14) predicted by the FEM model. The vertical effective stress (σ'_v) was related to k using k-σ'_v plots (Figure 4.6) obtained from the laboratory testing program.

The estimated k for the FB mix at different wall depths and times is shown in Figure 5.17. For all time steps, the hydraulic conductivity of the FB mix decreases with the depth of the wall. This is because the vertical effective stress gain at the bottom of the wall is more than at the top (due to self weight of the SB mix) (Figure 5.14). The k values at a depth of 5 m from the top at times of T = 0.5, 1, and 1.75 years (after which more than 95% of the excess pore pressure has dissipated) are 1×10^{-4}, 1×10^{-5}, and 3×10^{-6} m/s, respectively; corresponding values at a depth of 50 m are 7×10^{-7}, 4×10^{-7}, and 3×10^{-7} m/s.

Estimated hydraulic conductivity (k) values for all trial mixes used for this study are shown in Figures 5.18 through 5.20. For any given time, k decreases with increasing fines content in the mix. This is because the "final" σ'_v (Figure 5.16) value increases with increasing fines content in the mix at any give depth. This in turn reduces the void ratio in the soil matrix.

The maximum "final" achievable k values at a depth of 2 m from the top of the wall are 1×10^{-4}, 5×10^{-6}, 9×10^{-7}, and 3×10^{-9} m/s for TM1, FB, TM2, and TM3, respectively.

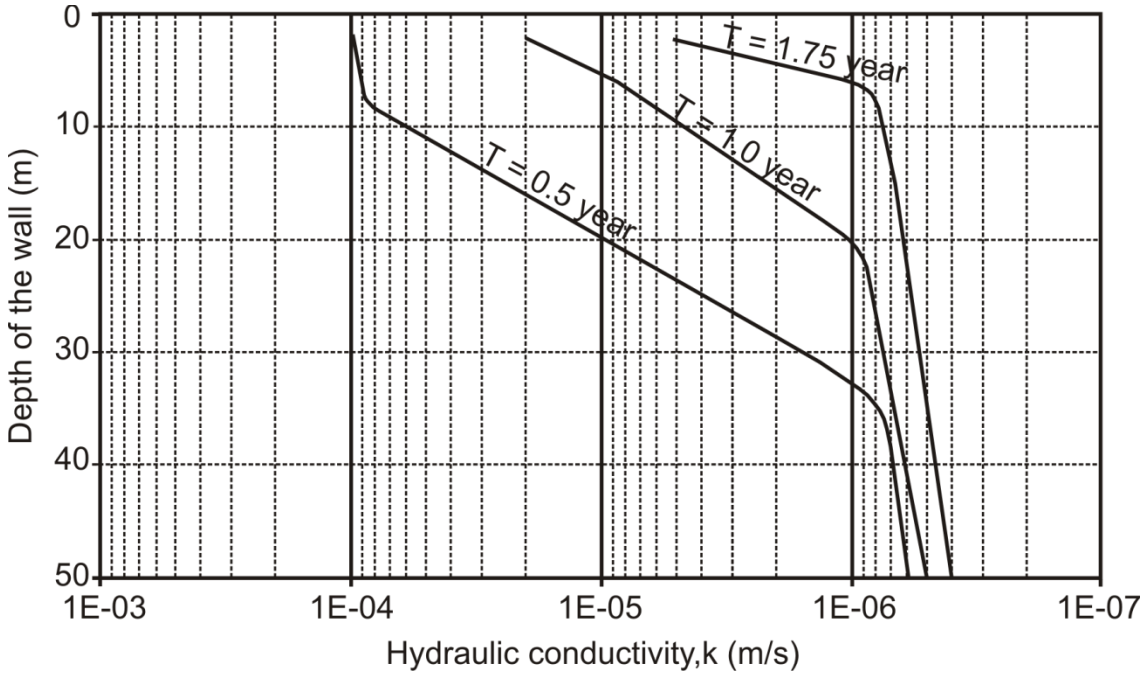

Figure 5.17 Estimated hydraulic conductivity with time for field backfill (FB).

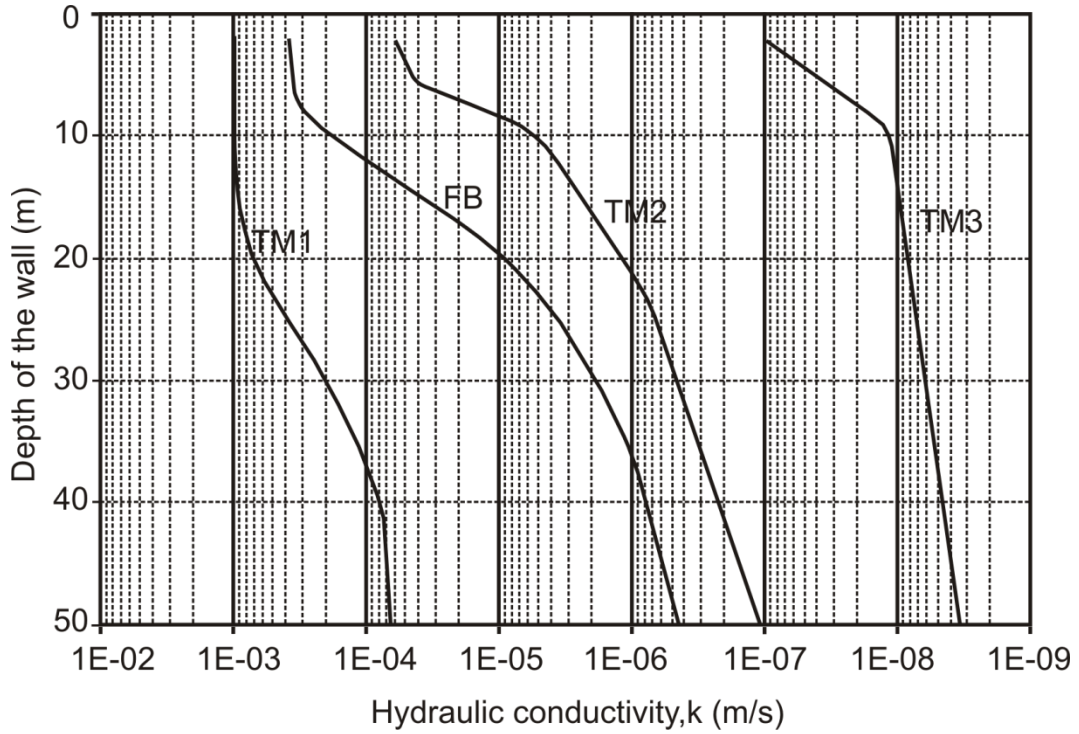

Figure 5.18. Comparison of estimated k for trial mixes at T = 0.5 years.

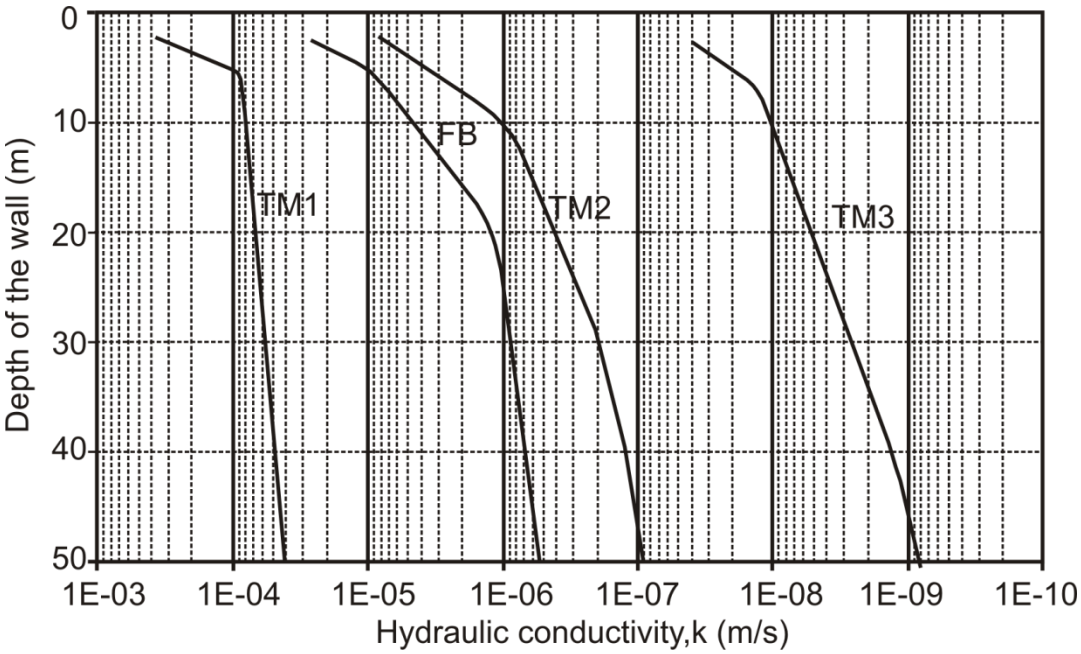

Figure 5.19. Comparison of estimated k for trial mixes at T = 1 year.

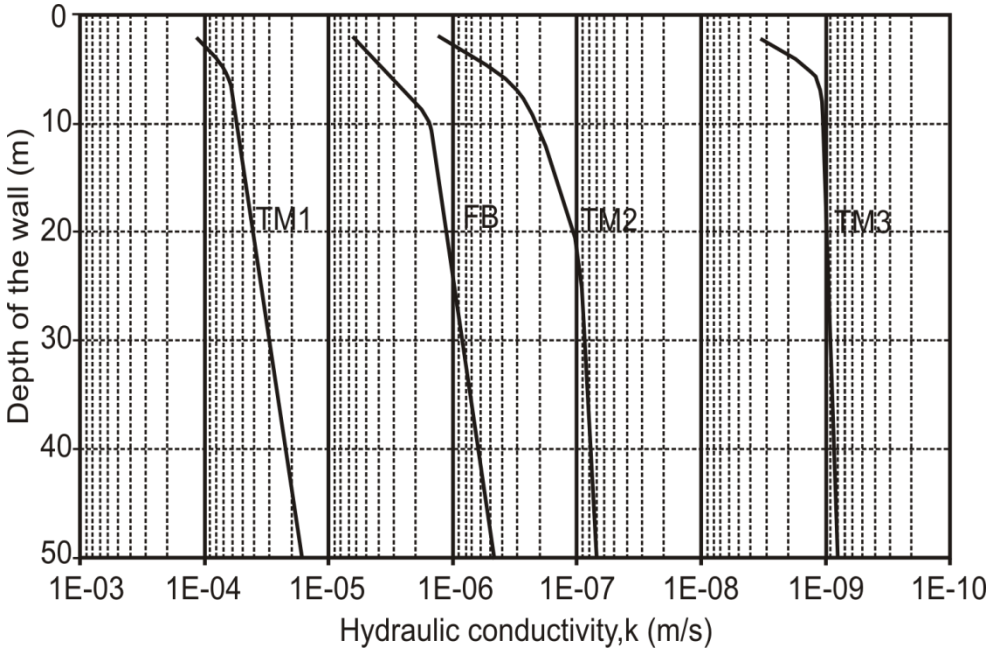

Figure 5.20. Comparison of estimated k for trial mixes at the end of consolidation.

5.5.4 Comparison of SB walls for different drainage conditions

Two different models of the SB slurry walls were used for this study by varying the drainage boundary conditions of the deep slurry trench. This was done to understand the sensitivity of the σ'_v distribution in the wall with drainage boundary conditions. The drainage conditions used are as follows:

1. Top drainage only (Appendix F).
2. Drainage from top and two vertical boundaries (k of the interface vertical elements was also varied).

A comparison of "Final" vertical effective stress for different flow boundary conditions is shown in Figure 5.21. The hydraulic conductivity of interface elements was chosen based on the k test results conducted on block samples of till obtained from Rocanville, SK (M.D. Haug and Associates Ltd., 1998). The interface elements with $k = 1 \times 10^{-8}$ and $k = 1 \times 10^{-13}$ m/s are considered to be two extreme vertical drainage boundaries. A comparison of geostatic stress and vertical effective stress for the SB wall with different drainage conditions at different depths after more than 95% of the excess pore pressure

has dissipated is summarized in Table 5.5 (refer also to Figures 5.22, 5.23). A comparison of estimated steady state ("final") k values for different drainage conditions is shown in Figure 5.22.The σ'_v distribution for interface elements with $k = 1 \times 10^{-13}$ m/s is lesser as compared to $k = 1 \times 10^{-8}$ m/s with the increase in depth. This is because excess pore pressure dissipation through the side boundary would be lesser with lower k. More pore pressure would be dissipated through the top.

Table 5.5 Vertical effective stress in the SB wall for different drainage conditions.

Depth of the wall (m)	Geostatic stress, $\gamma' H$ (kPa)	Vertical effective stress with top drainage only, kPa	Vertical effective stress with horizontal and vertical drainage, kPa	
			$k = 1 \times 10^{-8}$ m/s	$k = 1 \times 10^{-13}$ m/s
10	100.0	12.2	26.5	23.0
20	200.0	13.2	28.0	25.0
30	300.0	14.4	29.0	26.0
50	500.0	17.1	32.0	28.0

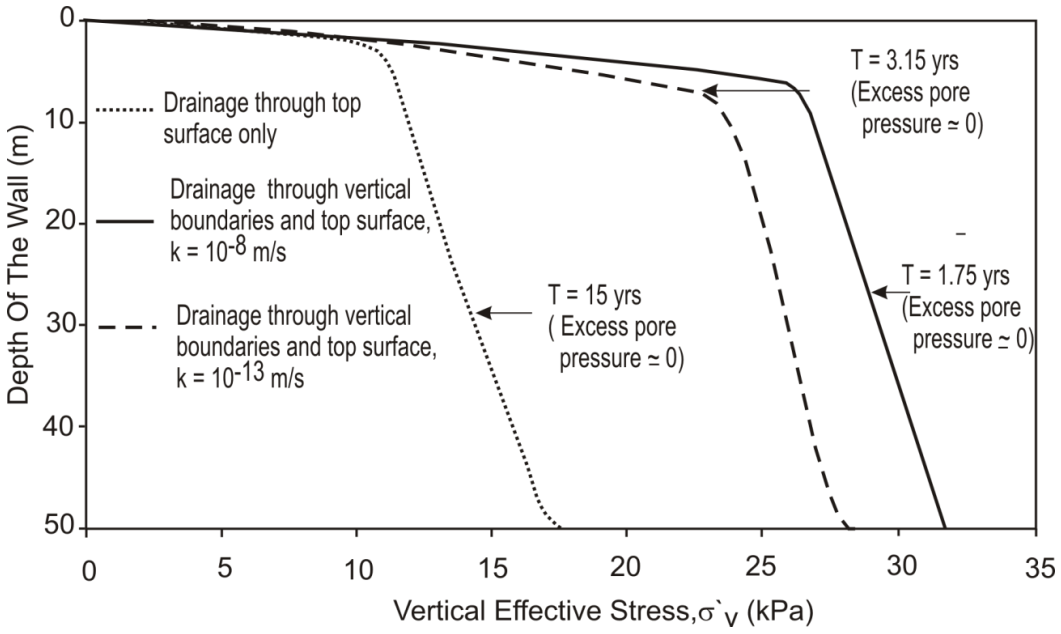

Figure 5.21 "Final" vertical effective stress, σ'_v, with depth of the wall.

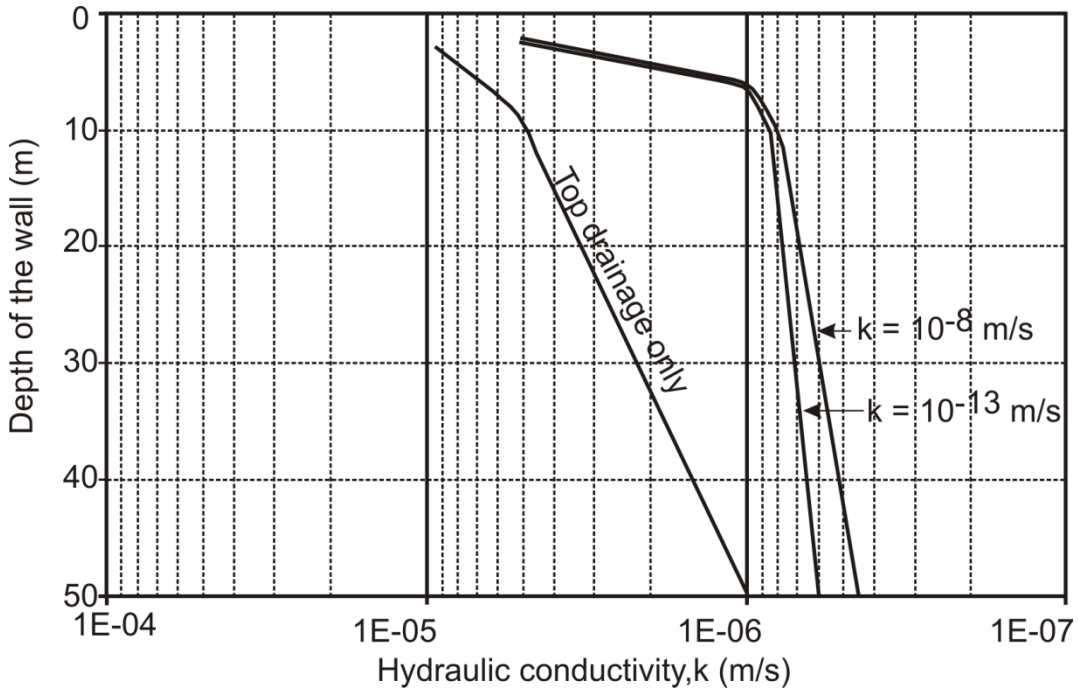

Figure 5.22 “Final” vertical effective stress, σ'_v, with depth of the wall.

5.6 Comparison of finite element models

A comparison of finite element predictions of vertical stress distribution (σ'_v) in a backfill stope made by Fahey et al. (2009) (Section 2.6) with the FEM predictions described in the previous section is presented in Figure 5.23. Fahey et al. modelled the vertical stress distribution in a backfilled stope, 20 m wide and 50 m deep, in a mine in Australia. Plaxis-2D (Version 8.6) software was used for modelling and analysis of the stope. Interface elements were placed on the boundary and the mesh closer to it was refined to allow intense shearing along the boundary. Table 5.6 shows the properties of the backfill materials used by Fahey et al. in their work. The backfilled mix consisted of rock-like materials.

The vertical effective stress distributions match over most of the depth (Figure 5.23). The vertical stress distribution is very close to the geostatic stress distribution up to 20 m depth. The σ'_v values predicted by GeoStudio 2007 and Plaxis 2D at a depth of 50 m are about 24 and 30% less, respectively, than the geostatic stress at the same depth.

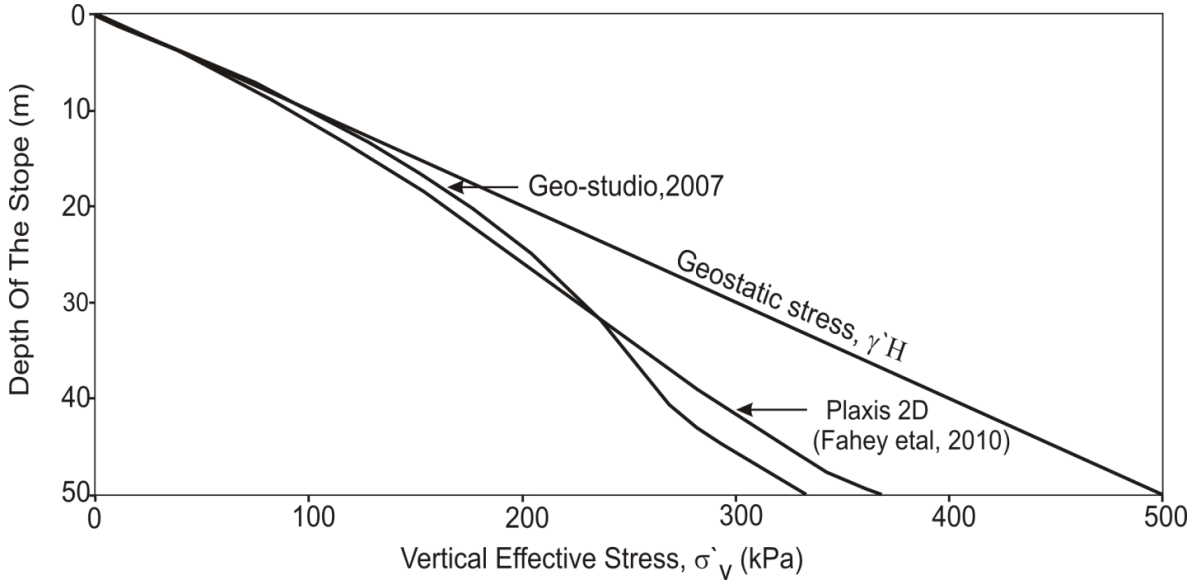

Figure 5.23. Comparison of Fahey et al. (2009) work with results using Plaxis 2D and GeoStudio software.

Table 5.6 Properties of the backfill material.

Properties of the material	Values
Young's modulus, E	10 MPa
Angle of friction, ϕ	45
Poisson's ratio, υ	0.2
Coefficient of permeability , k	1.15×10^{-8} m/s

5.7 Comparison of model predictions with field data

Field instrumentation and monitoring are effective ways to understand any soil-water interaction process. They provide good insight into the real process in the field. However, the finite element method is a faster and effective way of understanding any problem. It helps in predicting long-term behaviour in a cost-effective manner.

Pressure plates and vibrating wire piezometers were installed in the slurry wall at PCS Rocanville, SK in the fall of 2011 and left in place for long-term monitoring. Two pressure plates, one for horizontal stress measurement and the other for vertical stress

measurement, along with the vibrating wire piezometers were housed in a cage (Figure 5.24). Iron rails were attached to the bottom of the cage to make sure that the cage did not move during the backfilling process and afterwards. A data logger was attached to twice daily record pore pressure and total stress readings from the instruments.

The cage and instruments were then lowered to a depth of 47 m from the ground surface (bottom of the trench). It was ensured that the rails aligned longitudinally along the length of the slurry wall. The trench was then gradually backfilled with SB backfill mix.

Total stresses (horizontal and vertical) and backfill elevation measured in the field are shown in Figure 5.25. The secondary Y axis shows the backfill elevation (m). The primary X and Y axes show time (d) and total stress (kPa), respectively. The initial increasing trend simulates the backfill filling, as the stresses and the pore pressure increase with increasing backfill elevation. The decreasing trend of stress and pore pressure at a constant backfill elevation suggests the dissipation of excess pore pressure with time and arching in the SB slurry wall (lack of stress built up with time).

A comparison of the FEM predictions and field measurements with time is shown in Figure 5.26. To compare the results, total stress and pore pressure values from a node at a depth of 47 m from the ground surface were chosen. “Estimated” refers to the results predicted by the finite element model. Both plots show a decreasing trend in stresses and pore pressure. However, the field results have a steeper decreasing trend. This is could be due to “local arching”, as the stiffness of the iron cage (Figure 5.24) is high compared to the backfill material. This difference in stiffness might form an intermediate zone that may hold the consolidating backfill mix in place and prevent it from settling down and applying stress onto the pressure plates.

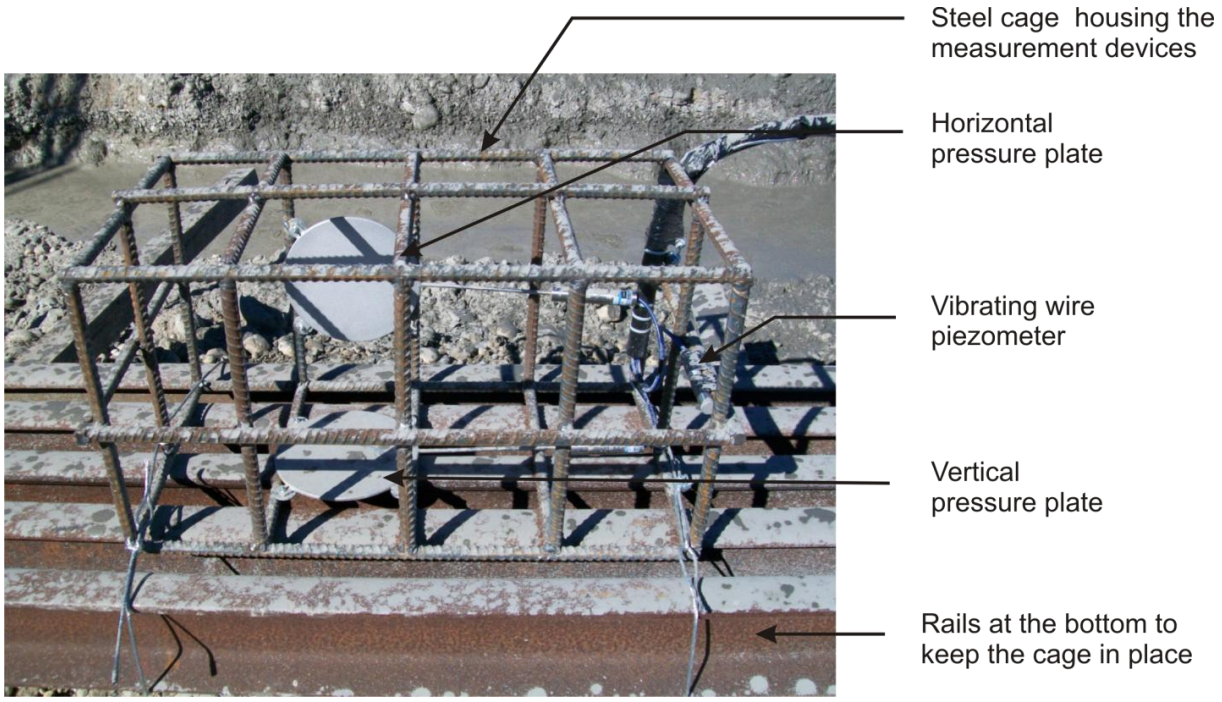

Figure 5.24 Field instrumentation.

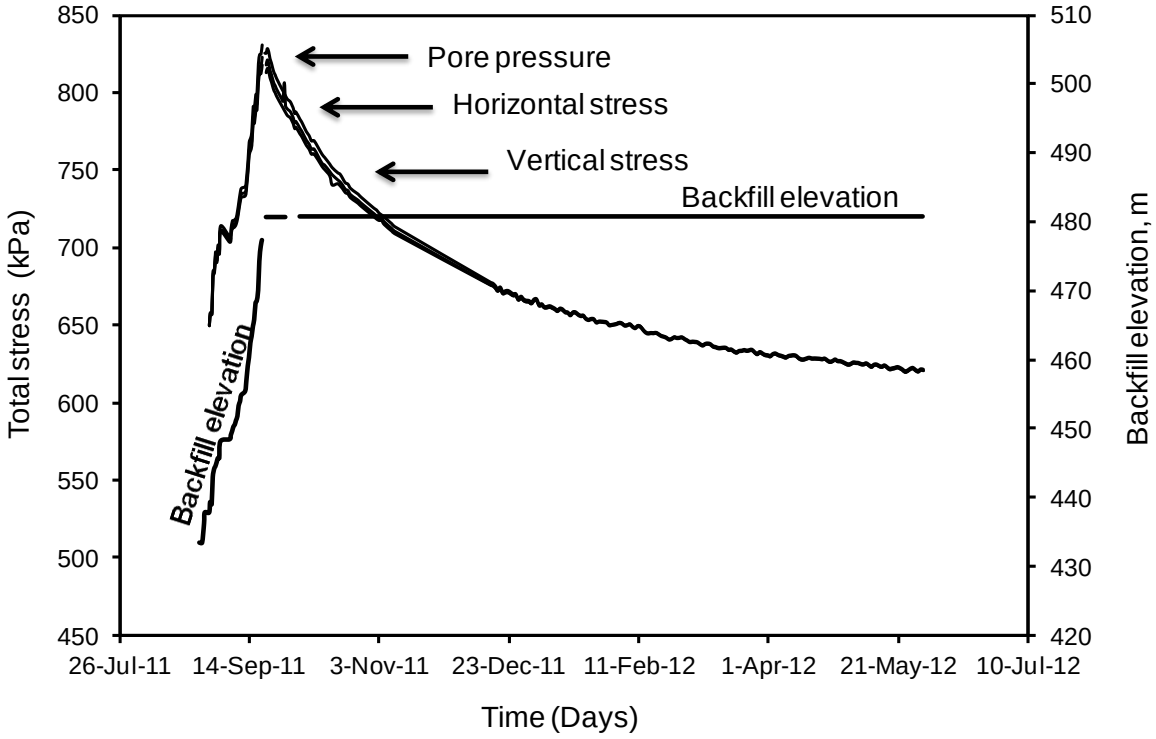

Figure 5.25 Total stress and pore pressure measured in the field.

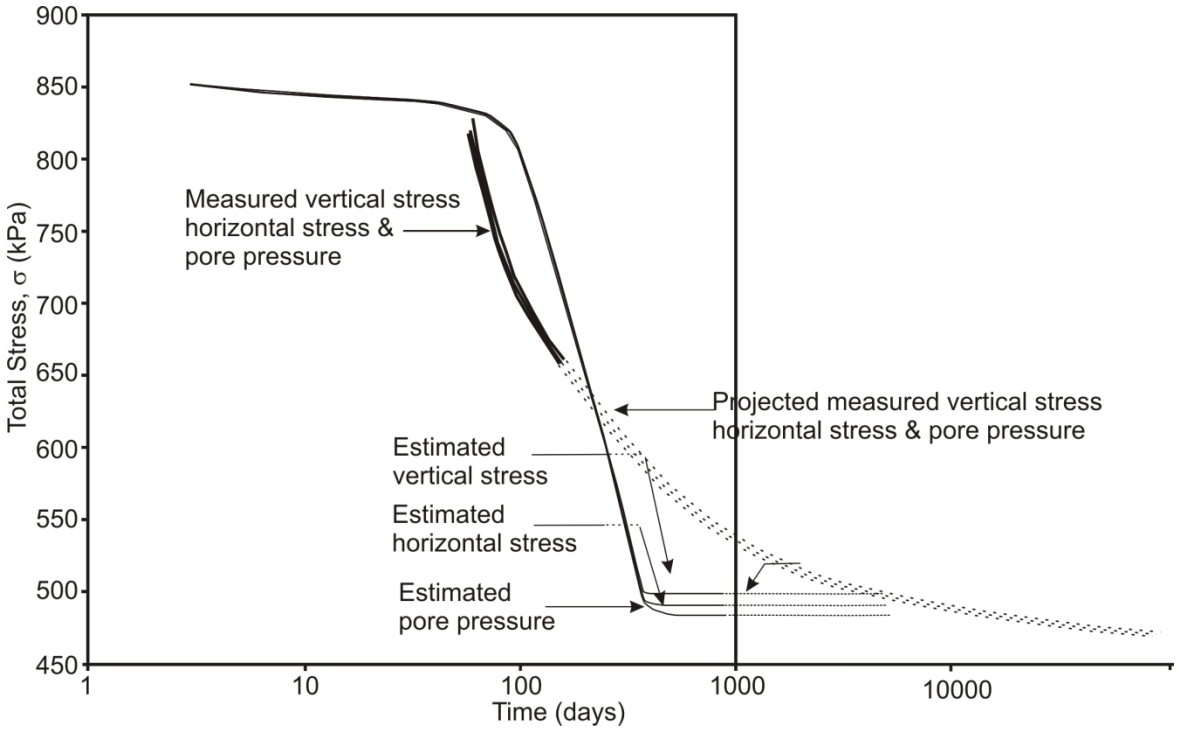

Figure 5.26 Comparison of estimated and measured total stress.

5.8 Parametric study using the finite element model

A parametric study on the SB slurry walls was conducted to understand the distribution in σ'_v with the depth of the wall due to surcharge berms and intermediate aquifers.

5.8.1 Surcharge berm

Research has shown that soil-bentonite materials coming into contact with brine undergo chemical (osmotic) consolidation (Haug 1983, Tang 1987). This is not desirable if the purpose of the backfill is to prevent the migration of brine into the regional groundwater regime. Further research (Haug et al., 1990) found that a 30 to 40 kPa surcharge on the backfill could limit brine-induced osmotic consolidation of the backfill and prevent a significant increase in the hydraulic conductivity of the wall. Application of a surcharge on the backfill can be accomplished by construction of a surcharge berm over the completed slurry wall, thus allowing slurry wall construction in

brine environments to be possible and successful. A surcharge berm is usually constructed 1 year after slurry wall construction. It is typically constructed using any stable material, such as till or gravel.

The cross-section and dimensions of the surcharge berm used in the finite element model are presented in Figure 5.27. The width of the crest of the berm is 4 m and the side slopes are 2H: 1V. The unit weight (γ) of the material used for the construction of the berm was assumed to be 20 kN/m^3. The step function used in the model to apply the load on the slurry wall is shown in Figure 5.28. It is assumed that only 80% of the load is transferred to the top of the slurry wall. Hence, only 32 kPa of load was applied to the top of the wall within a period of 5 d (360-365 d).

A comparison of “Final” vertical effective stress with depth of the wall, with and without the surcharge berm on top, is shown in Figure 5.29. The dashed line is the stress distribution with the surcharge berm at the top. The σ'_v value is greater with the surcharge berm than without, up to 10-12 m depth from the ground surface. At a depth of about 1.5 m from the top, the σ'_v with the surcharge berm on the top is 31 kPa, which is about seven times more than without the surcharge berm. This increase in σ'_v is reflected in a corresponding decrease in hydraulic conductivity at same depths (Figure 5.30). From the above discussion, it can be concluded that the addition of the surcharge berm retards the brine-induced osmotic consolidation of SB backfill and hence allows slurry wall construction in brine environments to be possible and successful.

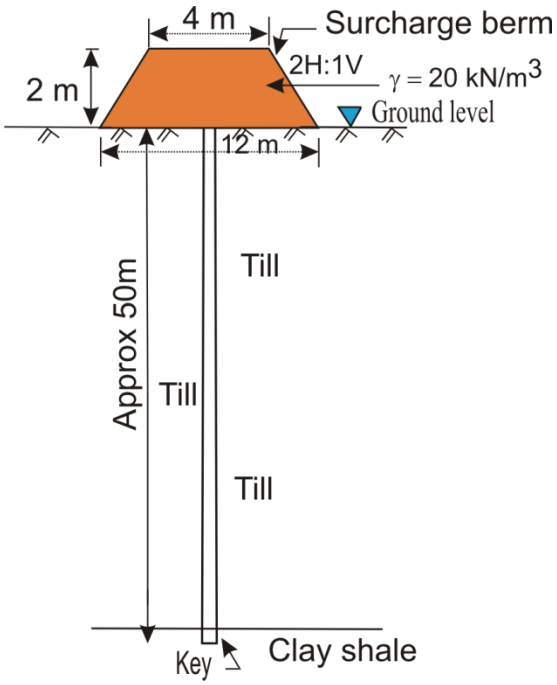

Figure 5.27 Cross-section of soil-bentonite wall with surcharge berm at the top.

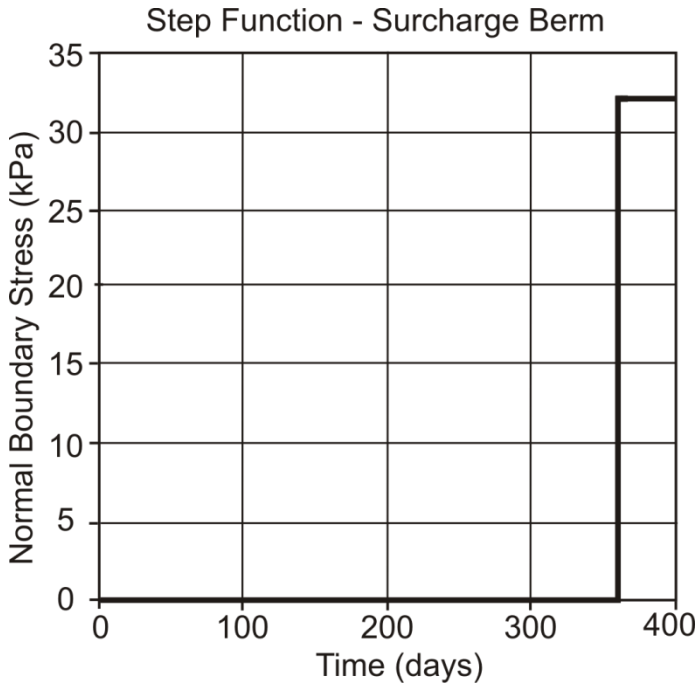

Figure 5.28 Step function for load application onto the slurry wall due to surcharge berm.

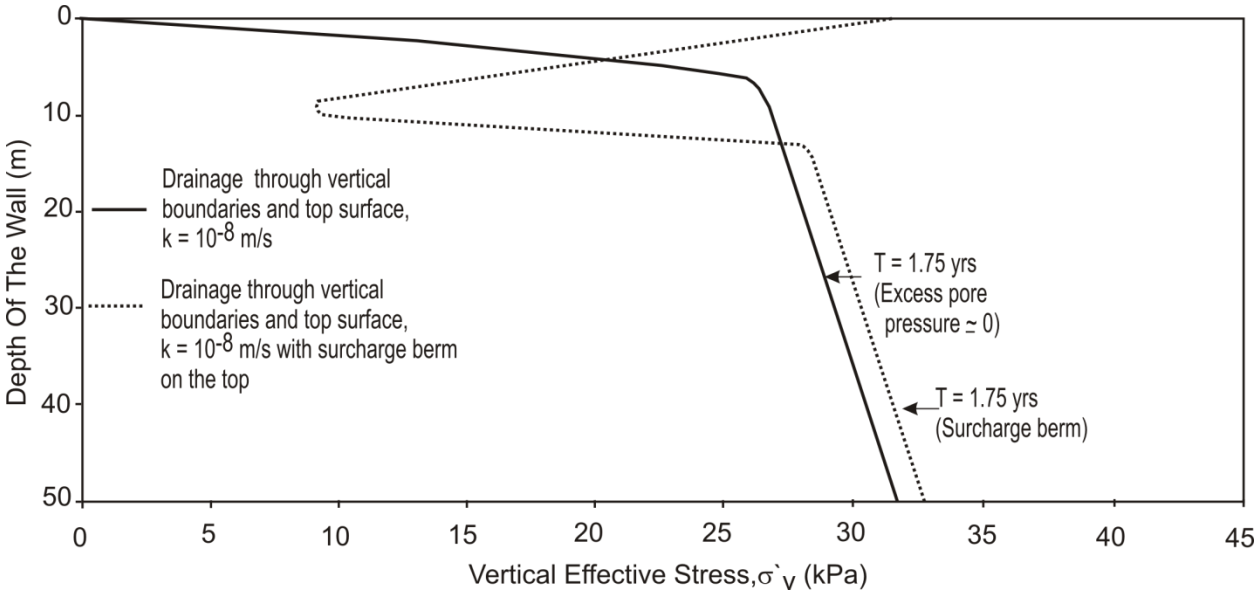

Figure 5.29 Comparison of "Final" vertical effective stress in an SB wall with and without a surcharge berm at the top.

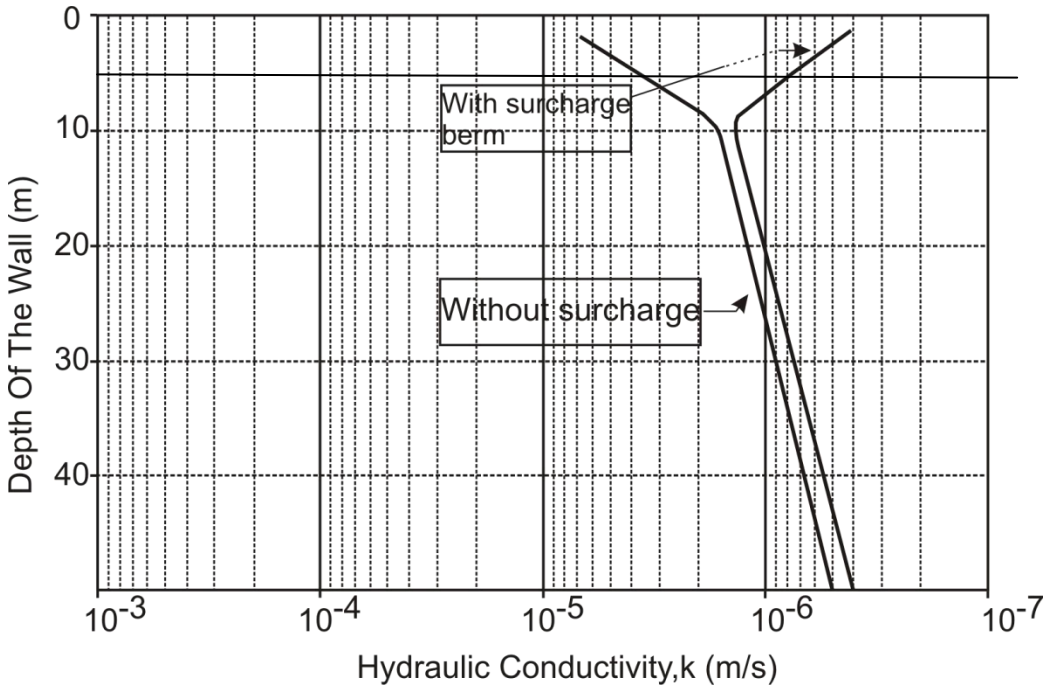

Figure 5.30 Comparison of "Final" hydraulic conductivity in an SB wall with and without a surcharge berm at the top.

CHAPTER 6 - CONCLUSIONS & RECOMMENDATIONS

6.1. Summary and conclusions

The primary conclusion of this research is that slurry wall backfill arching or “hang-up” significantly delays the magnitude and timing of vertical stress build-up in the backfill. The loss and timing of vertical stress build-up was found to be a function of: 1) backfill gradation, 2) the coefficient of lateral earth pressure for the backfill, 3) the depth and width of the slurry wall, 4) the hydraulic nature of the trench, and 5) the presence of any backfill surcharge. This loss of vertical stress results in backfill with lower density and higher hydraulic conductivity. The situation was found to be most critical for deep narrow slurry walls. It was also found that any advantage in using a coarser graded backfill was offset by higher backfill hydraulic conductivity. The net result is that the upper portions of slurry walls may not be able to achieve their hydraulic conductivity objectives as soon as expected, if at all. In addition, the backfill in the upper portion of the trench where σ'_v is less than 20 KPa may be susceptible to chemical attack and osmotic consolidation (Tang 1986, Haug 1990).

A parametric study using analytical and finite element modelling was conducted to examine the factors affecting arching in SB walls. The modelling results showed that the vertical stress in the SB wall is always less than the geostatic stress at any given depth.

Backfill gradation of the SB mix was found to significantly impact ϕ’ but have relatively little impact on K. The ϕ’ values for the SB mixes ranged from 23° for TM3 (53% fines) to 32° for TM1 (13% fines). Compressibility of the mix was found to be proportional to the amount of fines. Trial mix TM3 had the highest fines content and was the most compressible, while TM1 was the least compressible. Hydraulic conductivity of the SB backfill was found to be function of the amount of fines present in the mix. From the laboratory results, it was found that the hydraulic conductivity values for TM3 and TM1 at a consolidating pressure of 900 kPa were 2.80×10^{-10} and 5.28×10^{-8} m/s,

respectively. TM2 and FB, which has nearly the same fines content, have similar values of k at any given consolidating pressure.

The coefficient of lateral earth pressure (K) and angle of internal friction are related parameters. The coefficient of lateral earth pressure was found to be relatively independent of the quantity of fines present in the SB mix. Arching in SB walls was found to increase for higher coefficient of lateral earth pressure values. K for all of the test mixes used in the laboratory was approximately 0.34.

Arching or wall "hang-up" was also found to be highly dependent on the width of the SB walls. Narrow, deep walls were found to be more susceptible to arching. With increasing wall width, the vertical effective stress (σ'_v) distribution more closely aligned with the geostatic stress distribution. Vertical effective stress (σ'_v) at a depth of 2 m from the top of the slurry wall was found to be about 12 kPa for all widths. This is about 40% less than the geostatic stress at the same depth (20 kPa). The modelling results also showed that, for all widths, the difference between σ'_v and geostatic stress increases with increasing depth of the wall (trench). At a depth of 40 m from top, σ'_v values for w = 0.5, 1, 2, and 4 m were 16, 22, 44, and 90 kPa, respectively. These are about 96, 94, 89, and 77% less than the geostatic stress at the same depth.

Hydraulic conductivity is the governing design parameter for SB slurry walls. Hydraulic conductivity is dependent on the vertical stress state of the wall. For the conditions modelled, the upper portion of the trench (top 5-8 m) never reached the minimum acceptable value. At a depth of 5 m, k values for FB (field backfill) mix were 1×10^{-4}, 1×10^{-5}, and 9×10^{-7} m/s at the end of 0.5, 1, and 1.75 years (end of consolidation), respectively. The time required for k to reach the acceptable limit of 10^{-6} m/s was also found to be dependent on the fines content of the SB mix. As fines content in the mix increased, the stress in the wall also increased at any given depth and time; however, for backfill mixes of varying fines content, stress buildup with depth was not significant but its impact on k was higher. The maximum "Final" achievable k values for TM1, FB, TM2, and TM3 at a depth of 2 m from top of the wall were 1×10^{-4}, 5×10^{-6}, 9×10^{-7},

and 3×10^{-9} m/s, respectively. Although more fines (clay) in the mix helped to meet the k requirement, such mixes would be more susceptible to osmotic consolidation.

The hydraulic nature (boundary) of the trench also governs the performance of SB slurry walls. There is a significant difference in the vertical effective stress profiles under different drainage conditions. Two different drainage conditions were modelled. Modelling results showed that the vertical effective stress (σ'_v) at the bottom of the trench for top drainage only was 17 kPa and for drainage from top and vertical boundaries (horizontal direction) was 33 kPa. The presence of intermediate aquifers sped up the rate of pore pressure dissipation and resulted in faster consolidation. However, changing the thickness of the aquifer had a minimal effect on stress distribution in the wall.

The results of the modelling study also showed that building a surcharge berm over the slurry wall increases vertical stress and results in significantly lower (2 to 8 times) k values in the top 5 m. At a depth of 5 m from the top, the hydraulic conductivity (k) of the SB slurry wall with a surcharge berm over it was about 75% lower than for the wall without a surcharge berm. Building a surcharge berm on top of the slurry wall also helps to satisfy the k requirement for SB walls and lowers the risk of osmotic consolidation.

6.2 Recommendations

6.2.1 Use of visco-elastic/plastic material model

This study used an elastic-perfectly plastic material model. As a next step, it would be valuable to consider a more realistic material model, such as an elastic-viscoplastic model.

6.2.2 Accurate pore pressure measurement

In the laboratory tests in this study, a standing piezometer (conventional type) was used to measure pore pressures at various depths in the mold. This was unsuccessful due to clogging of the pipe connecting the mold and the piezometer.

It is recommended that an electronic piezometer be used for pore pressure measurements. This would enhance the measurement quality and would also allow for the use of a data logger.

6.2.3 Alternative design for SB slurry walls

Consolidation of SB backfill may take several years. The top few metres of the SB wall is the most critical section, as it is the most susceptible to osmotic consolidation when the fluid being contained has a high salt content. It is recommended that further research be carried out with an alternate design for the SB wall, as shown in Figure 6.1. The top few metres should be designed in a funnel shape. This will accommodate more backfill, which in turn would add more weight to the backfill below and hence would help to consolidate the backfill faster. This could potentially improve the stress distribution pattern in SB walls.

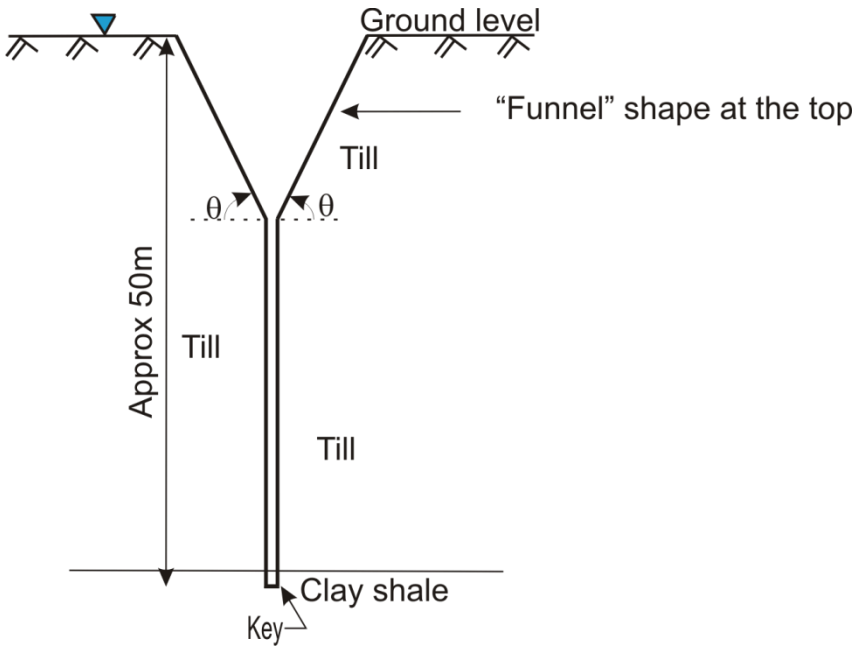

Figure 6.1 Alternate design for SB slurry walls.

REFERENCES

ASTM C143. Standard test method for slump of hydraulic cement concrete.

ASTM D2435-04. Standard test methods for one-dimensional consolidation properties of soils using incremental loading .

ASTM D2487-10. Standard practice for classification of soils for engineering purposes (United Soil Classification System).

ASTM D3080-04. Standard test method for direct shear test of soils under consolidated drained conditions.

ASTM D4318-00. Standard test methods for liquid limit, plastic limit and plasticity index of soils.

ASTM D422-63. Standard test method for particle size analysis of soils.

ASTM D854-02. Standard test methods for specific gravity of soil solids by water pycnometer.

API. 1990. “Recommended practice for standard procedures for field testing water-based drilling fluids.” API Recommended Practice 13-B-1, Dallas, TX.

Aubertin, M., Li, L., Arnodi, S., Belem, T., Bussiere, B., Benzaazoua, M., and Simon R. 2003. “Interaction between backfill and rock mass in narrow stopes”. In Proceedings of 12th Pan-American conference on soil mechanics and geotechnical engineering and 39th U.S. rock mechanics symposium, 22-26 June, Boston, MA, 1: 1157-1164.

Baxter, D.Y. 2001. “Mechanical behaviour of soil-bentonite cut-off walls.” Ph.D. Dissertation, Virginia Polytechnic Institute and State University, Blacksburg, VA.

Belem, T., and Benzaazoua, M. 2008. “Design and Application of underground mine paste backfill technology”. Geotech Geol Eng, 26: 147-174.

Clark, I.H. 1994. “Modeling of soil-bentonite cut off wall.” Proceedings of ANCOLD Conference on Dams, Tasmania, Australia.

Clough, G.W. and Duncan, J.M. 1991. “Earth Pressures.” *Foundation Engineering Handbook, 2nd ed*, Chapter 6, Fang, H. Y., ed., Van Nostrand Reinhold, New York, NY.

D'Appolonia, D. 1980. "Soil-bentonite slurry trench cut-offs". Journal of Geotechnical Engineering Division, 106(4): 399-417.

Das, B.M. 2008. Advanced soil mechanics, Taylor & Francis, New York, NY.

Duncan, J.M. 1993. "Limitation of conventional analysis of consolidation settlements". Journal of Geotechnical Engineering Division, 119(9):1331-1359.

Engemoen, W.O., and Hensley, P.J. 1986. "ECPT investigation of a slurry trench cutoff wall." Use of In Situ Tests in Geotechnical Engineering, Geotech. Special Publ. No. 6, S. P. Clemence, ed., ASCE, New York, NY: 514-528.

Evans, J.C. 1991. "Geotechnics of hazardous waste control systems", Chapter 20, Foundation Engineering Handbook, 2nd Edition, H. Y. Fang, ed., Van Nostran Reinhold, New York, NY: 765-777.

Evans, J.C. 1994. "Hydraulic conductivity of vertical cut-off walls". Hydraulic conductivity and waster contaminant transport in soil, ASTM STP 1142, D.E. Daniel and S.J Trautwein, eds., Chapman and Hall, London, UK: 430-454.

Evans, J.C., and Ryan, C. 2005. "Time dependent strength behaviour of soil – bentonite slurry wall backfill." Proceedings of Geo Frontier 2005, ASCE Geotechnical Special Publication No. 130-142: 3779-3787.

Evans, J.C., Costa, M.J., and Cooley, B. 1995. "The state-of-stress in soil-bentonite slurry trench cutoff walls." Proceedings of Geoenvironment 2000, ASCE Geotechnical Special Publication No. 46, Y.B. Acar and D.E. Daniel, eds., New Orleans, LA: 1173-1191.

Fahey, M., Helinski, M., and Fourie A. 2009. "Some aspects of the mechanics of arching in backfilled stopes". Canadian Geotechnical Journal, 46: 1322-1336

Federico, A., Elia, G., and Germano V. 2008. "A Short note on the earth pressure and mobilized angle of internal friction in one-dimensional compression of soils". Journal of GeoEngineering, 3(1): 41-46

Filz, G.M. 1996. Consolidation stresses in soil – bentonite backfilled trenches. Proceedings of the 2nd Int. Congress on Environmental Geotechnics, M. Kamon, ed., Balkema, Rotterdam, The Netherlands: 497-502

Filz, G.M., Boyer, R.D. and Davidson, R.R. 1997. “Bentonite-water slurry rheology and cut-off wall trench stability”. In situ Remediation of the Geoenvironment, GSP No. 71, ASCE, Reston VA: 139-153.

Gan, J, Nader, I.B and Haug, M.D. 2011 Consolidation and hydraulic conductivity testing of Slurries. TAILINGS AND MINE WASTE ’11, Proceedings of the 15th International Conference on Talings and Mine Waste, Vancouver, BC, November 6 to 9, 2011: 259-265.

GEOSLOPE International Ltd. 2010a. Seepage modelling with SEEP/W 2007: An engineering methodology, 4th edition. February 2010. Calgary, AB.

GEOSLOPE International Ltd. 2010b. Stress-deformation analysis with SIGMA/W 2007: An engineering methodology, 4th edition. February 2010. Calgary, AB.

Handy, R.L. 1985. “The arch in soil arching”. Journal of Geotechnical Engineering., ASCE, Vol. 111(3): 302-319.

Haug, M.D. and Kozicki,P.1983. “Selection criteria for slurry trench cut-offs”. Canadian Journal of Civil Engineering, 10(3): 527-537.

Haug, M.D., Barbour, S.L. and Tang, R. 1990. “Hydraulic performance of slurry trench backfill in brine environment”. Proceedings of Canadian Society for Civil Engineers Annual Conference.

Henry, L.B., Filz, G.M., and Davidson, R.R. 1998. “Formation and properties of bentonite filter cakes”. Filtration and Drainage in Geotechnical/ Geoenvironmental Engineering, GSP No.78, ASCE, L.N. Reddy and M.V.S Bonala, eds., Reston, VA: 69-88.

Jacobson, B. 1958. “On pressure in silos.” Proceedings of the Conference on earth pressure problems, Brussels, Belgium, 1:49-54.

Jaky, J. 1948. “Pressure in silos”. Proceedings of the 2nd International Conference on Soil Mechanics and Foundation Engineering, ICSMFE,London,June,1:103-107.

Jeeravipoolvarn, S., Scott, J.D. and Chalaturnyk, R.J. 2009. “10 m standpipe tests on oil sands tailings: long term experimental results and prediction.” Canadian Geotechnical Journal, 46: 875-888.

Khoury, M.A., Fayad, P.H., and Ladd, R.S. 1992. “Design, construction, and performance of a soil-bentonite cutoff wall constructed in two stages.” Slurry Walls: Design, Construction, and Quality Control, ASTM STP 1129, D. B. Paul, R. R.Davidson, and N. J. Cavalli, eds., ASTM, Philadelphia, PA.

Kutter, B. L., and Sathialingam, N. 1992. “Elastic-viscoplastic modelling of the rate dependent behaviour of clays.” Geotechnique, 42(3): 27-441.

LaGrega, M.D., Buckingham, P.L., and Evans, J.C. 1994. Hazardous waste management, McGraw Hill, New York, NY.

Leonards, G.A. and Ramiah, B.K. 1959. “Time effects in the consolidation of clay.”ASTM STP 254: 116-130.

Li, L, Aubertin, M., and Belem T. 2005. “Formulation of a three dimensional analytical solution to evaluate stresses in backfilled vertical narrow openings”. Canadian Geotechnical Journal, 42: 1705-1717.

Marston, A. 1930. “The Theory of External Loads on Closed Conduits in the Light of the latest experiments”. Iowa Engineering Experiment Station, Bulletin No. 96.

Marston, A. and Anderson, A.V. 1913. “The Theory of Loads on Pipes in Ditches and Tests of Cement and Clay Drain Tile and Sewer Pipe”. Bulletin 31, Iowa State College, IA.

McCandless, R. M. and Bodocsi, A. 1988. “Hydraulic characteristics of model soil bentonite slurry cutoff walls.” Proceedings of the Fifth National Conf. on Hazardous Wastes and Hazardous Materials ’88, Las Vegas, NV, 198-201.

M.D. Haug & Associates Ltd. 1998. “PCS Rocanville slurry wall report, construction and analysis”.

Mesri, G., and Olson, R.E. 1971. “Mechanisms controlling the permeability of clays”. Clays and Clay Minerals, 19: 151-158.

Mesri, G., and Hayat, T.M. 1993. “The coefficient of earth pressure at rest”. Canadian Geotechnical Journal, 30: 647-666.

Mesri, G., and Hayat, T.M. 1993. “The coefficient of earth pressure at rest”. Canadian Geotechnical Journal, 30: 647-666.

Michalowski, R.L.2005. “Coefficient of earth pressure at rest”. Journal of Geotechnical and Geoenvironmental Engineering, 131(11): 1429-1433.

Pandian, N.S., Nagaraj, T.S., and Raju, P.S.R.N. 1995 “Permeability and Compressibility behaviour of bentonite sand/soil mixes”. Geotechnical Testing Journal, 18(1): 86-93.

Ranjan, G., and Rao, A.S.R. 2005. Basic and Applied Soil Mechanics, New Age International Publishers, New Delhi, India.

Ryan, C.R. 1987. Soil bentonite cut-off walls, Geotechnical practice for waste disposal’87, R.D Woods, ed., ASCE, New York: 182-204.

Sauer, E.K., Egeland, A.K. and Christiansen, E.A. 1993. “Preconsolidation of Tills and Intertill Clays by Glacial Loading in Southern Saskatchewan”. Canadian Journal of Earth Sciences, 30(3): 420-433.

Singh, S., Shukla, S.K. and Sivakugan, N. 2011. “Arching in Inclined and Vertical Mine stopes”. Geotechnical and Geological Engineering, DOI 10.1007/s 10706-011-9410-4.

Skempton, A.W. 1944. “Notes on compressibility of clays.”Geological Society of London, Quarterly Journal, 100(397-98): 119-135.

Spangler, M.G., and Handy, R.L. 1973. “Loads on underground conduits”. Soil-Engineering, Harper Collins, New York: 727-763.

Tang, K.R. 1987. “Hydraulic conductivity of slurry trench backfill in brine.” Master’s. Dissertation, Department of Civil and Geological Engineering, University of Saskatchewan, Saskatoon, SK, Canada.

Tavenas, P., Leblond, P., Jean, P. and Leroueil, S. 1983. “The permeability of natural soft clays. Part I: Methods of laboratory measurement”. Canadian geotechnical Journal, 20: 629-644.

Tavenas, P., Jean, P., Leblond, P. and Leroueil, S. 1983. “The permeability of natural soft clays. Part II: Permeability characteristics”. Canadian geotechnical Journal, 20: 645-660.

Terzaghi, K. 1943. Theoretical Soil Mechanics. John Wiley & Sons, New York.

Terzaghi, K., and Peck, R.B. 1948. Soil Mechanics in Engineering Practice, John Wiley and Sons, New York.

Tien, H.J. 1996. “A literature study of the arching effect” Master’s Dissertation, Department of Civil and Environmental Engineering, Massachusetts Institute of Technology, Cambridge, MA.

Woodcock, J.C., and Miller, K.R. 1971. “Slurry wall construction in deep mined area”. ASCE Geotechnical special publication: 197-211.

Xanthakos, P.P. 1979. Slurry walls, McGraw Hill, New York, NY.

Yeo, S.S., Shackelford, C.D., and Evans, J.C. 2005. “Consolidation and hydraulic conductivity of nine model soil-bentonite backfills”. Journal of Geotechnical and Geoenvironmental Engineering, 131(10): 1189-1198.

Appendix A

Bentonite properties as supplied by the manufacturer

Description: Premium Gel is natural, powdered, high-swelling Wyoming sodium bentonite. Premium Gel meets API Specification 13A for Drilling Fluid Materials.

Applications: Soil/Bentonite liners; Slurry Trenching, Tunnel Boring, and Foundation Drilling.

Slurry Properties (6.1% suspension)	Typical	Specification
Viscosity FANN 600 rpm	40	30 min
Marsh funnel, s/quart	38	
Apparent viscosity, cps	18.5	
Plastic viscosity (PV)	12	10 min
Yield point, kg/100 m^2	68.35	3 $\times$ PV max
Filter cake, cm	0.23	

Construction properties	Typical	Specification
Moisture (%)	7.4	
Swell index (mL)	28	
Specific gravity	2.50	
pH, 6% suspension	9.5	
Bulk density, uncompacted	848	Kg/m^3
Bulk density, compacted	1153	Kg/m^3
Fluid loss	14	15 mL max

Bentonite Properties

Free swell	16 mL/2 g minimum (ACC 1010)
Filtrate loss	18 mL maximum (API 13A)
Barrel yield	90 minimum (API 13A)
Particle sizing	70 percent minimum passing #200 mesh (75 mm) sieve (ASTM D422)
Chemical formula	A tri-layer expanding mineral structure of approximately: $(Al, Fe_{1.67}, Mg_{0.33})\ Si_4O_{10}(OH_2)\ Na^{+}Ca^{2+}{}_{0.33}$

Appendix B

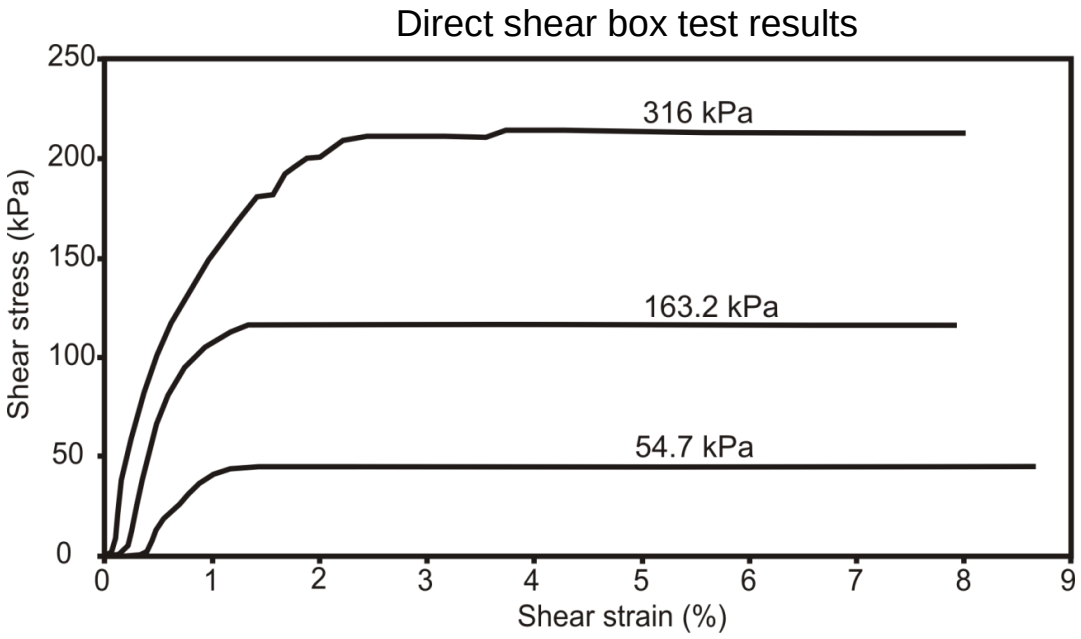

Figure B1: Shear stress vs. shear strain for TM1.

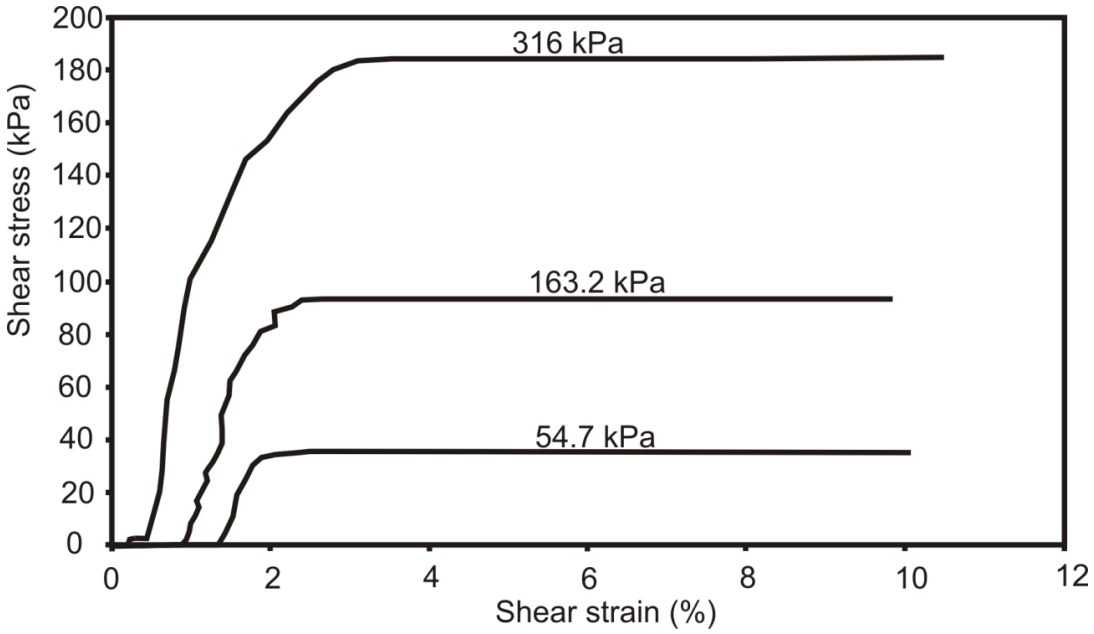

Figure B2: Shear stress vs. shear strain for FB.

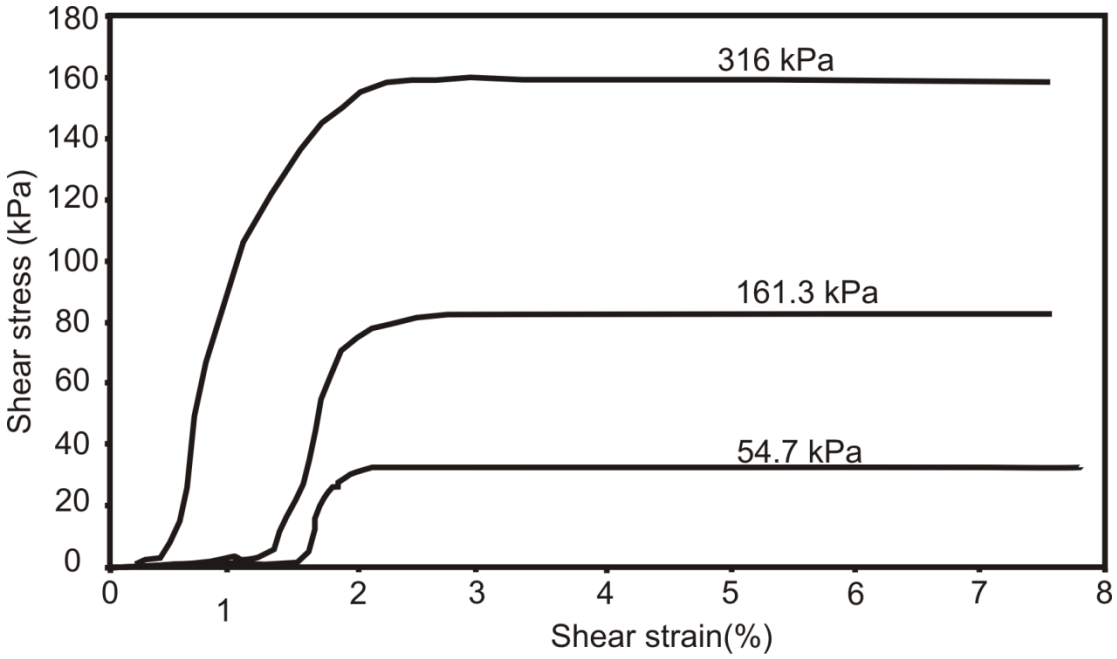

Figure B3: Shear stress vs. shear strain for TM2.

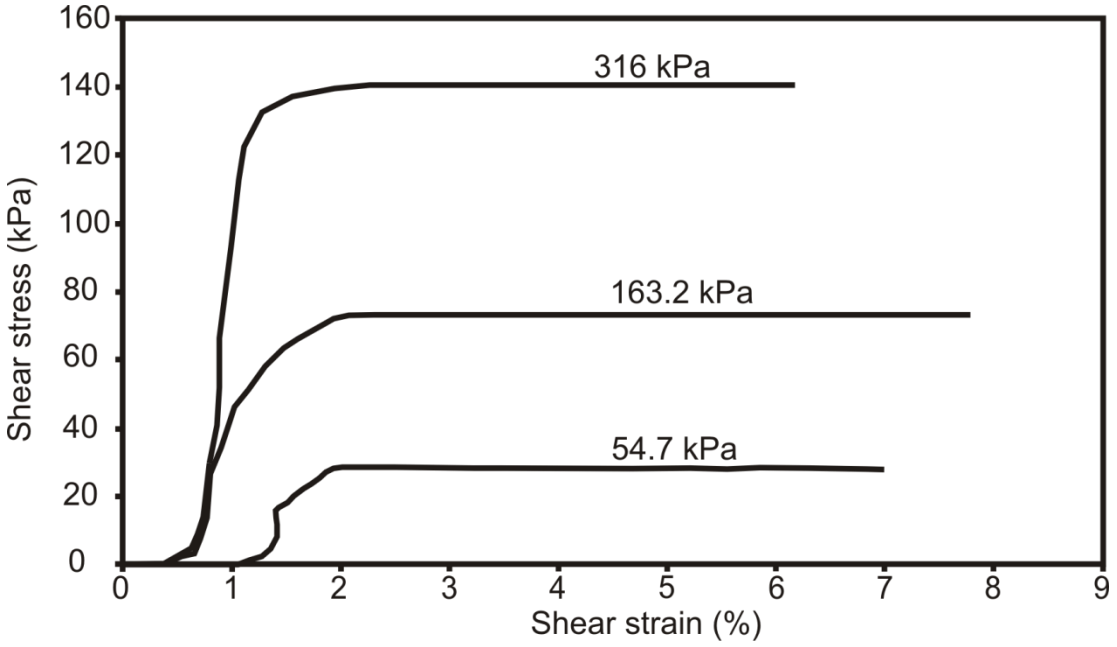

Figure B4: Shear stress vs. shear strain for TM3.

Appendix C

Example showing calculation of Young's modulus (E) from consolidation test results.

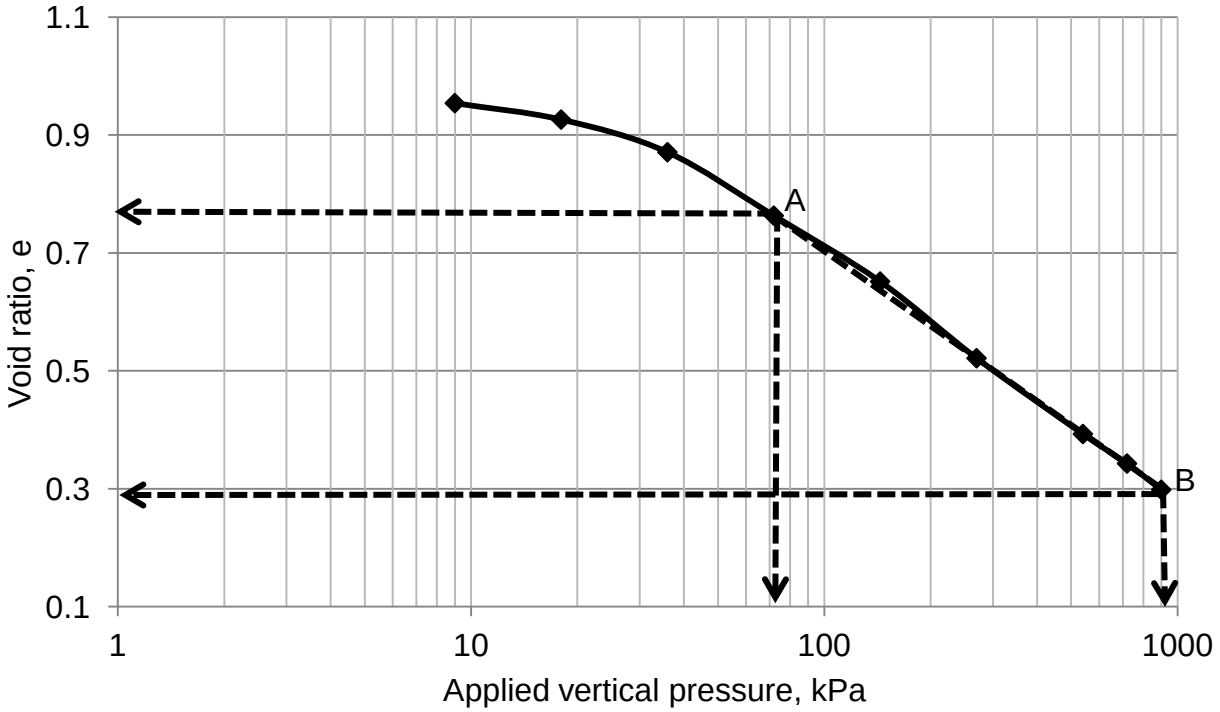

Figure C1.Calculation of Young's modulus from e-log p curve.

From the following relationship,

Young's modulus, $E = [M (1 + \upsilon)*(1 - 2\upsilon)] / [(1 - \upsilon)]$ [1]

constraint modulus, $M = 1/ m_v$ [2]

$m_v = \Delta e / (1 + e_0) * \Delta\sigma_v$ [3]

where M = constraint modulus;

υ = Poisson's ratio;

m_v = coefficient of volume compressibility;

e_0 = initial void ratio; and

Δe = change in void ratio for corresponding change in stress (σ).

In an e-log p curve, locate the straight line portion as shown in figure above. Choose any two points along the straight line. Determine the corresponding void ratio and the vertical stress at that point. Use formula [1] to calculate m_v. Subsequently calculate M and E.

The initial void ratio, e_o, at which the samples were compacted = 1.1883.

From the above figure, the corresponding e and σ at A are 0.7632 and 72 kPa, respectively, and at B are 0.2983 and 900 kPa, respectively.

Now, $m_v = (0.7632-0.2983) / (1 + 1.1883) * (900-72)$,

$m_v = 2.5657 * 10^{-4}$ / kPa,

$M = 1/ m_v = 3897.42$ kPa,

$\upsilon = 0.254$.

Hence, Young's modulus, E, using relation 1 = 0.32231×10^4 kPa.

Appendix D

Comparison of finite element and analytical solution for 1-D consolidation

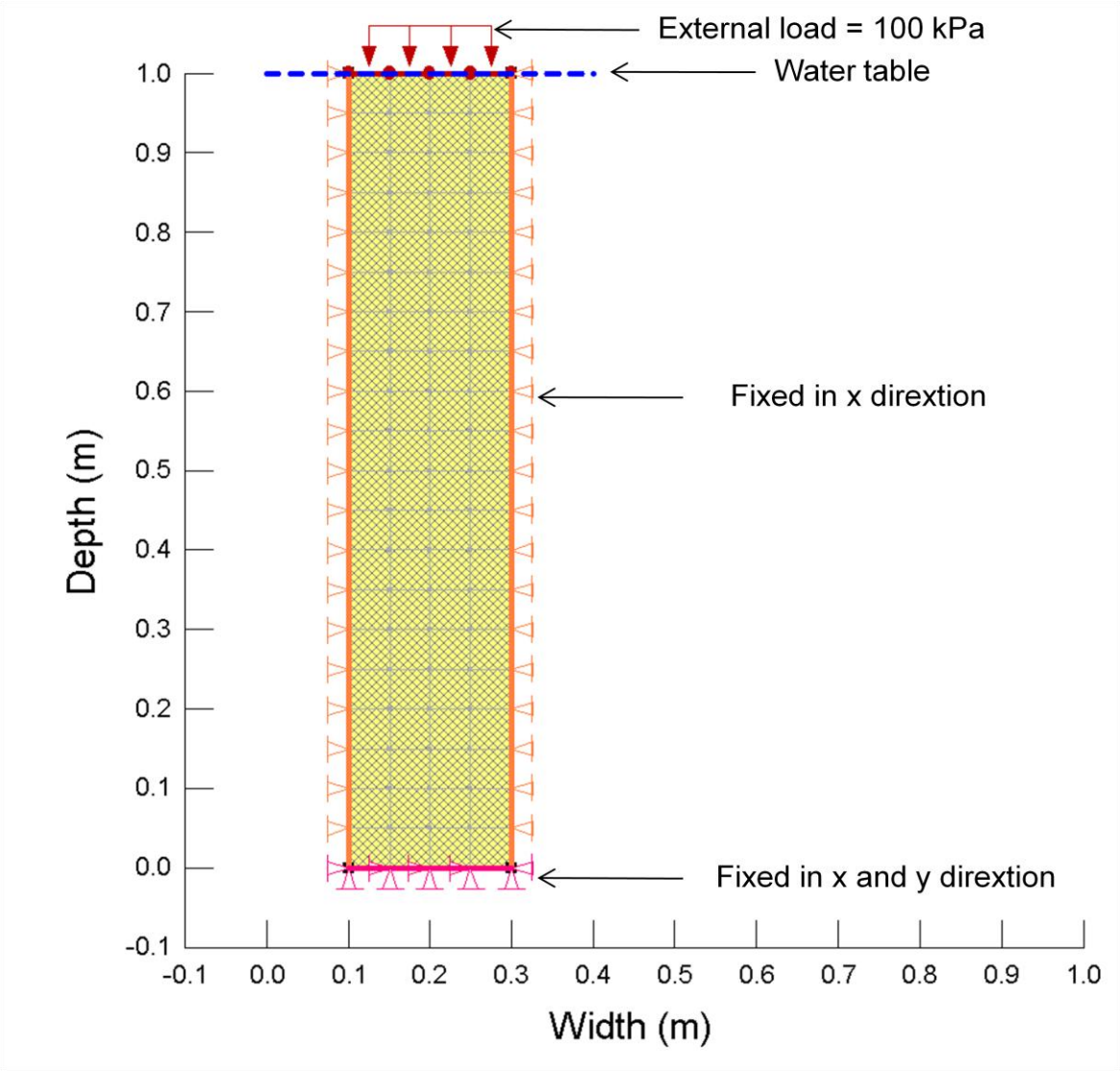

Figure D1. Column used for 1-D consolidation analysis.

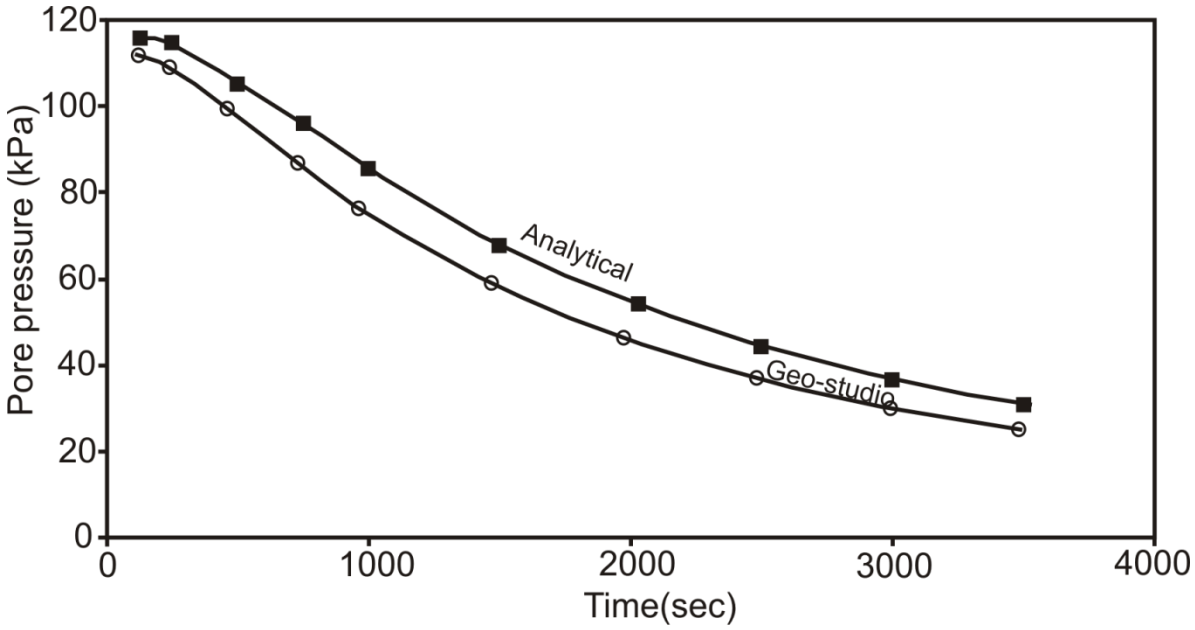

Figure D2. Comparison of analytical and GeoStudio pore pressure calculation at the bottom of the column.

Consider a column 1 m deep and 0.2 m wide. An external load of 100 kPa is applied at the top of the sample.

1. Material model: Linear elastic

2. Material properties
   i. Young's modulus, E = 2000 kPa
   ii. Poisson's ratio, m = 0.334
   iii. Hydraulic conductivity, $k = 1 \times 10^{-6}$ m/s
   iv. Coefficient of volume compressibility, $mv = 1/E = 5 \times 10^{-4}$ /kPa

3. Boundary conditions
   i. Force boundary
      a) Along depth: Fixed in x direction; y direction free

b) Along width: Fixed in x and y directions

ii. Flow boundary

a) Water table at the top

b) Drainage from the top

4. Calculation

The time factor (T) can be calculated using the relation, $T = \frac{C_V t}{H^2}$ with $C_v = \frac{k_{sat}}{\gamma_w m_v}$,

where C_v = coefficient of consolidation (m^2/s);

t = time (s);

H = depth of the column (m);

Ksat = saturated hydraulic conductivity of the mix (m/s);

γ_w = unit weight of water (kN/m^3); and

m_v = coefficient of volume compressibility (/kPa),

The percentage of pore pressure dissipation at the bottom of the column can be estimated using isochrones curves (Refer to Das 2008, p. 285).

Using the above relations, the following table can be created:

Table D1. Calculation of pore pressure at the base of the column.

Time, t (sec)	T_v (at the base)	u/u_o (from the curve)	Pore pressure at the base, u (u_o = 110kPa)
250	0.05	0.99	109.9
500	0.1	0.956	105.2
750	0.15	0.873	96.1
1000	0.2	0.776	85.4
1500	0.3	0.616	67.8
2000	0.4	0.497	54.7

2500	0.5	0.403	44.4
3000	0.6	0.333	36.7
3500	0.7	0.280	30.9

The calculated pore pressure listed in the above table is compared with the GeoStudio estimated pore pressure shown in Figure D2.

Appendix E

Pore pressure dissipation and vertical effective stress curves for the trial mixes ($k = 1 \times 10^{-8}$ m/s)

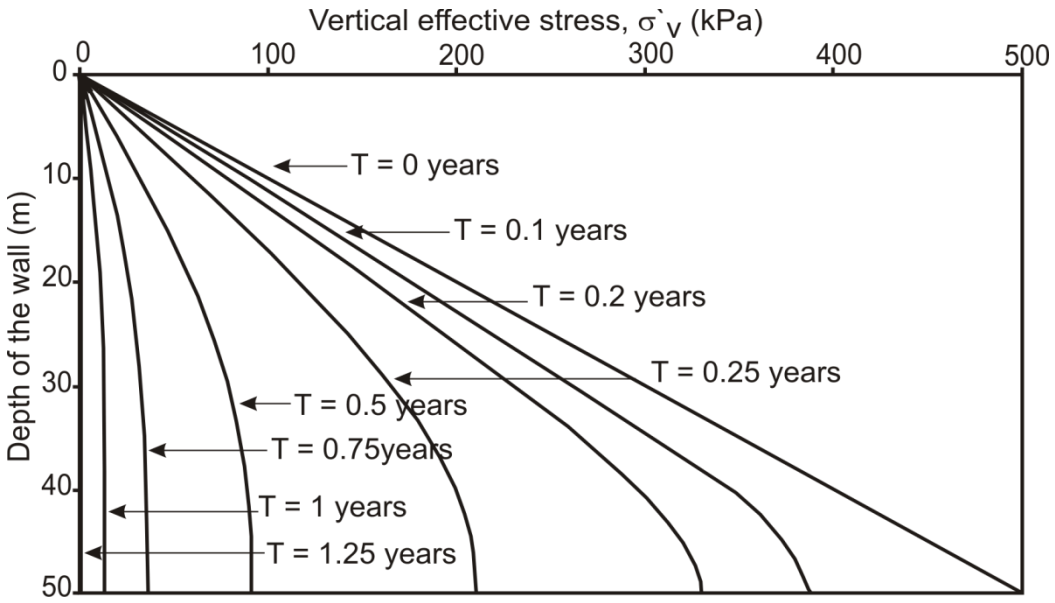

Figure E1. Dissipation of excess pore pressure with time for TM1.

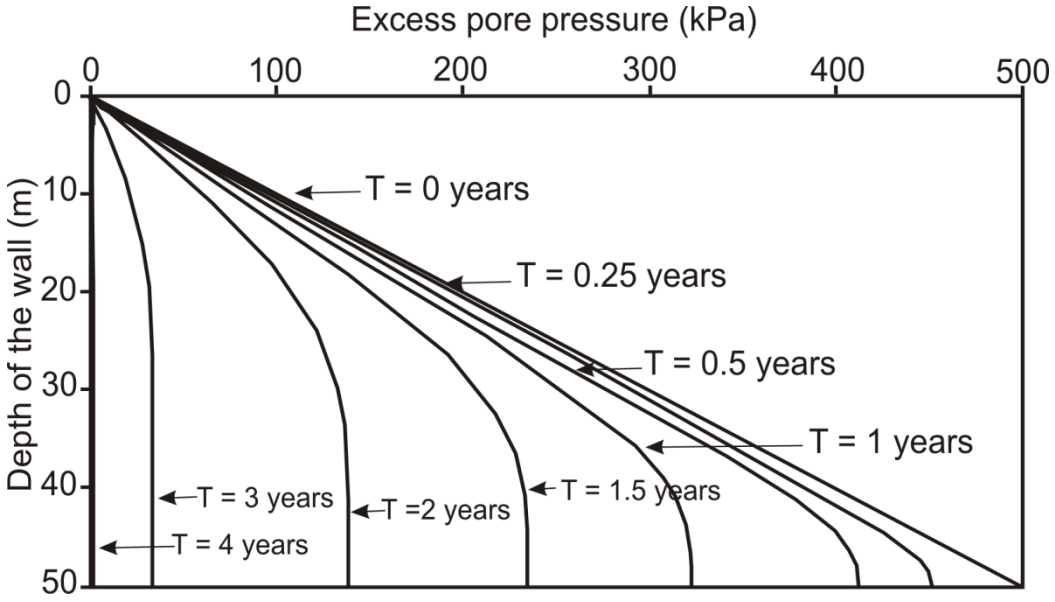

Figure E2. Dissipation of excess pore pressure with time for TM2.

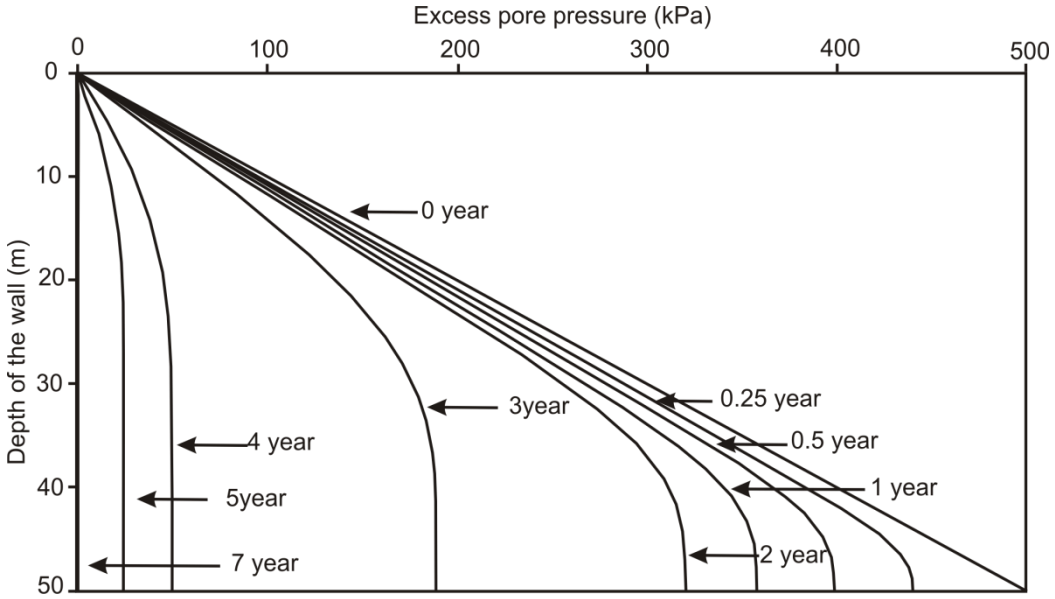

Figure E3. Dissipation of excess pore pressure with time for TM3.

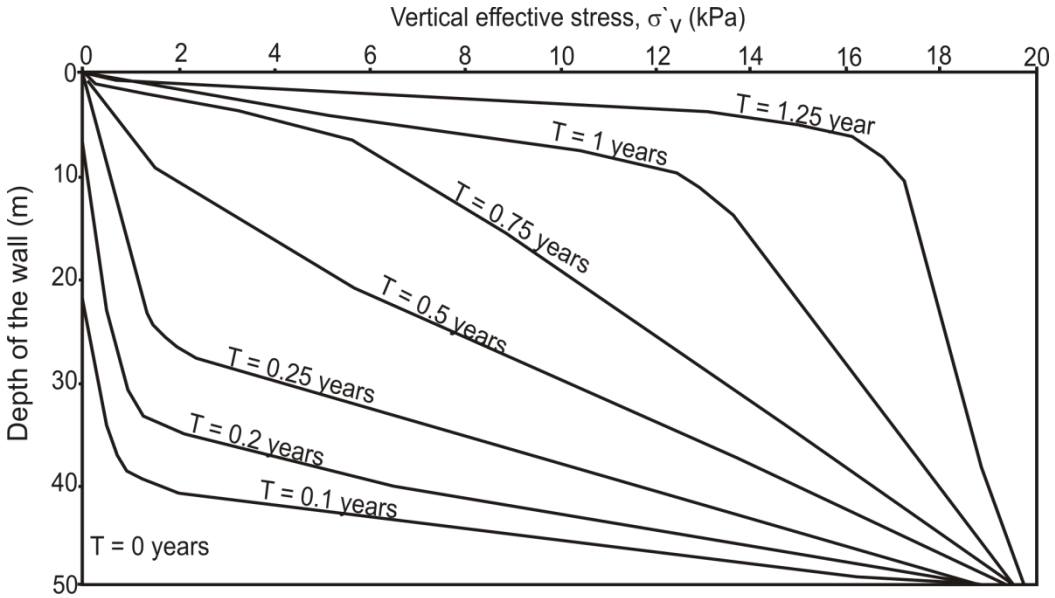

Figure E4. Variation of vertical effective stress with depth for TM1.

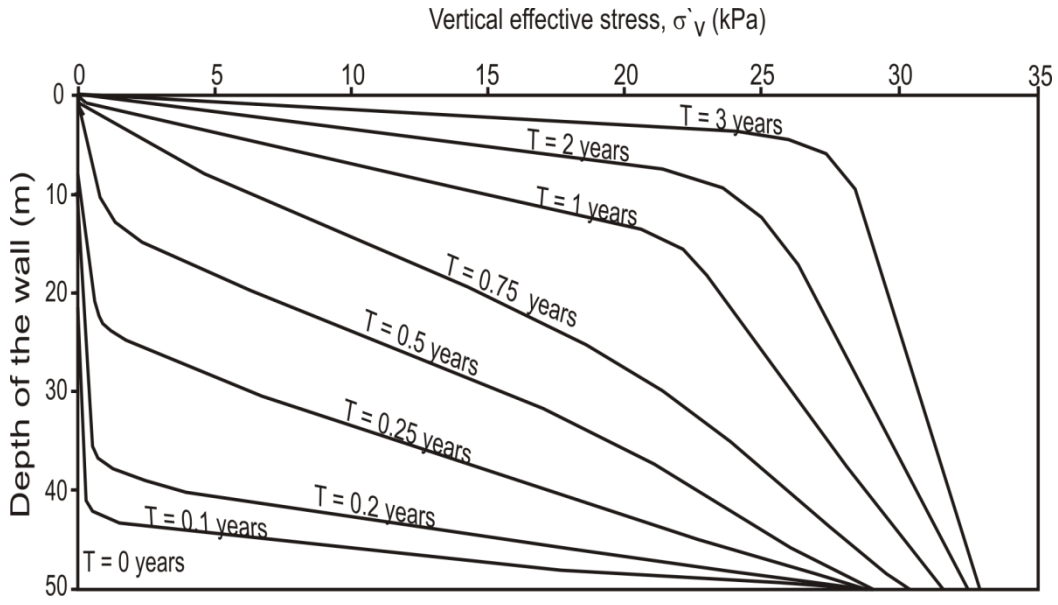

Figure E5. Variation of vertical effective stress with depth for TM2.

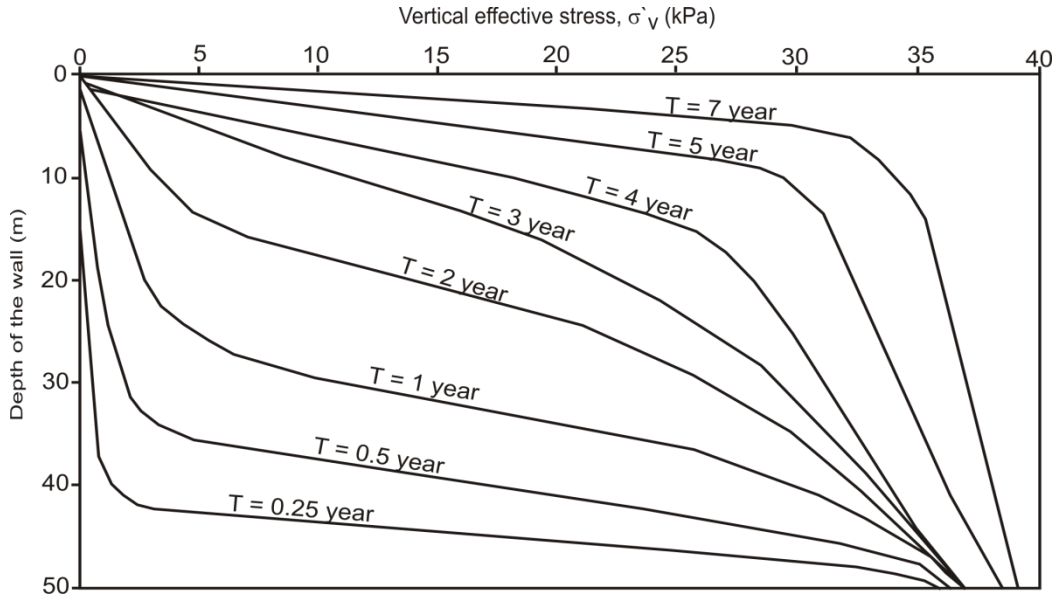

Figure E6. Variation of vertical effective stress with depth for TM3.

Appendix F

Pore pressure dissipation and vertical effective stress curves for the trial mixes and FB with top drainage only

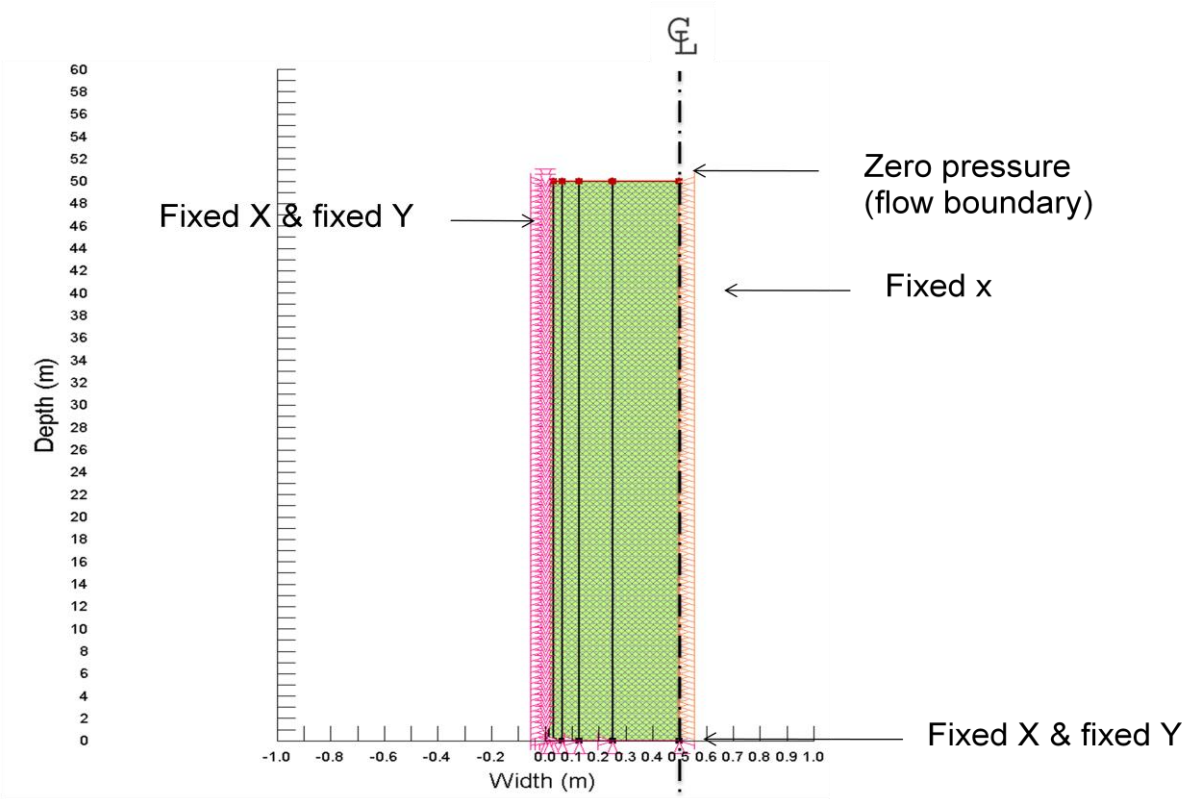

Figure F1. Boundary conditions used for transient analysis.

The hydraulic and displacement boundary conditions used in the present modelling are shown in Figure F1. The displacement boundary conditions are identical to the SB wall described in Chapter 5 (Table 5.3). The drainage boundaries allow excess pore pressure dissipation only from the top surface. Dissipation of excess pore pressure with time and variation of vertical effective stress with depth for the test materials is presented below.

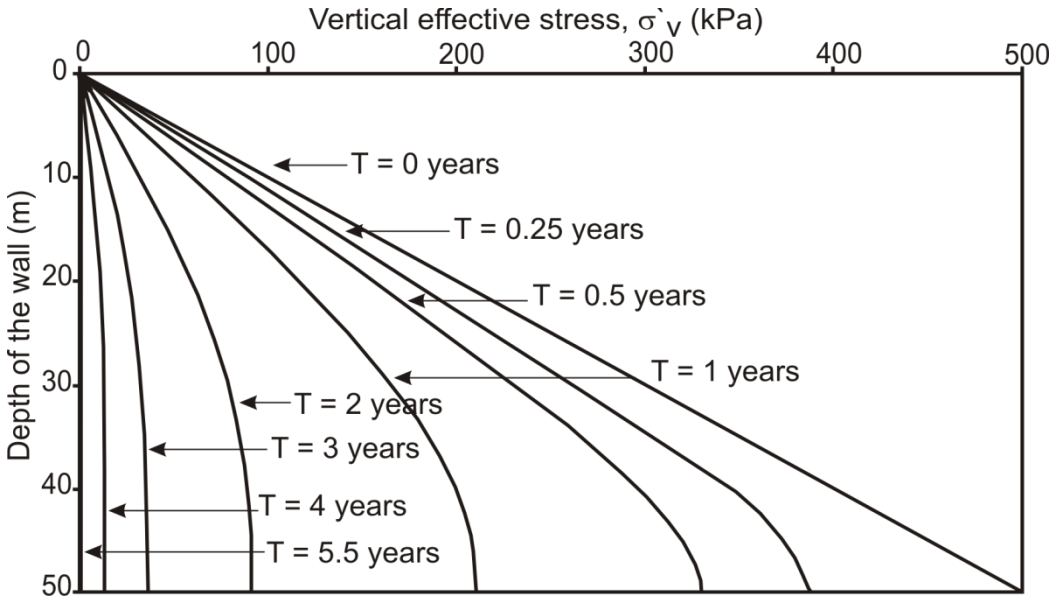

Figure F2. Dissipation of excess pore pressure with time for TM1.

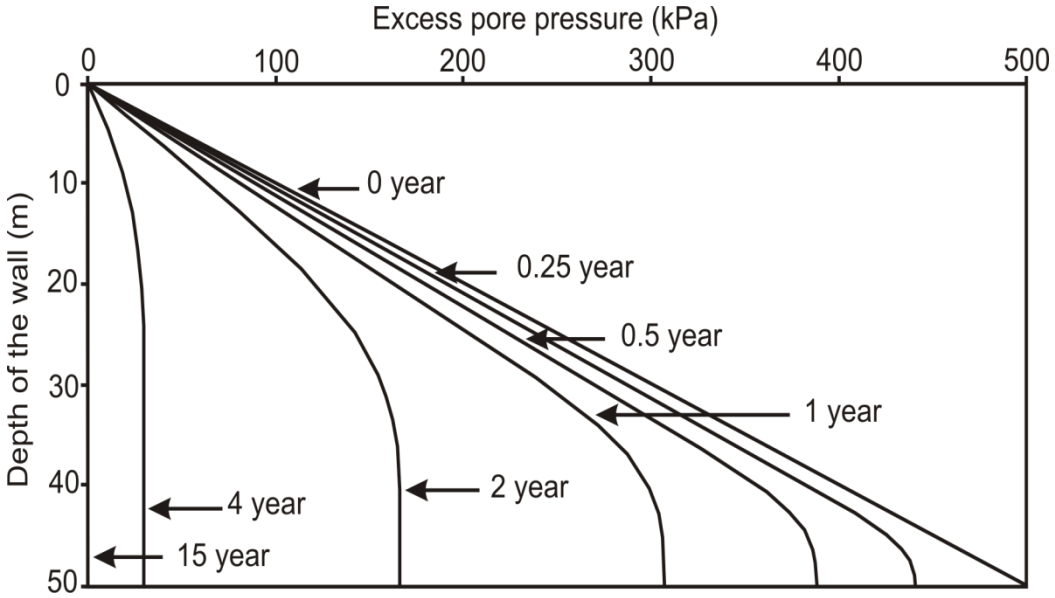

Figure F3. Dissipation of excess pore pressure with time for FB.

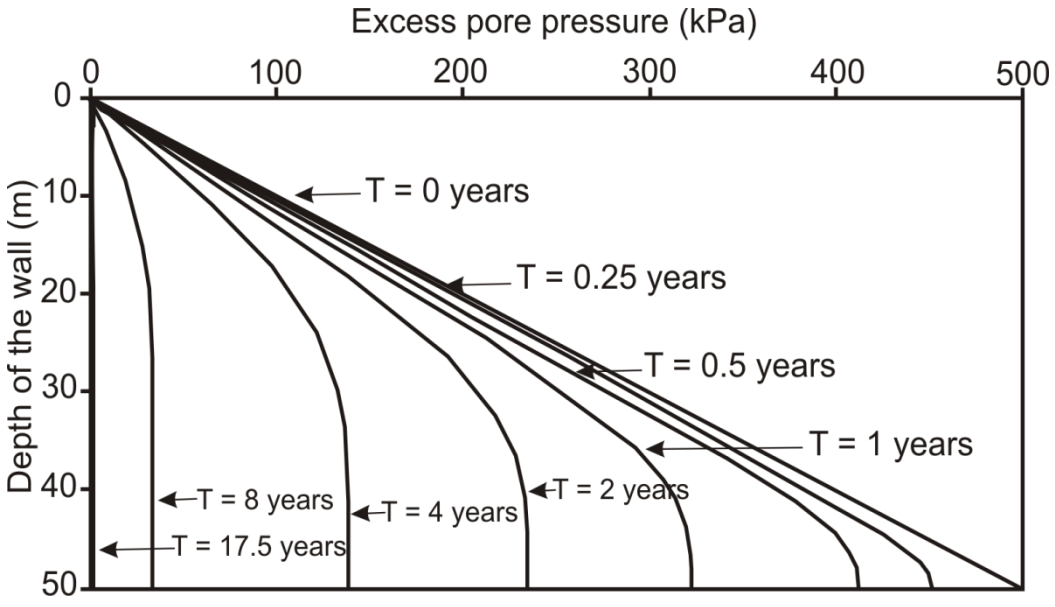

Figure F4. Dissipation of excess pore pressure with time for TM2.

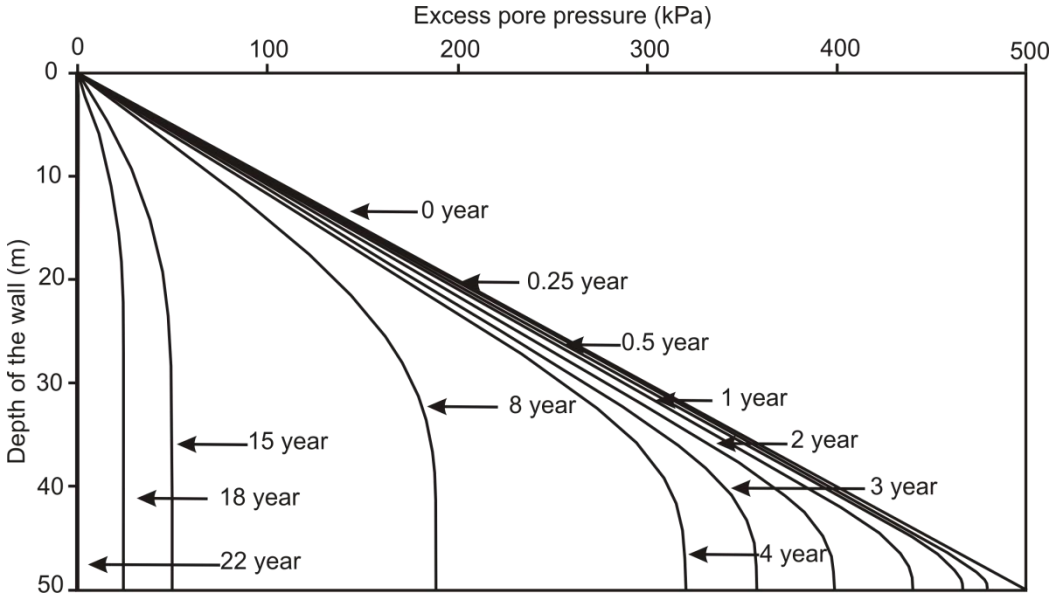

Figure F5. Dissipation of excess pore pressure with time for TM3.

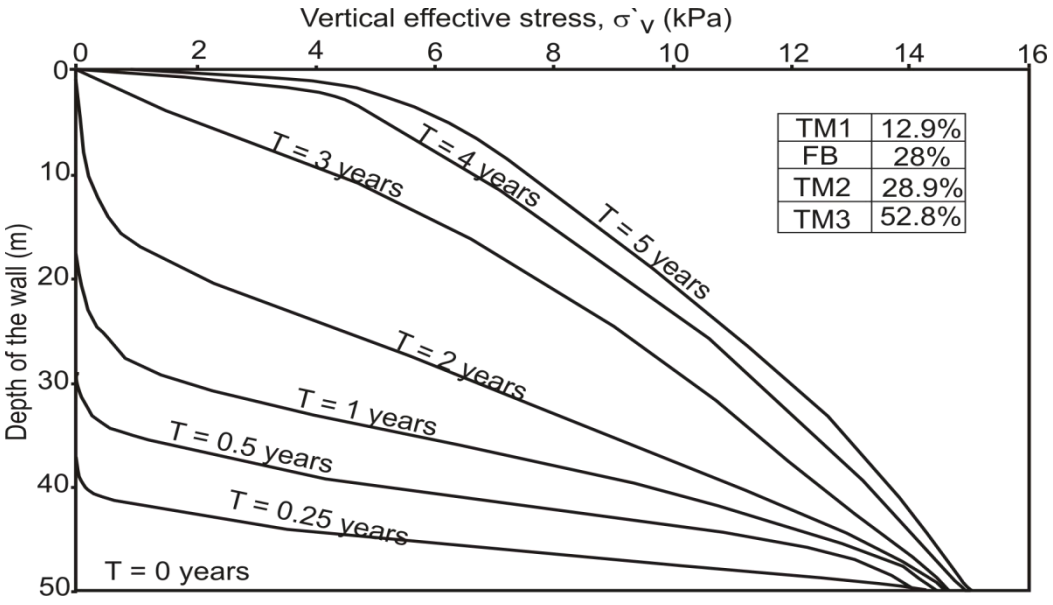

Figure F6. Variation of vertical effective stress with depth for TM1.

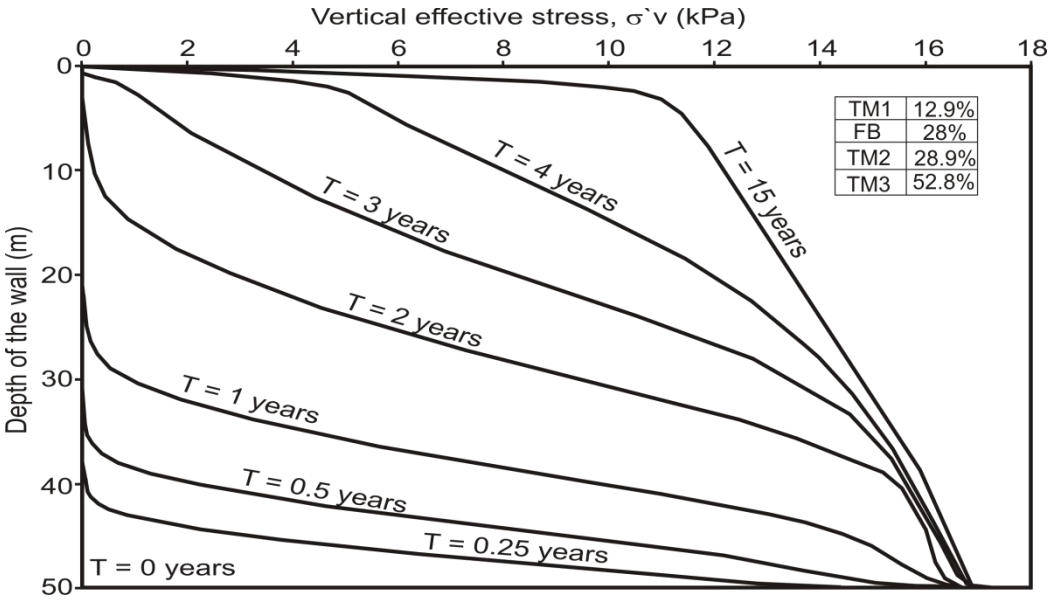

Figure F7. Variation of vertical effective stress with depth for FB.

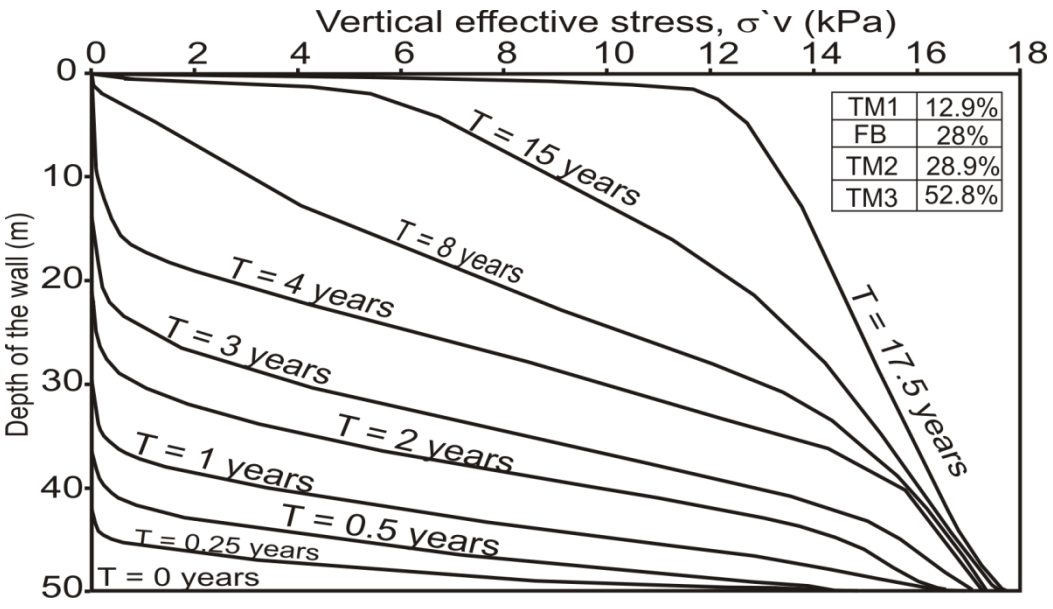

Figure F8. Variation of vertical effective stress with depth for TM2.

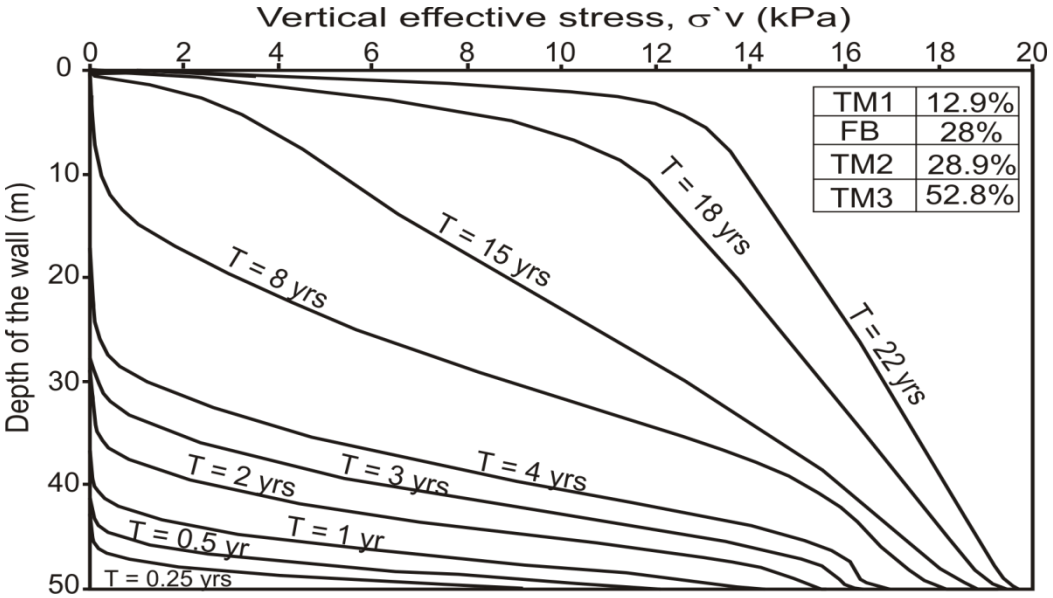

Figure F9. Variation of vertical effective stress with depth for TM3.

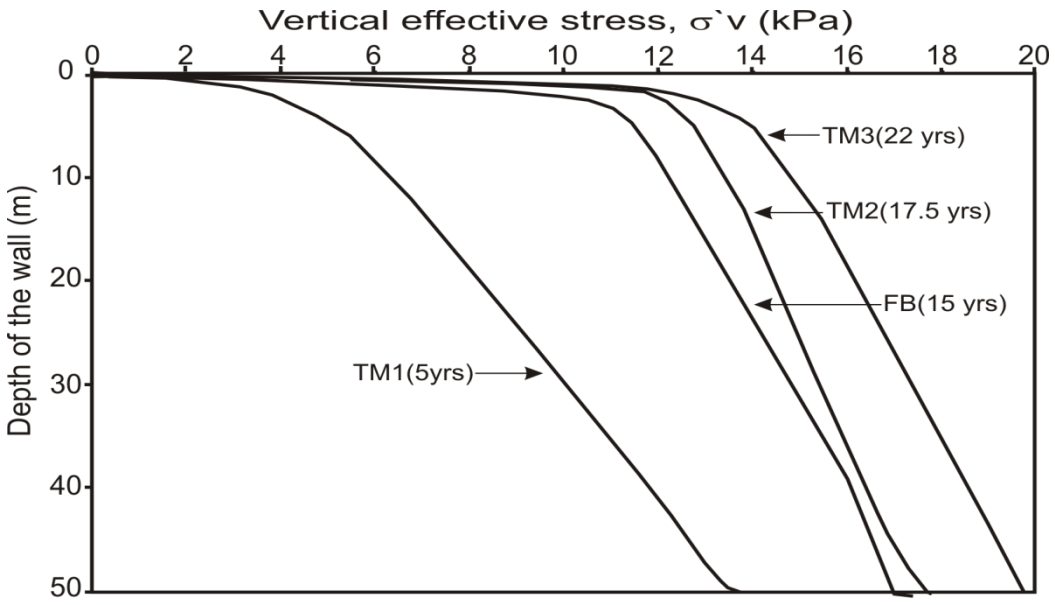

Figure F10. “Final” vertical effective stress with depth of the wall.

Appendix G

Calculation of Hydraulic conductivity from consolidation experiments

Table G1. Calculation of k from consolidation result and its comparison with measured k for Trial mix 1 (TM1)

Vertical effective stress, σ'_v (kPa)	Void ratio, e	Co-efficient of consolidation, c_v (cm^2/s)	Coefficient of compressibility, m_v (per kPa)	Calculated k $k = c_v*\gamma_w*m_v$ (m/s)	Measured hydraulic conductivity (m/s)
9	1.1288	3.16E-03	1.093773028	3.39E-06	7.66E-05
18	1.1161	3.41E-03	0.507219642	1.70E-06	1.99E-05
36	1.1005	2.62E-03	0.196490492	5.05E-07	6.88E-06
72	1.0776	2.21E-04	0.097664913	2.11E-08	1.98E-06
144	1.0372	1.97E-04	0.085512205	1.65E-08	5.65E-07
270	0.9956	8.62E-05	0.046703619	3.95E-09	1.88E-07
540	0.9523	9.54E-06	0.187124587	1.75E-09	8.88E-08
720	0.937	8.50E-06	0.121487101	1.01E-09	6.54E-08
900	0.9237	9.51E-06	0.046471326	4.33E-10	5.28E-08

Table G2. Calculation of k from consolidation result and its comparison with measured k for Field backfill (FB)

Vertical effective stress, σ'_v (kPa)	Void ratio, e	Co-efficient of consolidation, c_v (cm^2/s)	Coefficient of compressibility, m_v (per kPa)	Calculated k $k = c_v*\gamma_w*m_v$ (m/s)	Measured hydraulic conductivity (m/s)
9	1.1178	3.16E-05	1.093773028	3.39E-08	5.60E-06
18	1.1029	2.31E-05	0.507219642	1.15E-08	9.81E-07
36	1.0887	2.62E-05	0.196490492	5.05E-09	3.76E-07
72	1.0394	2.21E-05	0.097664913	2.11E-09	2.89E-08
144	0.9779	2.97E-06	0.085512205	2.49E-10	5.60E-09
270	0.9136	2.62E-06	0.046703619	1.20E-10	1.98E-09
540	0.8291	2.54E-06	0.028712459	7.14E-11	1.09E-09
720	0.8023	4.50E-06	0.01214871	5.36E-11	9.46E-10
900	0.7781	9.51E-06	0.004647133	7.33E-11	9.32E-10

Table G3. Calculation of k from consolidation result and its comparison with measured k for Trial mix2 (TM2)

Vertical effective stress, σ'_v (kPa)	Void ratio, e	Co-efficient of consolidation, c_v (cm^2/s)	Coefficient of compressibility ,m_v (per kPa)	Calculated k $k = c_v*\gamma_w*m_v$ (m/s)	Measured hydraulic conductivity (m/s)
9	1.1027	2.16E-05	1.093773028	2.32E-08	1.36E-06
18	1.0884	2.81E-05	0.507219642	1.40E-08	3.63E-07
36	1.0735	2.12E-05	0.196490492	4.09E-09	9.88E-08
72	1.0158	2.41E-05	0.097664913	2.31E-09	6.30E-09
144	0.9163	2.77E-06	0.085512205	2.32E-10	1.38E-09
270	0.8197	2.62E-06	0.046703619	1.20E-10	8.99E-10
540	0.7309	2.54E-06	0.028712459	7.14E-11	9.12E-10
720	0.6976	4.50E-06	0.01214871	5.36E-11	9.21E-10
900	0.6667	9.51E-06	0.004647133	4.03E-11	9.67E-10

Table G4. Calculation of k from consolidation result and its comparison with measured k for Trial mix 3 (TM3)

Vertical effective stress, σ'_v (kPa)	Void ratio, e	Co-efficient of consolidation, c_v (cm^2/s)	Coefficient of compressibility ,m_v (per kPa)	Calculated k $k = c_v*\gamma_w*m_v$ (m/s)	Measured hydraulic conductivity (m/s)
9	0.9541	2.16E-07	2.093773028	4.44E-10	1.68E-09
18	0.9263	2.81E-07	0.307219642	8.46E-11	1.20E-09
36	0.8709	6.12E-07	0.096490492	5.79E-11	8.10E-10
72	0.7632	1.41E-06	0.009766491	1.35E-11	6.58E-10
144	0.6515	1.77E-06	0.005551221	9.61E-12	5.17E-10
270	0.5215	9.62E-07	0.005670362	5.35E-12	3.99E-10
540	0.3929	8.44E-07	0.003571246	2.95E-12	3.27E-10
720	0.3428	7.50E-07	0.003214871	2.36E-12	2.90E-10
900	0.2983	8.51E-07	0.002647133	2.21E-12	2.80E-10

Appendix H

Intermediate aquifers

The field construction site (Section 5.7) has intermediate aquifers intersecting the slurry wall at different depths. These aquifers may act as a drainage path if the filter cake (Section 2.2) falls. This could be happen either during excavation with the clamshell or during the filling process.

A parametric study was initiated to investigate the effect of the aquifers on consolidation of the SB material. A simplified model of the site as shown in Figure H1 was used for this study. The study was carried on an aquifer of 1 m thickness, starting at a depth of 39 m depth from the ground surface. The pressure head (P) in the aquifer was 40 m.

The vertical effective stress variation with time and depth of the wall for a pressure head of 40 m is shown in Figure H3. The σ'_v distribution shifts upwards with time before reaching steady state. The σ'_v at the aquifer is more than for the rest of the wall with depth. This is because the aquifer acts as a drainage path.

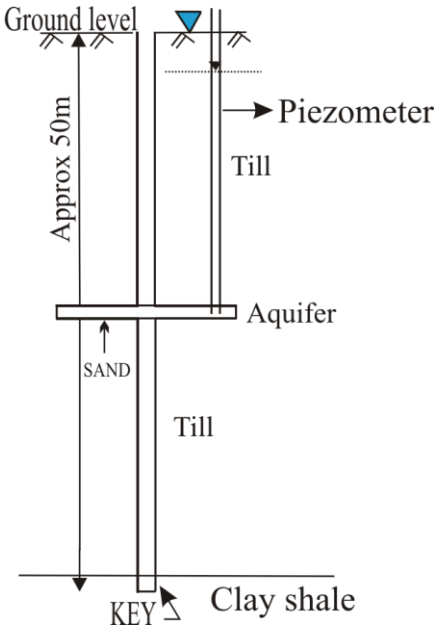

Figure H1 Cross-section of an SB wall with an intermediate aquifer.

A steady state pore pressure profile with depth, obtained by varying the pressure head in the aquifer, is shown in Figure H3. Pore water pressure dissipation is dependent on the number of drainage paths. The presence of an intermediate aquifer, which acts as a drainage path, speeds up the process of consolidation.

A parametric study was carried out on the intermediate aquifers by varying the pressure head (P) in the aquifer and the thickness (T_c) of the aquifer.

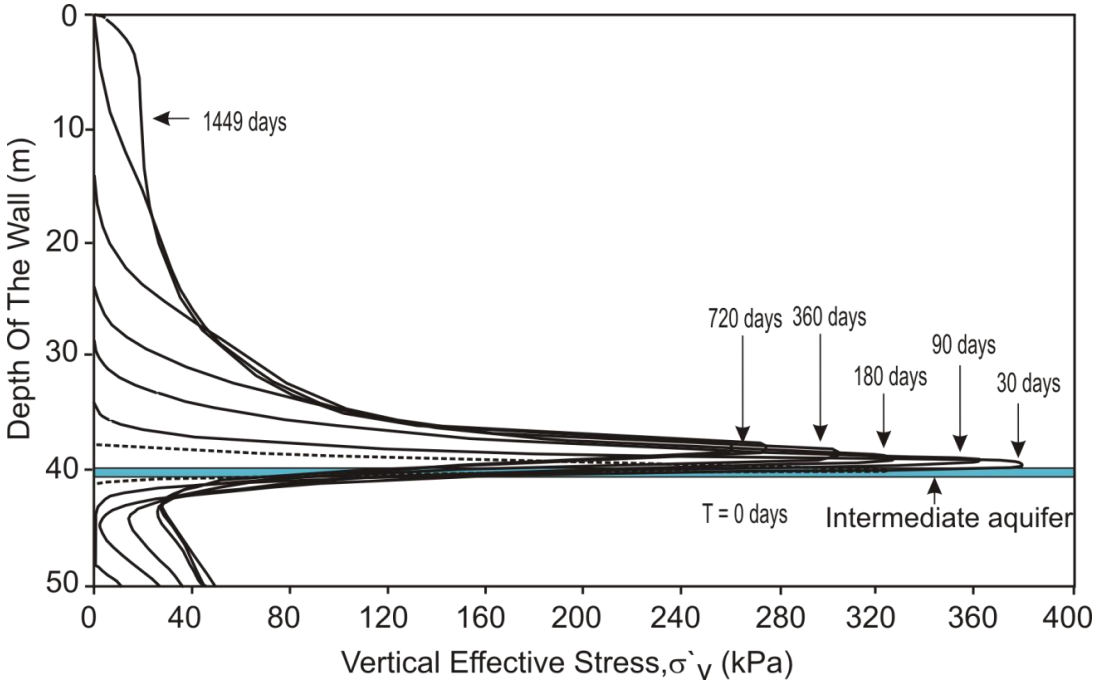

Figure H2 Variation of vertical effective stress in the SB wall with time.

5.9.2.1 Pressure head in the aquifer

Values considered for the pressure head, P, in the aquifer were 5, 10, 20, and 40 m. This was done to study the influence of pressure head on the σ'_v profile in the SB wall. The "Final" σ'_v profiles for aquifers with different pressure heads are shown in Figure H4. With increasing aquifer pressure, the σ'_v value at the aquifer decreases. The σ'_v profile (Figure H4) indicates that the void ratio initially decreased from 0 to 38 m and then increased up to 40 m (based on σ'_v distribution, more the effective stress, lesser

the void ratio). The decreasing trend of the curve (lower density) from 38 to 40 m depth makes the zone more susceptible to hydraulic fracturing and brine attack.

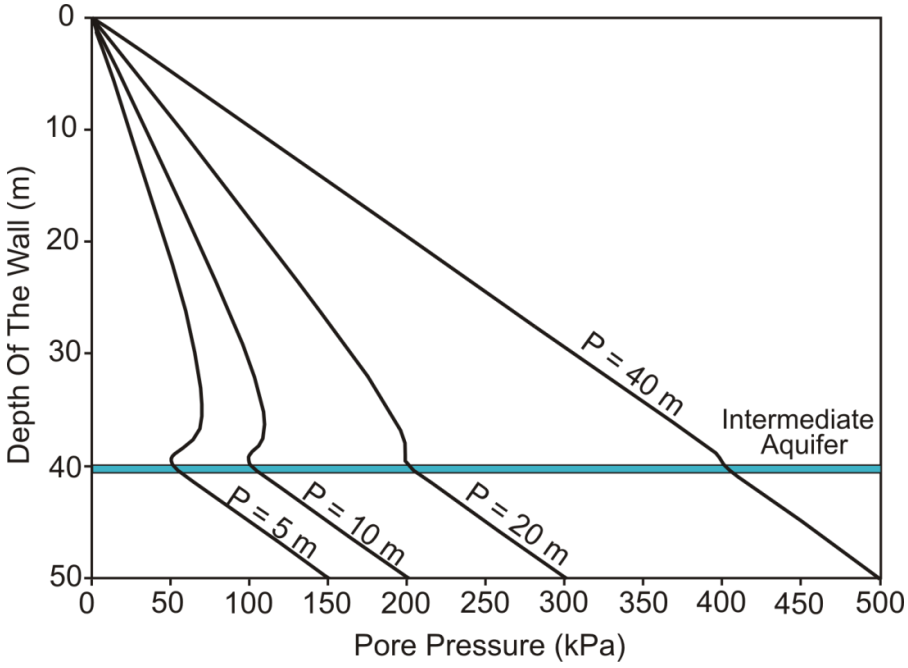

Figure H3 Steady state pore pressure.

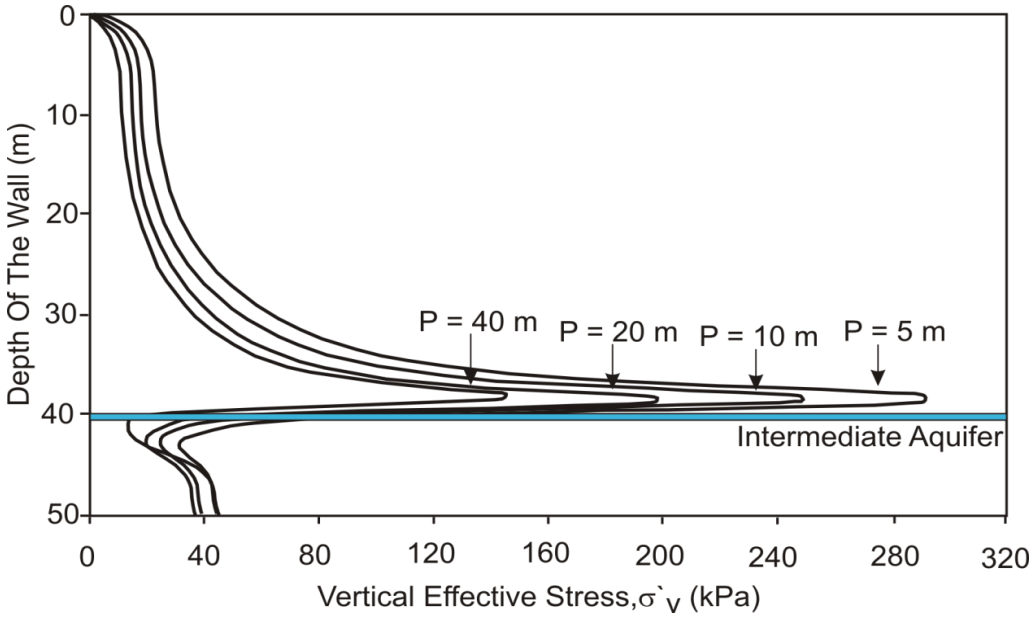

Figure H4 Variation of “Final” vertical effective stress in the SB wall by varying the pressure head in the aquifer.

5.9.2.2 Thickness (T_c) of the aquifer

Values considered for the thickness (T_c) of the aquifer were 0.5, 1, 2, and 4 m for a given pressure head of 40 m. This was done to study the influence of the thickness of the aquifer on the σ'_v profile with the depth of the wall. The “Final” stress profile (after more than 95% of the excess pore pressure has dissipated) for different aquifer a thickness is shown in Figure H5. It is clear from the figure that the thickness of the aquifer has little effect on vertical stress distribution in the SB walls.

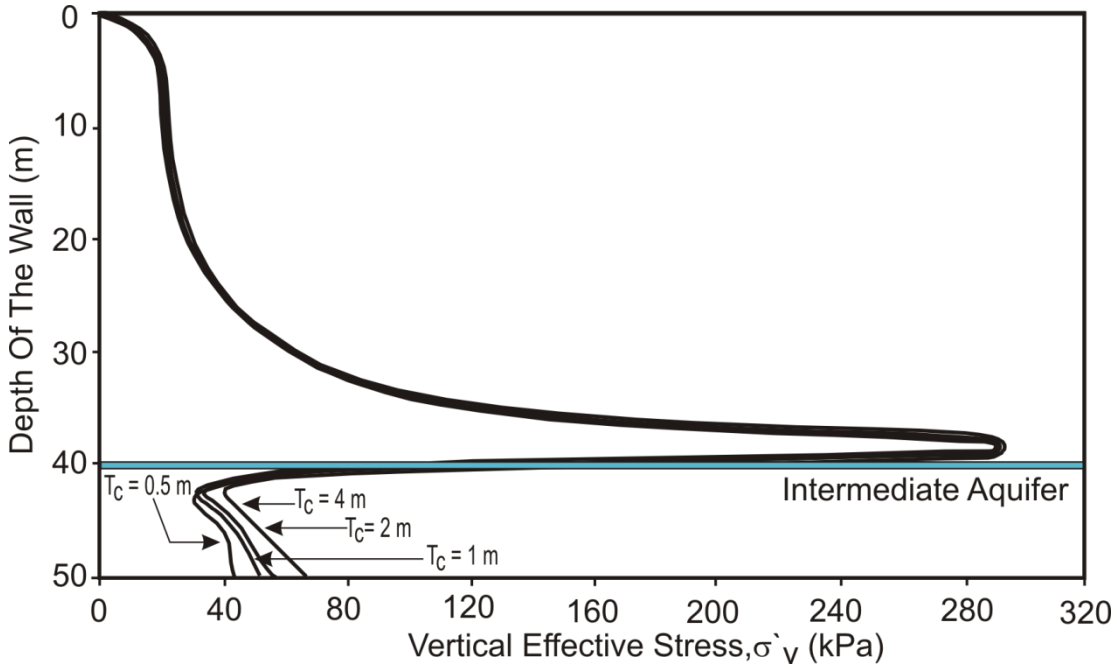

Figure H5 Variation of “Final” vertical effective stress in the SB wall by varying the thickness of the aquifer.